INVESTIGATION OF THE HERSCHEL-QUINCKE TUBE CONCEPT AS A NOISE CONTROL DEVICE FOR TURBOFAN ENGINES

By

Raphaël F. Hallez

Thesis submitted to the Faculty of the
Virginia Polytechnic Institute and State University
in partial fulfillment of the requirements for the degree of

Master of Science
in
Mechanical Engineering

Ricardo A. Burdisso, Chair
Marty E. Johnson
Don J. Leo

January 29, 2001
Blacksburg, Virginia

Keywords: Fan noise, aeroacoustics, Herschel-Quincke tube, higher-order modes

INVESTIGATION OF THE HERSCHEL-QUINCKE TUBE CONCEPT AS A NOISE CONTROL DEVICE FOR TURBOFAN ENGINES

By

Raphaël F. Hallez

Committee chairman: Ricardo A. Burdisso, Mechanical Engineering

(ABSTRACT)

An innovative implementation of the Herschel-Quincke tubes concept for the reduction of noise from turbofan engines is proposed here. The approach consists of installing circumferential arrays of Herschel-Quincke (HQ) tubes or waveguides in the inlet of the turbofan engine. An analytical technique was developed to predict the effects of HQ tubes applied to circular inlets. The modeling technique involves modeling the tubes-inlet interfaces as finite piston sources that couple the acoustic field inside the inlet with the acoustic field within the HQ tubes. An optimization technique based on genetic algorithms was also developed to be able to design and optimize the system parameters. The accuracy of the model was validated with experimental data obtained from two types of turbofan engines. Analytical predictions are shown to correlate well with experimental data. The analytical model is then used to provide insight into the noise control mechanisms involved in the system. It is shown that the energy in an incident mode is in part reflected back to the fan and that some energy is also scattered into other higher-order modes. Thus, the suppression of a particular mode is due to the combination of the scattered contributions from the various incident modes. The effects of the system parameters were analyzed and parametric studies were conducted. Different configurations for the arrays of HQ tubes such as helical patterns or tubes at an angle with respect to the inlet axis were also investigated. The results show the great potential of the HQ tubes system to reduce noise from turbofan engines.

Acknowledgments

I would like to thank my research advisor, Prof. Ricardo Burdisso, for giving me the opportunity to work on a challenging research project. Working under his supervision has been a truly exciting experience. I would also like to thank Jerome.Smith, who has provided helpful guidance and suggestions at the beginning of this work. I also wish to thank Prof. Marty Johnson and Prof. Don Leo for serving on my advisory committee.

I appreciate Mrs. Jaffrin, Mrs. Behin and Dr. Mahan, coordinators of the exchange program between Virginia Tech and the Université de Technologie de Compiègne, for giving me the opportunity to study in Blacksburg.

Many thanks go to all my friends in the Vibration and Acoustics Laboratories who have helped me during the course of this work. In particular, I would like to thank Arnaud Charpentier, Simon Esteve, Pierre Marcotte, Arthur Blanc and many others for their technical support and most importantly their friendship. I also wish to thank my faithful friend, Benjamin Soulé de Bas, for his support and encouragements throughout this work.

I am obviously indebted to the Aeroacoustics branch of the NASA Langley Research Center for their financial and technical support. I wish to particularly thank the technical monitors of this work, Dr. Carl Gerhold and Dr. Joe Posey.

My parents, my brother and my grandmother in France deserve all my gratitude for their moral support and their encouragements throughout this work. Finally, I would like to thank my girlfriend, Julia, who accepted my choice to come study in the United States. Her voice and her letters have been my source of energy during this period far from her.

Contents

List of figures

List of tables

Chapter 1. Introduction

As air traffic continues to escalate, turbofan engines represent an increasingly significant source of noise pollution, particularly at airports and the surrounding communities. At the same time, the search for higher performance propulsion systems results in the development of turbofan engines with ultra-high bypass ratio (bypass ratios of 5 to 6 are currently used and future engines are planned to have bypass ratios in the range of 10 to 15). In these modern turbofan engines, the pure tones produced by the fan are a significant source of noise. Thus, fan tonal noise constitutes the main target for noise control of turbofan engines. Traditionally, acoustic wall treatment has been used as a method to address this noise problem. However, this passive technique has only made small reductions in fan inlet and aft noise levels and remains a complex and expensive system. More innovative systems such as active noise control were investigated more recently to attenuate noise from turbofan engines. Although these systems can show very good noise attenuation of tonal component, they tend to be very complex and still unpractical for the application on a real engine. Therefore, the door is left open for innovative systems which could provide significant sound reduction and be easily implemented on the turbofan engine. The present study proposes to investigate the potential of the Herschel-Quincke tube concept to reduce the noise from turbofan engines. In particular, the system investigated here consists of placing the HQ tubes on the inlet of a turbofan engine, with no acoustic treatment on the inlet wall.

In this first chapter, a description of the turbofan engine noise is first presented. The different components present in the acoustic spectrum of a turbofan engine are

explained. The generation and propagation mechanisms of noise in an engine inlet are also presented. Then, a brief review of the existing systems to control turbofan engine noise will be performed. The principle of the Herschel-Quincke (HQ) tube system applied to plane wave control will be explained and the previous studies on this system will be reviewed. Finally, the objectives and organization of the study are presented in the last two sections.

1.1 Turbofan engine noise

In order to find an efficient system to reduce noise from turbofan engines, it is important to understand the properties of the sound field inside the engine. In the 1960's, Tyler and Sofrin performed experiments to investigate the characteristics of the pressure field generated by an axial flow compressor [1]. Two aspects of their study will be explained here, i.e. the generation mechanisms of the fan noise and the propagation characteristics of the noise down the inlet of the engine.

A typical fan acoustic spectrum includes a broadband noise level and tones at the fan blade passage frequency (BPF) and its harmonics. The broadband noise can be caused by vortex shedding, boundary layer turbulence, interaction between the blade pressure fields, wall boundary layers, and so forth. It is present at every frequency and is typically equally distributed among all frequencies. The most dominant components in the fan spectrum are the blade passage frequency tones. These tones are often at least 10-15 dB above the broadband level. Tyler and Sofrin showed that the generation of these components is mainly due to the interaction between the rotor blades and the stator vanes. The sources of this interaction noise are the cutting of wakes of upstream stators by rotor blades, the impringement of rotating blade wakes on downstream stators and interruption of the rotating periodic pressure field of the rotor by the proximity of reflecting objects, apart from wake effects. The tones are generated at specific frequencies called the blade passage frequency, or BPF, and its harmonics. This frequency is calculated from the following equation

$$BPF = \frac{N}{60} B \tag{1.1}$$

where N is the rotational speed of the rotor in RPM and B is the number of fan blades. As the rotor passes near a stator, the wake of the rotor passes by the stator causing a peak in the pressure field. These peaks will rotate at a certain frequency to generate sound at the BPF and the harmonics. The corresponding pressure pattern constitutes a spinning mode. Therefore, only certain modes will be generated by the interaction between rotor and stator. The circumferential order of these modes depends on the number of fan blades and number of stator vanes as shown in the following equation

$$m_{RS} = nB + kV \tag{1.2}$$

where m_{RS} is the circumferential order mode which is generated by the stator-rotor interaction, n is the harmonic of the BPF, B is the number of rotor blades, k is any integer number, i.e. k=0, ±1, ±2, ±3,…and V is the number of stator vanes.

Depending on the circumferential order of the mode m_{RS}, the rotation speed will change to generate noise at the BPF frequency or its harmonics. The angular velocity Ω_m of mode m_{RS} can be calculated from the equation

$$\Omega_m = \frac{nB}{m_{RS}}\Omega \tag{1.3}$$

where n is the BPF harmonic index, B is the number of rotor blades, m_{RS} is the circumferential order of the mode and Ω is the shaft angular velocity (in rad/s).

As explained above, the pressure field due to the rotor-stator interaction is made of spinning patterns called modes. Depending on the number of blades and vanes, modes of specific circumferential order will be excited. This order, also called m index, corresponds to the number of pressure lobes around the circumference of the inlet duct. However, circumferential modes can have different pressure variation along the radius. This radial variation is defined by the radial order n, which corresponds to the number of pressure nodes along the radius. As an illustration, Figure 1-1 shows some examples of pressure variation on the cross-sectional plane of the inlet for modes of different radial and circumferential order. On these plots, the black areas represent regions where the pressure is out of phase with the pressure on white areas.

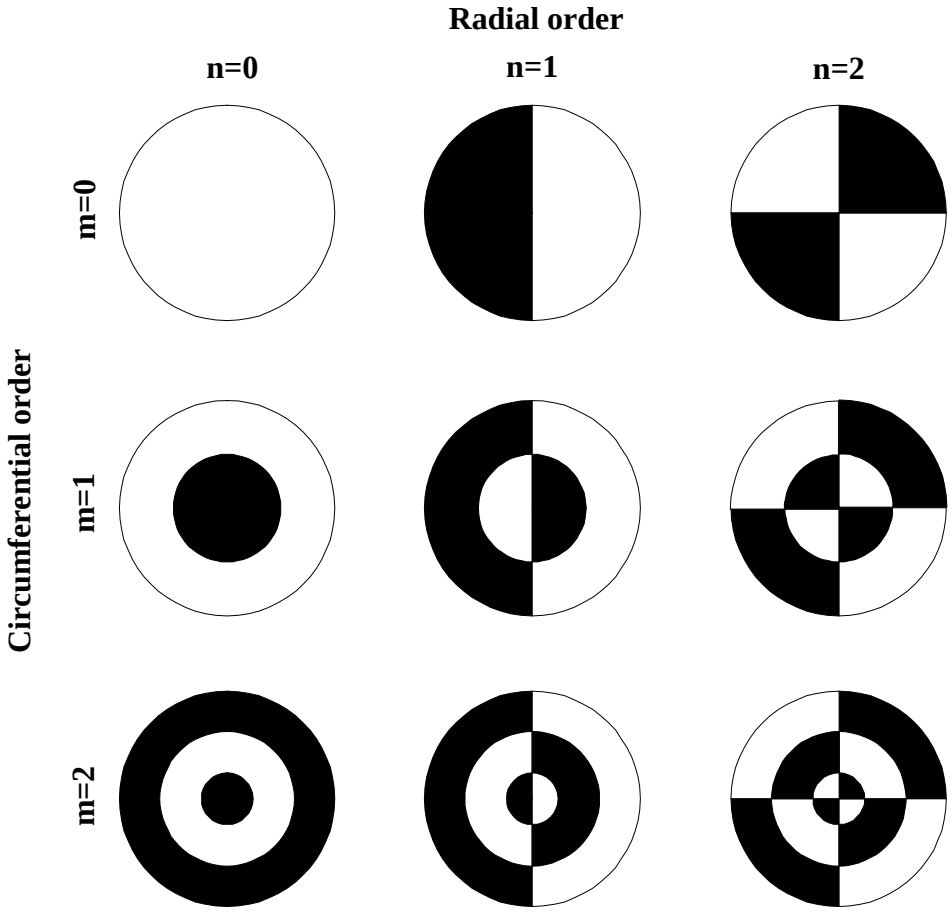

Figure 1-1: Mode patterns in the cross-sectional plane of the inlet.

The pressure field in the inlet duct is made of an infinite superposition of mode patterns. However, the propagation characteristics of these modes will be different depending on their order. These characteristics are dictated by a limit frequency, above which a mode starts to propagate. This frequency is called cut-off frequency. If the driving frequency is lower than the mode cut-off frequency, then the wave will decay exponentially as it propagates down the axis of the inlet. In this case, the acoustic mode is considered to be "cut-off" and will not propagate to the far field. However, for a given mode, if the driving frequency is higher than the cut-off frequency, then the acoustic energy in this mode will propagate down the inlet with unchanged amplitude in a duct with no acoustic treatment. The mode is said to be "cut-on" and will radiate to the far field. Therefore, the cut-off frequency is a determinant criterion that dictates the propagation characteristics of the modes. This frequency is a function of the flow Mach

number and mode order, i.e. the cut-off frequency increases as the mode order increases. The expression for this frequency will be given in equation (2.20). Each mode radiating in the far field has a different directivity pattern. However, for the purpose of this study, only the sound power and sound pressure levels at the open end of the inlet will be considered here.

1.2 Noise control systems for turbofan engines

In the last decades, various attempts have been made to try to reduce the fan noise. One way of reducing fan noise is by changing directly the design of the fan. For example, the geometry of the fan blades and the rotor vanes can be modified to reduce the noise generation due to rotor-stator interaction [2-3]. Such systems with various spacing between rotor and stator as well as fan with leaned blades were investigated. Although these systems allow to achieve significant noise reduction, these innovative systems raise new issues such as additional vortex shedding generation or stress concentration at the same time.

On the other hand, passive treatments have been extensively used to reduce fan noise [4]. These porous material systems are typically placed on the inlet walls of the engine and their efficiency is proportional to the length of treatment used. The liners systems can be classified as the absorber type, the resonator type and a type which has a combination of both these characteristics. Absorber liners consist of a thick layer of porous material and will attenuate a broad band of noise but are not particularly suitable for attenuating large amplitude components of discrete frequency. Resonant liners consist of a thin sheet of perforated facing material separated from an impervious surface by a cavity divided into compartments by a honeycomb spacer structure; this forms an array of resonators which effectively attenuate a predominantly narrow frequency band of noise but are not very effective over a broader band frequency range. Lastly, a liner combining the essential features of both types, consisting of a thin porous absorptive facing material backed by resonant cavities, has good attenuation characteristics over a wide range of frequencies.

Although the principle of the liners is simple, these systems tend to be very complex to build, which makes it a very expensive acoustic treatment. Moreover, there is a tradeoff in the design of the liner impedance. Either the impedance is chosen such that it can

provide attenuation in several modes, or it is designed to attenuate the acoustic energy in a specific mode. On the other hand, one of the results of the continuing search for higher performance propulsion systems is the development of ultra high bypass turbofan engines. These large engines will have an even greater fan tonal noise component at lower frequencies. Moreover, the shorter and wider inlet duct inherent to the ultra high bypass turbofan engines will make passive liner technology less effective for attenuating the fan tones.

Because of these difficulties, the potential of new techniques such as active noise control was investigated for the control of turbofan noise [5, 6, 7]. However, despite the recent advances in active noise control methods for controlling the BPF tone and harmonics, the complexity of these systems implies that the implementation of a practical system for production may be still many years away. The presence of multiple higher-order modes in a duct can require a large number of sensors and actuators for an effective active noise control system, and the expense of such systems increases rapidly with the complexity of the sound field. Furthermore, it has been reported that simply reducing the BPF tone and harmonics, i.e., without any reduction in the broadband levels, may result in little or no reduction in the EPNL (Effective Perceived Noise Level), which is the metric used to quantify aircraft flyover noise. Thus, it is likely that a noise control methodology resulting in fan tone noise control in combination with broadband noise control will have to be implemented to produce an effective noise control solution for turbofan engines.

1.3 The Herschel-Quincke technique

Here a novel approach to control both tonal and broadband noise from turbofan engines will be investigated. The approach consists of installing circumferential arrays of Herschel-Quincke (HQ) waveguides in the inlet of the turbofan engine. A HQ waveguide is essentially a hollow side-tube that travels along (but not necessarily parallel to) the engine axis and attaches to the inlet at each of the two ends of the tube. The HQ concept as applied to a turbofan engine inlet is illustrated in Figure 1-2, where a single circumferential array of HQ tubes is positioned on an engine inlet.

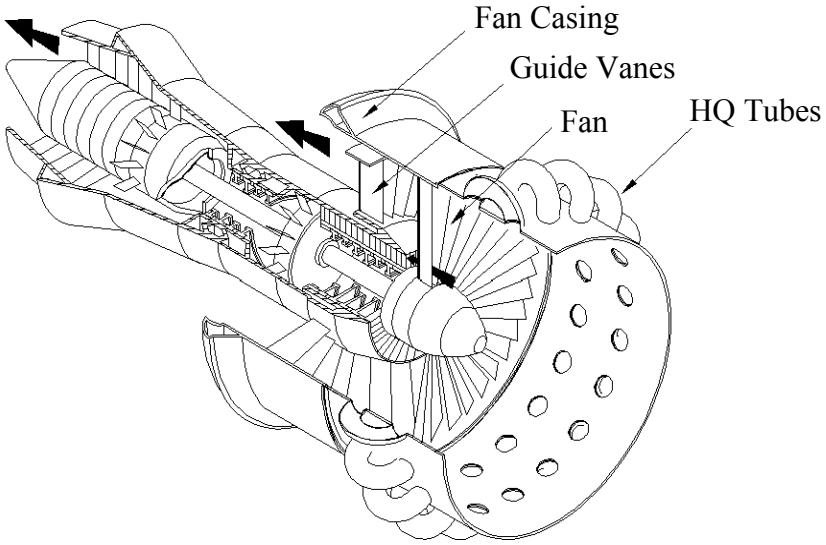

Figure 1-2: Schematic of the Herschel-Quincke tube concept applied to the inlet of a turbofan engine.

The case of a single HQ tube for the control of plane wave control is illustrated in Figure 1-3. A simplistic explanation of the noise cancellation observed with the HQ tube in the case of the plane wave is that some of the sound energy traveling in the main-duct goes into the HQ tube at its entrance, travels through the tube, and recombines with the remaining energy traveling through the main-duct at the exit of the tube. Since the sound in the tube has traveled a larger distance, frequencies exist where the sound in the tube exit is out-of-phase with the sound in the main-duct and would therefore cancel at those frequencies. These frequencies are dictated by the geometrical parameters of the HQ tubes such L, D or S. This explanation is indeed an oversimplified one, the actual dynamics are much more complex, as sound waves can propagate in both directions within the main duct and the tubes.

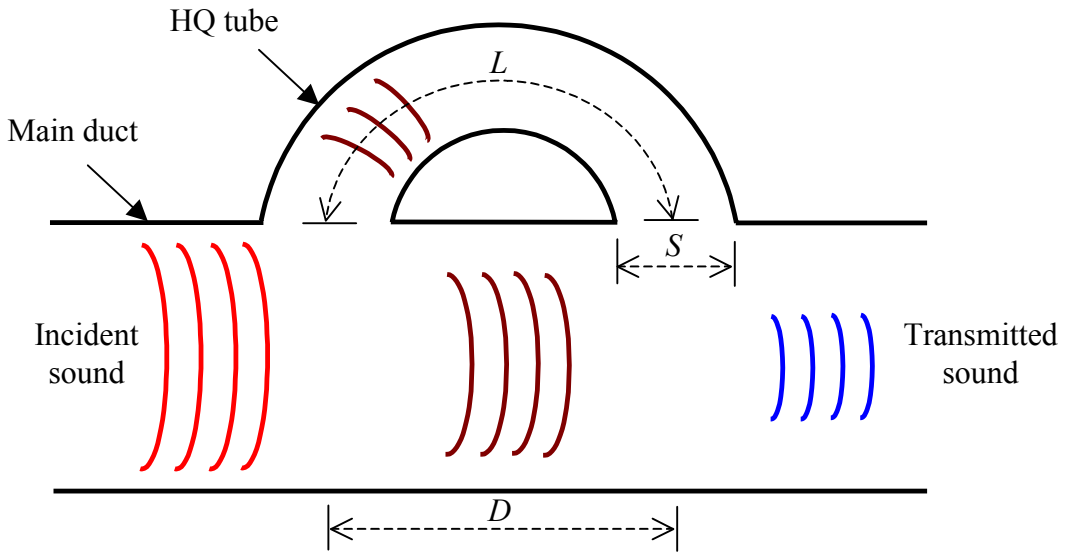

Figure 1-3: Schematic of Herschel-Quincke tube for the control of plane wave.

Previous work of the HQ concept has been restricted to the control of simple one-dimensional plane waves in ducts. Herschel [8] first discussed the idea of acoustic interference of musical tones with such a system in 1833. He predicted that the cancellation of tones would occur when the path length difference between the recombined signals was $(2m+1)(\lambda/2)$, where λ is the wavelength of the acoustic wave and m is any integer. Later, in 1866, Quincke [9] experimentally validated that Herschel's system did effectively cancel sound. Stewart [10], in the 20th century, found Herschel's theoretical explanation to be insufficient to interpret experimental data he had observed. Using a plane wave analysis, Stewart derived an analytical model describing the ratio of transmitted to incident sound intensity in the system. He verified that cancellation does occur when the path length difference is $(2m+1)(\lambda/2)$, but also when the path length difference is $m\lambda$, with limited attenuation at other transitional frequencies. However, Stewart's model assumed that the cross-sectional areas of the parallel duct sections were equal. More recently, Selamet, et. al. [11], extended Stewart's work by deriving an analytical model without the limitations on duct cross-sectional geometry. The effect of multiple HQ tubes and reflection at the duct opening was more recently addressed again for plane-wave only [12].

Only recently has the potential of HQ waveguides for attenuating higher-order modes in two-dimensional ducts been analytically investigated [13]. This study proposed

a model to predict the effect of a HQ tube in the presence of higher-order modes and showed that the noise attenuation mechanisms involved reflection of incident energy as well as scattering and recombination of energy between radial modes.

The above one- and two-dimensional situations should be contrasted to the more complicated three-dimensional pressure fields that exist in ducts in the presence of higher-order modes. In the case of turbofan engine inlets in particular, the sound field at the BPF tone is made up of propagating spinning modes with multiple circumferential and radial orders. This results in a complex pressure field in the cross-sectional plane of the inlet with non-uniform circumferential variation in the acoustic pressure. The same simplistic description of the noise cancellation process for the plane wave case can be extended to the configuration in Figure 1-2. However, due to the circumferential variation of the acoustic pressure on the inlet wall, an array of independent HQ tubes is necessary to account for and preserve the circumferential variation in the pressure. With a circumferential array of independent tubes, the acoustic pressure from tube to tube has the same variation as the circumferential variation in the duct. This is critical to the implementation of the concept to result in significant sound cancellation, i.e., when the sound in the tubes and in the inlet recombine out-of-phase, the sound at the exit of the tubes must be out-of-phase and of the same circumferential variation as the sound in the inlet. The potential of HQ tubes to reduce noise from turbofan engines was recently investigated on a running Pratt & Whitney JT15D turbofan engine by Burdisso et. al. [14]. The results showed very good reduction of tonal noise at discrete frequencies as well as broadband noise. This study demonstrated the remarkable potential of the Herschel-Quincke concept for reducing noise from turbofan engines.

1.4 Objectives

The study performed here will focus on the analytical aspect of the HQ concept applied to turbofan engines. Therefore, the first objective of this work is to develop a model of the HQ tube system mounted on the engine inlet. The modeling technique will be developed to take into account the propagation of higher-order modes in a cylindrical duct and a computer code will be written based on this technique. The code will allow to

predict the radiation of acoustic energy in the inlet duct mounted with a HQ system. The HQ systems considered in the model can have various geometries since the dimension of each tube is defined individually.

After validating the model with experimental data on two different engines, the next objective is to investigate the noise control mechanisms involved in the HQ system. The model will thus be used to try understanding the behavior of the HQ tube system. The goal of the study is to investigate the influence of the parameters in the HQ system on the sound reduction and draw conclusions to help the design of the HQ system and be able to apply it to various engines.

1.5 Organization

The remainder of this report is organized into four chapters. The theoretical development of the study is presented in Chapter 2. In this chapter, the technique used to model the HQ system mounted on a cylindrical duct is first explained. Then, the approach used to optimize the HQ system parameters with genetic algorithms is presented. In chapter 3, the modeling technique will be validated with experimental data. The test setup for two different engines is first presented and predictions for broadband and tonal noise are compared to experimental data. A convergence study will also be performed to determine the number of modes necessary to get accurate prediction results. Then, the computer code is used to get insight into the noise control mechanisms involved in the HQ system. An impedance analysis is first achieved to investigate the resonances of the system. The scattering mechanisms will then be presented for radial and circumferential modes. The next section presents a parametric study where the effect of the configuration of the system on its performance was investigated. Finally, different geometries for the HQ system are tested based on the concept of mode propagating along helixes. Systems where tubes are placed in helix patterns or where tubes are rotated at an angle relative to the inlet axis will be investigated. The last system consists of a combination of the previous two and places the HQ tubes in helix patterns with tubes rotated at an angle. Finally, conclusions drawn from this study, along with recommendations for further research, are presented in Chapter 5.

Chapter 2. Theoretical development

In this chapter, the theoretical formulations are presented. The technique used to model the HQ tubes in the cylindrical inlet is first explained in section 2.1. In this section, the equations used in the model will be presented in detail. After having found the general expression for the sound pressure inside a rigid wall duct, the sound field generated by a finite piston source on the inlet duct wall will be expressed. Then, the sound field inside the duct and the sound field inside the HQ tubes will be developed. Both systems will be coupled at the tube-duct interfaces allowing to find an expression for the average velocity of each piston source. Finally, the sound power radiated upstream of the HQ system will be calculated.

In order to design the various parameters of the HQ system, an optimization technique based on genetic algorithms is developed and is presented in section 2.2. After explaining the main principle of these algorithms, this section will focus on the key concepts used in this technique. A definition of the fitness function will thus be given. Then, the selection, crossover, mutation and replacement processes will be explained.

2.1 Modeling technique

In this section, the modeling of the HQ tube system mounted on a cylindrical duct is developed. First of all, the eigenvalue problem is solved for the rigid-wall infinite duct to find the acoustics modes that are then used to expand the pressure field inside the duct. Then, the Green's function corresponding to the pressure field generated by a point

source on the duct wall is calculated. This function allows to find the expression for the sound field radiated by a finite piston source on the duct wall.

Once these general expressions are found, the actual model of the acoustic field inside the duct with HQ tubes can be developed. The technique used in the modeling approach is illustrated in Figure 2-1. The reflections at the open end of the inlet and on the fan is neglected in the model, therefore, the inlet of the turbofan engine is modeled as an infinite rigid-wall duct as shown in Figure 2-1b. The model for the sound field inside the duct (Figure 2-1c) and inside the HQ tubes (Figure 2-1d) are developed individually and then fully coupled by matching the acoustic variables, i.e. pressure and particle velocity, at the interfaces between the duct and the HQ tubes. An expression for the sound power radiated at the end of the duct is finally derived.

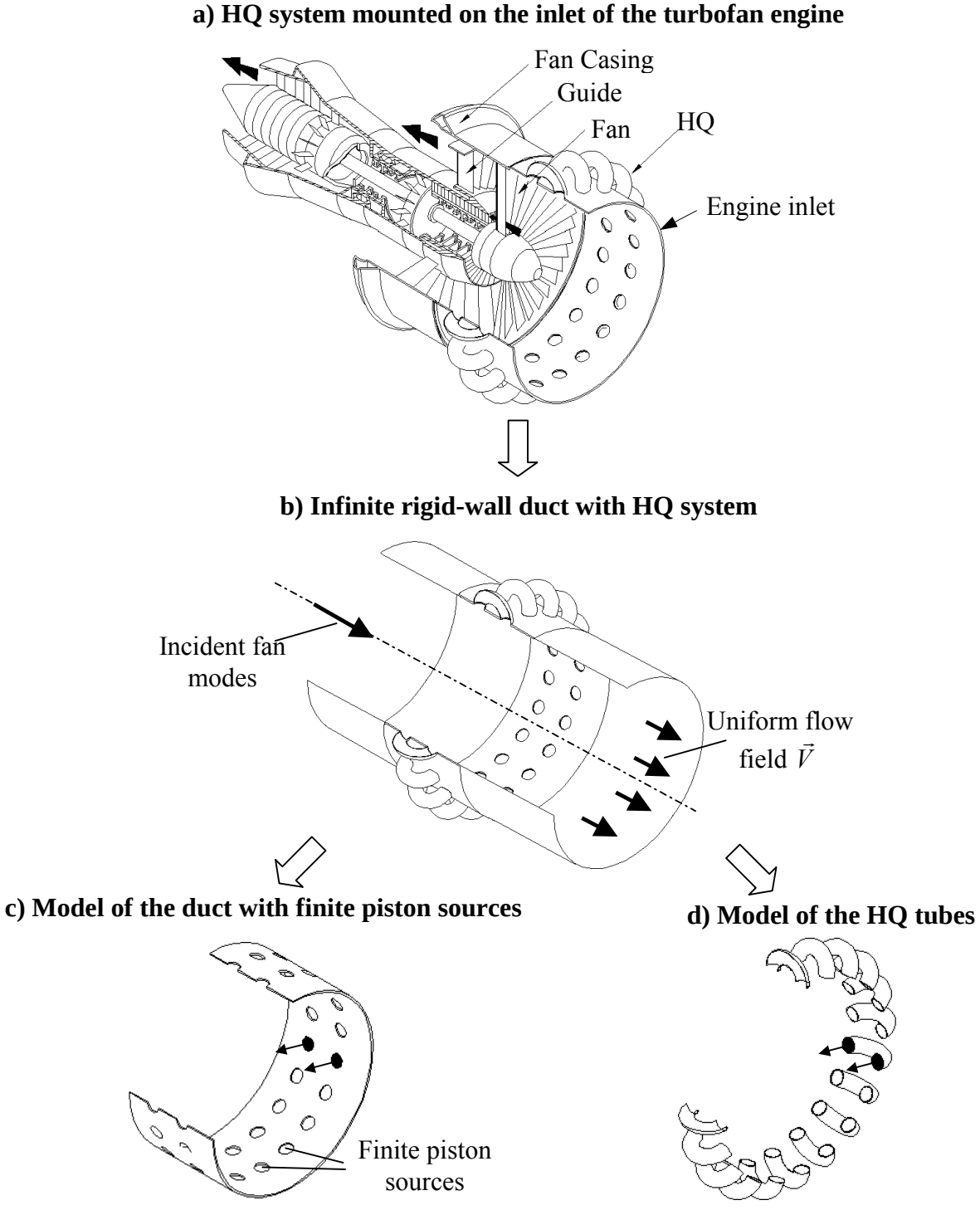

Figure 2-1: Modeling approach. a) Engine inlet mounted with HQ tubes is modeled as b) an infinite duct. Model of sound fields c) inside the duct and d) inside the HQ tubes are developed individually.

2.1.1 Eigenvalue problem

The first step of the modeling process consists of considering a cylindrical duct with hard wall, and finding an expression for the acoustic pressure field inside the duct. In other words, the eigenvalues and mode shapes need to be found. The duct considered here is of infinite length and of radius *a*. The cylindrical coordinates system used in the analysis is shown in Figure 2-2. The positive *z*-direction is chosen to be the direction of sound propagation. It is assumed that a uniform flow field with Mach number *M* (the Mach number is the flow velocity divided by the speed of sound) is propagating in the positive *z*-direction. For the particular case of turbofan engines, this Mach number will be negative since the flow is propagating in the opposite direction.

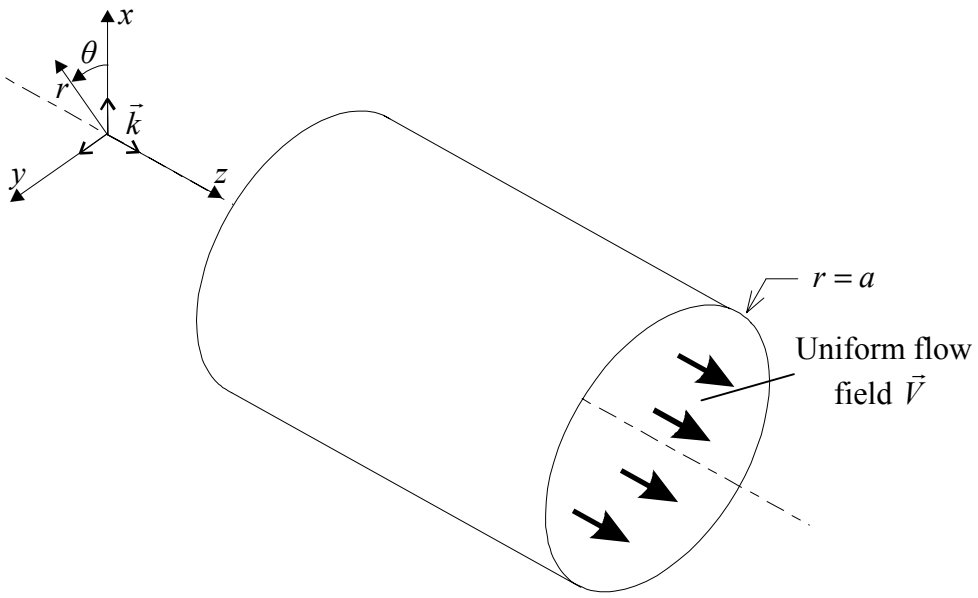

Figure 2-2: Model of the infinite cylindrical duct with flow.

The general form of the acoustic wave equation in a moving media is given as [15]

$$\nabla^2 p = \frac{1}{c^2}\left(\frac{\partial}{\partial t} + \vec{V}\cdot\nabla\right)^2 p \tag{2.1}$$

where ∇^2 is the Laplacian operator, c is the speed of sound, p is the acoustic pressure, and $\vec{V}$ is the flow velocity field vector. Assuming a uniform flow field in the positive *z*-direction (along the duct axis), i.e. $\vec{V} = cM\vec{k}$ where $\vec{k}$ is the unit vector in the *z*-direction, and considering a harmonic motion, equation (2.1) in cylindrical coordinates becomes

$$\frac{\partial^2 p}{\partial r^2}+\frac{1}{r}\frac{\partial p}{\partial r}+\frac{1}{r^2}\frac{\partial^2 p}{\partial \theta^2}+\frac{\partial^2 p}{\partial z^2}=-k_o^2 p+2ik_o M\frac{\partial p}{\partial z}+M^2\frac{\partial^2 p}{\partial z^2} \tag{2.2}$$

where k_o is the free field wavenumber. The solution to the partial differential equation (2.2) is assumed to be a propagating wave in the z-direction and have the form

$$p(r,\theta,z,t)=\Phi(r,\theta)e^{-ik_z z}e^{i\omega t} \tag{2.3}$$

where k_z is the axial wave number and $\Phi(r,\theta)$ is the acoustic mode shape function. The time function $e^{i\omega t}$ is omitted for the rest of the derivation.

Replacing (2.3) into equation (2.2) and canceling out the term $e^{-ik_z z}$ gives

$$\frac{\partial^2\Phi}{\partial r^2}+\frac{1}{r}\frac{\partial\Phi}{\partial r}+\frac{1}{r^2}\frac{\partial^2\Phi}{\partial\theta^2}+\left\{k_o^2-k_z^2\left(1-M^2\right)-2k_o k_z M\right\}\Phi=0 \tag{2.4}$$

The solution of this equation is obtained using separation of variables as

$$\Phi(r,\theta)=R(r)\Theta(\theta) \tag{2.5}$$

Replacing (2.5) into (2.4) and multiplying by $r^2/\left[R(r)\Theta(\theta)\right]$ gives

$$\frac{r^2}{R}\left(\frac{d^2R}{dr^2}+\frac{1}{r}\frac{dR}{dr}\right)+\frac{1}{\Theta}\frac{d^2\Theta}{d\theta^2}+r^2k_{mn}^2=0 \tag{2.6}$$

where

$$k_{mn}^2=k_o^2-k_z^2(1-M^2)-2k_o k_z M \tag{2.7}$$

Each term in equation (2.6) must be a constant and thus implies that

$$\frac{1}{\Theta}\frac{d^2\Theta}{d\theta^2}=-m^2 \tag{2.8}$$

where $\Theta(\theta)$ must be a periodic function with period 2π. Therefore, for stationary modes, the solution of equation (2.8) takes the form

$$\Theta(\theta)=A\cos(m\theta)+B\sin(m\theta) \qquad m=0,\ 1,\ 2,\ldots \tag{2.9}$$

The solution to (2.8) can also take the form of spinning modes as

$$\Theta(\theta)=Ae^{im\theta}+Be^{-im\theta} \qquad m=0,\ 1,\ 2,\ldots \tag{2.10}$$

where A and B are the amplitudes of the mode spinning in the negative and positive θ-direction, respectively.

Equation (2.6) is written in term of *R(r)* as

$$\frac{r^2}{R}\left(\frac{d^2R}{dr^2}+\frac{1}{r}\frac{dR}{dr}\right)-m^2+r^2k_{mn}^2=0 \tag{2.11}$$

The solution of this equation takes the form

$$R(r)=CJ_m(k_{mn}r)+DY_m(k_{mn}r) \tag{2.12}$$

where J_m is the first kind Bessel function of m^{th} order, Y_m is the second kind Bessel function or Neumann's function of m^{th} order and C and D are constants. Because Y_m has a singularity at the origin and the pressure field has to be bounded for any $r \le a$, the constant D is set to zero. Thus, equation (2.12) can be written as

$$R(r)=CJ_m(k_{mn}r) \tag{2.13}$$

For a rigid-wall duct, the radial particle velocity on the wall must vanish. Therefore

$$\left.\frac{\partial p}{\partial r}\right|_{r=a}=\left.\frac{\partial \Phi}{\partial r}\right|_{r=a}=\left.\frac{dR}{dr}\right|_{r=a}=0 \tag{2.14}$$

Thus, replacing equation (2.13) into the preceding boundary condition (2.14) yields

$$\left.\frac{dJ_m}{dr}(k_{mn}r)\right|_{r=a}=0 \tag{2.15}$$

where k_{mn} are the values that satisfy the boundary condition. For each m value, there are actually many roots that satisfy this equation. The k_{mn} values are called the eigenvalues and are written as

$$k_{mn}=\frac{\chi_{mn}}{a} \qquad m=0, 1, 2, \ldots\ n=0, 1, 2,\ldots \tag{2.16}$$

defining χ_{mn} as the inflection points of the Bessel's function of the first kind of order m. For each m index, there are many values that satisfy equation (2.16), these values are designated by the index n, where n=0 corresponds to the first value.

Finally, the expression for the mode shapes is

$$\Phi_{mn}(r,\theta)=\Theta(\theta)J_m(k_{mn}r) \qquad m=0, 1, 2, \ldots\ n=0, 1, 2,\ldots \tag{2.17}$$

where the function $\Theta(\theta)$ corresponds to stationary or spinning waves as shown in equations (2.9) and (2.10) respectively, depending on the actual excitations.

The axial wavenumber k_z is found using

$$k_{mn}^2 = k_o^2 - k_z^2\left(1-M^2\right) - 2k_o k_z M \tag{2.18}$$

which yields

$$k_z = \left\{-Mk_o \pm \sqrt{k_o^2 - \left(1-M^2\right)k_{mn}^2}\right\} / \left(1-M^2\right) \tag{2.19}$$

Thus, there are two values for k_z corresponding to positive and negative traveling waves. The modes can also be propagating or decaying depending on the following conditions:

(i) If $k_o > k_{mn}\sqrt{\left(1-M^2\right)}$ the mode will propagate

(ii) If $k_o < k_{mn}\sqrt{\left(1-M^2\right)}$ the mode will decay

The frequency where $k_o = k_{mn}\sqrt{\left(1-M^2\right)}$ is called cut-off frequency and is written as

$$f_{cut-off} = \frac{c}{2\pi} k_{mn}\sqrt{\left(1-M^2\right)} \tag{2.20}$$

Based on the above conditions, there are four possible cases for the axial wavenumber

i) Positive traveling mode: $$k_z^{(+)} = \left\{-Mk_o + \sqrt{k_o^2 - \left(1-M^2\right)k_{mn}^2}\right\} / \left(1-M^2\right) \tag{2.21}$$

ii) Positive decaying mode: $$k_z^{(+)} = \left\{-Mk_o - i\sqrt{\left(1-M^2\right)k_{mn}^2 - k_o^2}\right\} / \left(1-M^2\right) \tag{2.22}$$

iii) Negative traveling mode: $$k_z^{(-)} = \left\{-Mk_o - \sqrt{k_o^2 - \left(1-M^2\right)k_{mn}^2}\right\} / \left(1-M^2\right) \tag{2.23}$$

iv) Negative decaying mode: $$k_z^{(-)} = \left\{-Mk_o + i\sqrt{\left(1-M^2\right)k_{mn}^2 - k_o^2}\right\} / \left(1-M^2\right) \tag{2.24}$$

Finally, the pressure field in the duct can be expressed as a sum of circumferential and radial modes traveling in both directions as

$$p(r,\theta,z) = \sum_{m=0}^{N_\theta}\sum_{n=0}^{N_r} A_{mn}^{(+)}\Phi_{mn}(r,\theta)e^{-ik_z^{(+)}z} + \sum_{m=0}^{N_\theta}\sum_{n=0}^{N_r} A_{mn}^{(-)}\Phi_{mn}(r,\theta)e^{-ik_z^{(-)}z} \tag{2.25}$$

where $A_{mn}^{(+)}$ and $A_{mn}^{(-)}$ are the amplitude of the positive and negative waves, respectively, and N_θ and N_r are the number of circumferential and radial modes used in the expansion, respectively.

2.1.2 Finite source radiation

Once the expression for the pressure field in the rigid wall duct is found, one must find the Green's function, i.e. the pressure field generated by a point source on the duct wall. The Green's function will then be used to find the pressure field radiated by a piston source on the duct wall. This will allow to model the effect of the tubes on the duct, since each interface between the duct and the HQ tubes is modeled as a finite piston source. Finally, the average pressure over a source due to another piston source with unit velocity, i.e. impedance function, will be developed.

To find an expression for the Green's function, the following differential equation needs to be solved (see equation (2.2))

$$\frac{\partial^2 g}{\partial r^2}+\frac{1}{r}\frac{\partial g}{\partial r}+\frac{1}{r^2}\frac{\partial^2 g}{\partial \theta^2}+\frac{\partial^2 g}{\partial z^2}\left(1-M^2\right)-2Mik_o\frac{\partial g}{\partial z}+k_o^2 g=\delta\left(r-r_o\right)\delta\left(\theta-\theta_o\right)\delta\left(z-z_o\right) \quad (2.26)$$

where $g(r,\theta,z\,|\,r_o,\theta_o,z_o)$ is the Green's function for a point source located at $\left(r_o,\theta_o,z_o\right)$. The solution to this equation is expanded in terms of the rigid-walled duct mode shapes found in the previous section as

$$g(r,\theta,z\,|\,r_o,\theta_o,z_o)=\sum_{m=0}^{Mg}\sum_{n=0}^{Ng}F_{mn}(z)\Phi_{mn}(r,\theta) \quad (2.27)$$

where M_g and N_g indicate the number of circumferential and radial modes included in the Green's function, respectively. To satisfy the symmetry of the sound field with respect to the plane defined by the point $\left(r_o,\theta_o\right)$ and the z-axis, the duct modes are selected as

$$\Phi_{mn}\left(r,\theta\right)=\cos\left[m\left(\theta-\theta_o\right)\right]J_m\left(k_{mn}r\right) \quad (2.28)$$

Replacing equation (2.27) into (2.26) gives

$$\sum_{m=0}^{M_g}\sum_{n=0}^{N_g}\left\{\frac{d^2F_{mn}}{dz^2}(1-M^2)-2iMk_o\frac{dF_{mn}}{dz}-k_{mn}^2F_{mn}+k_o^2F_{mn}\right\}\Phi_{mn}(r,\theta) = \delta\left(r-r_o\right)\delta\left(\theta-\theta_o\right)\delta\left(z-z_o\right) \quad (2.29)$$

where (from equations (2.4) and (2.7))

$$-k_{mn}^2 \Phi_{mn} = \frac{\partial^2 \Phi_{mn}}{\partial r^2} + \frac{1}{r}\frac{\partial \Phi_{mn}}{\partial r} + \frac{1}{r^2}\frac{\partial^2 \Phi_{mn}}{\partial \theta^2} \tag{2.30}$$

By definition, the mode shapes are orthogonal and the orthogonality condition is written as

$$\int_0^{2\pi}\int_0^a \Phi_{rs}(r,\theta)\Phi_{mn}(r,\theta) r dr d\theta = \pi a^2 \Lambda_{mn} \delta_{rm} \delta_{sn} \tag{2.31}$$

where the orthogonality constant is given by

$$\Lambda_{mn} = \begin{cases} J_m^2\left(k_{mn}a\right) & \text{if } m = 0 \\ \frac{1}{2}\left[1 - \frac{m^2}{\left(k_{mn}a\right)^2}\right] J_m^2\left(k_{mn}a\right) & \text{if } m \neq 0 \end{cases} \tag{2.32}$$

Thus, premultiplying equation (2.29) by the mode shape $\Phi_{rs}(r,\theta)$ of mode (r,s), integrating over the duct cross-section, and considering the orthogonality condition gives

$$\frac{d^2 F_{mn}}{dz^2}(1-M^2) - 2iMk_o \frac{dF_{mn}}{dz} - \left(k_{mn}^2 - k_o^2\right) F_{mn} = \delta(z - z_o)\frac{\Phi_{mn}(r_o,\theta_o)}{\pi a^2 \Lambda_{mn}} \tag{2.33}$$

Equation (2.33) is an ordinary differential equation in z, which is solved assuming the solutions for positions upstream and downstream of the source as

$$F_{mn}(z) = \mathrm{A}_{mn} e^{-ik_z^{(+)}(z - z_o)} \qquad for\ z \geq z_o \tag{2.34}$$

$$F_{mn}(z) = \mathrm{A}_{mn} e^{-ik_z^{(-)}(z - z_o)} \qquad for\ z \leq z_o \tag{2.35}$$

Note that by selecting the same amplitude A_{mn} for both solutions, the sound field is uniquely defined at $z=z_0$.

To find the unknown amplitude A_{mn}, the following integral needs to be solved

$$\lim_{\varepsilon \to 0} \int_{z_o - \varepsilon}^{z_o + \varepsilon} \left[\frac{d^2 F_{mn}}{dz^2}(1-M^2) - 2iMk_o \frac{dF_{mn}}{dz} - \left(k_{mn}^2 - k_o^2\right) F_{mn} \right] dz = \frac{\Phi_{mn}(r_o,\theta_o)}{\pi a^2 \Lambda_{mn}} \tag{2.36}$$

thus

$$\lim_{\varepsilon \to 0} \left\{ (1-M^2) \left[\left.\frac{dF_{mn}}{dz}\right|_{z_o + \varepsilon} - \left.\frac{dF_{mn}}{dz}\right|_{z_o - \varepsilon} \right] \right\} = \frac{\Phi_{mn}(r_o,\theta_o)}{\pi a^2 \Lambda_{mn}} \tag{2.37}$$

Replacing equations (2.34) and (2.35) for the upper and lower limits respectively in (2.37) yields

$$\lim_{\varepsilon\to 0}\left(1-M^2\right)\left[\mathrm{A}_{mn}\left(-ik_z^{(+)}\right)e^{ik_z^{(+)}(+\varepsilon)}-\mathrm{A}_{mn}\left(-ik_z^{(-)}\right)e^{ik_z^{(-)}(-\varepsilon)}\right]=\frac{\Phi_{mn}(r_o,\theta_o)}{\pi a^2\Lambda_{mn}} \tag{2.38}$$

Taking the limit yields

$$-\mathrm{A}_{mn}i\left(1-M^2\right)\left(k_z^{(+)}-k_z^{(-)}\right)=\frac{\Phi_{mn}(r_o,\theta_o)}{\pi a^2\Lambda_{mn}} \tag{2.39}$$

Solving for A_{mn} and replacing back into (2.34) and (2.35) and then into (2.27) gives

$$g^{(+)}\left(r,\theta,z\,|\,r_o,\theta_o,z_o\right)=\frac{i}{\pi a^2}\sum_{m=0}^{M_g}\sum_{n=0}^{N_g}\frac{\Phi_{mn}(r,\theta)\Phi_{mn}(r_o,\theta_o)}{\Lambda_{mn}\left(1-M^2\right)\left(k_z^{(+)}-k_z^{(-)}\right)}e^{-ik_z^{(+)}(z-z_o)}\quad for\ z\geq z_o \tag{2.40}$$

$$g^{(-)}\left(r,\theta,z\,|\,r_o,\theta_o,z_o\right)=\frac{i}{\pi a^2}\sum_{m=0}^{M_g}\sum_{n=0}^{N_g}\frac{\Phi_{mn}(r,\theta)\Phi_{mn}(r_o,\theta_o)}{\Lambda_{mn}\left(1-M^2\right)\left(k_z^{(+)}-k_z^{(-)}\right)}e^{-ik_z^{(-)}(z-z_o)}\quad for\ z\leq z_o \tag{2.41}$$

which are the Green's functions for positive and negative *z*-propagation direction, respectively.

Once the Green's function for a point source on the duct wall is found, the sound field generated by a finite piston source as illustrated in Figure 2-3 can be derived. The finite piston source of normal velocity *v* radiating into the duct is the model of a Herschel-Quincke tube end at the interface with the duct.

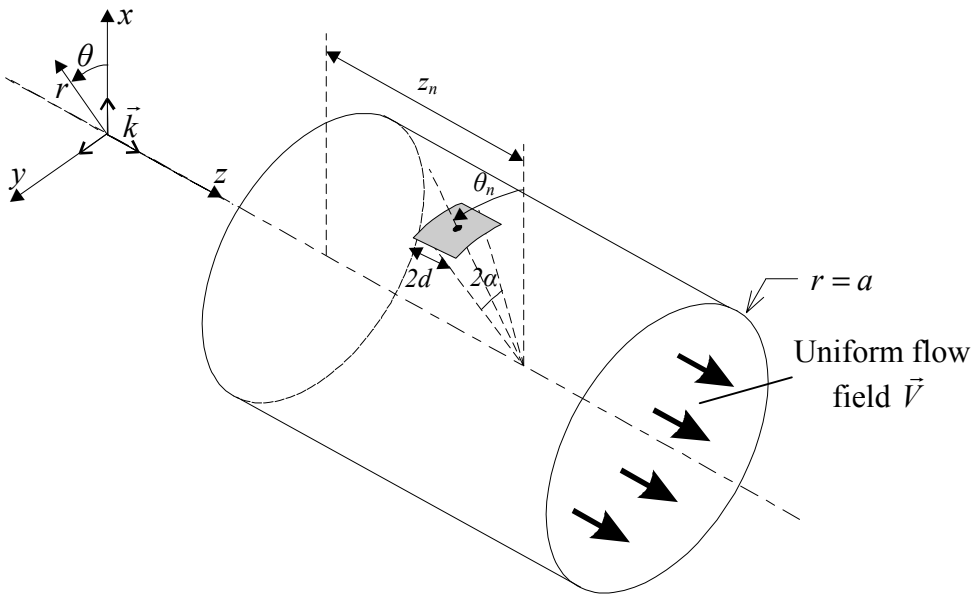

Figure 2-3: Piston Source radiating into the duct.

The pressure at *(r,θ,z)* due to the n^{th} piston source located at (a,θ_n,z_n) with source velocity v_n is obtained by integrating the Green's function over the surface of the source as

$$p(r,\theta,z|a,\theta_n,z_n) = -i\omega\rho v_n \int_{z_n-d}^{z_n+d}\int_{\theta_n-\alpha}^{\theta_n+\alpha} g(r,\theta,z\,|\,a,\tilde{\theta},\tilde{z})ad\tilde{\theta}d\tilde{z} \tag{2.42}$$

where (a,θ_n,z_n) is the location of the source center as defined in Figure 2-3. Replacing (2.40) or (2.41) into (2.42), it is clear that there are two integrals that need to be solved. The first one with respect to θ is easily obtained as

$$\int_{\theta_n-\alpha}^{\theta_n+\alpha} \cos m\left(\theta-\tilde{\theta}\right)ad\tilde{\theta} = \kappa_\theta(\alpha)\cos m\left(\theta-\theta_n\right) \tag{2.43}$$

where $\kappa_\theta(\alpha) = \dfrac{2a\alpha\sin(m\alpha)}{m\alpha}$

For the special case of m=0 equation (2.43) gives $2a\alpha$.

The solution of the second integral depends on the position of the observation point z relative to the piston source position z_n. Three cases are considered as illustrated in Figure 2-4.

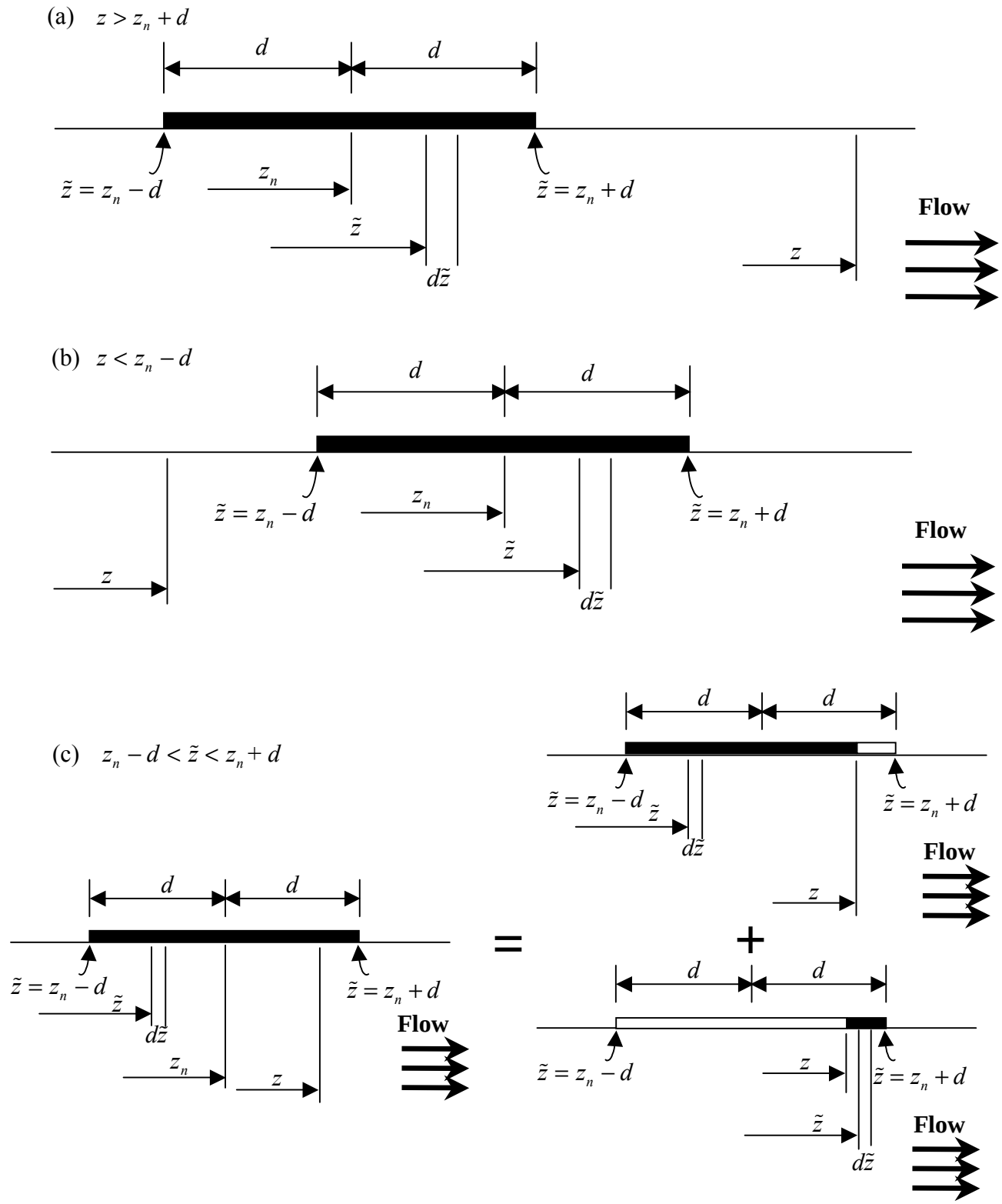

Figure 2-4: Elements of integration over the source surface (a) case 1: observation point is downstream of the source, (b) case 2: observation point is upstream of the source, (c) case 3: observation point is on the surface of the source.

CASE 1: The observation point is downstream of the source, i.e. $z > z_n + d$. This case is illustrated in Figure 2-4a and implies that $z > \tilde{z}$. Thus, the following integral is solved as

$$\int_{z_n-d}^{z_n+d} e^{-ik_z^{+}(z-\tilde{z})} d\tilde{z} = e^{-ik_z^{(+)}(z-z_n)} \frac{\sin(k_z^{(+)}d)}{k_z^{(+)}d} 2d \tag{2.44}$$

The pressure due to the source positioned at (a,θ_n,z_n) is then

$$\begin{aligned} p(r,\theta,z \mid a,\theta_n,z_n) = v_n \frac{k_0 \rho c}{\pi a^2} \sum_m^{M_g} \sum_n^{N_g} & \frac{\kappa_\theta(\alpha)\cos m(\theta-\theta_n) J_m(k_{mn}r) J_m(k_{mn}a)}{\Lambda_{mn}(1-M^2)(k_z^{(+)}-k_z^{(-)})} \\ & \times e^{-ik_z^{(+)}(z-z_n)} \frac{\sin(k_z^{(+)}d)}{k_z^{(+)}d} 2d \end{aligned} \tag{2.45}$$

CASE 2: The observation point is upstream of the source, i.e. $z < z_n - d$. This case is illustrated in Figure 2-4b and implies that $z < \tilde{z}$. Thus, the following integral is solved as

$$\int_{z_n-d}^{z_n+d} e^{-ik_z^{(-)}(z-\tilde{z})} d\tilde{z} = e^{-ik_z^{(-)}(z-z_n)} \frac{\sin(k_z^{(-)}d)}{k_z^{(-)}d} 2d \tag{2.46}$$

The pressure due to the source is then written as

$$\begin{aligned} p(r,\theta,z \mid a,\theta_n,z_n) = v_n \frac{k_0 \rho c}{\pi a^2} \sum_m^{M_g} \sum_n^{N_g} & \frac{\kappa_\theta(\alpha)\cos m(\theta-\theta_n) J_m(k_{mn}r) J_m(k_{mn}a)}{\Lambda_{mn}(1-M^2)(k_z^{(+)}-k_z^{(-)})} \\ & \times e^{-ik_z^{(-)}(z-z_n)} \frac{\sin(k_z^{(-)}d)}{k_z^{(-)}d} 2d \end{aligned} \tag{2.47}$$

CASE 3: The observation point is on the surface of the source, i.e. $z_n - d < z < z_n + d$. This case is illustrated in Figure 2-4c and requires to solve the integral with the two terms

$$\int_{z_n-d}^{z} e^{-ik_z^{(+)}(z-\tilde{z})} d\tilde{z} + \int_{z}^{z_n+d} e^{-ik_z^{(-)}(z-\tilde{z})} d\tilde{z} = \frac{1-e^{-ik_z^{(+)}(z-z_n+d)}}{ik_z^{(+)}} - \frac{1-e^{-ik_z^{(-)}(z-z_n-d)}}{ik_z^{(-)}} \tag{2.48}$$

The pressure due to the source is then written as

$$\begin{aligned} p(r,\theta,z \mid a,\theta_n,z_n) = v_n \frac{k_0 \rho c}{\pi a^2} \sum_m^{M_g} \sum_n^{N_g} & \frac{\kappa_\theta(\alpha)\cos m(\theta-\theta_n) J_m(k_{mn}r) J_m(k_{mn}a)}{\Lambda_{mn}(1-M^2)(k_z^{(+)}-k_z^{(-)})} \\ & \times \left[\frac{1-e^{-ik_z^{(+)}(z-z_n+d)}}{ik_z^{(+)}} - \frac{1-e^{-ik_z^{(-)}(z-z_n-d)}}{ik_z^{(-)}} \right] \end{aligned} \tag{2.49}$$

In the development of the model, it is also required to compute the average pressure over a source due to another piston source with unit velocity, i.e. impedance function. The average pressure over a piston source "*r*" located at (a,θ_r,z_r) due to another source "*s*" located at (a,θ_s,z_s) with unit velocity is simply given as

$$Z_{rs} = \frac{1}{S_r} \int_{z_r-d_r}^{z_r+d_r} \int_{\theta_r-\alpha_r}^{\theta_r+\alpha_r} p(a,\theta,z \mid a,\theta_s,z_s) a d\theta dz \tag{2.50}$$

where S_r is the area of the piston source "*r*". Once again, two integrals need to be solved separately. The first integral with respect to θ is

$$\int_{\theta_r-\alpha_r}^{\theta_r+\alpha_r} \cos m\left(\theta-\theta_s\right) a d\theta = \kappa_\theta(\alpha_r) \cos m\left(\theta_r-\theta_s\right) \tag{2.51}$$

The second integral is with respect to the *z*-coordinate which depends on the location of the observation source "*r*" relative to the "*s*" source. Three cases are again possible as illustrated in Figure 2-5.

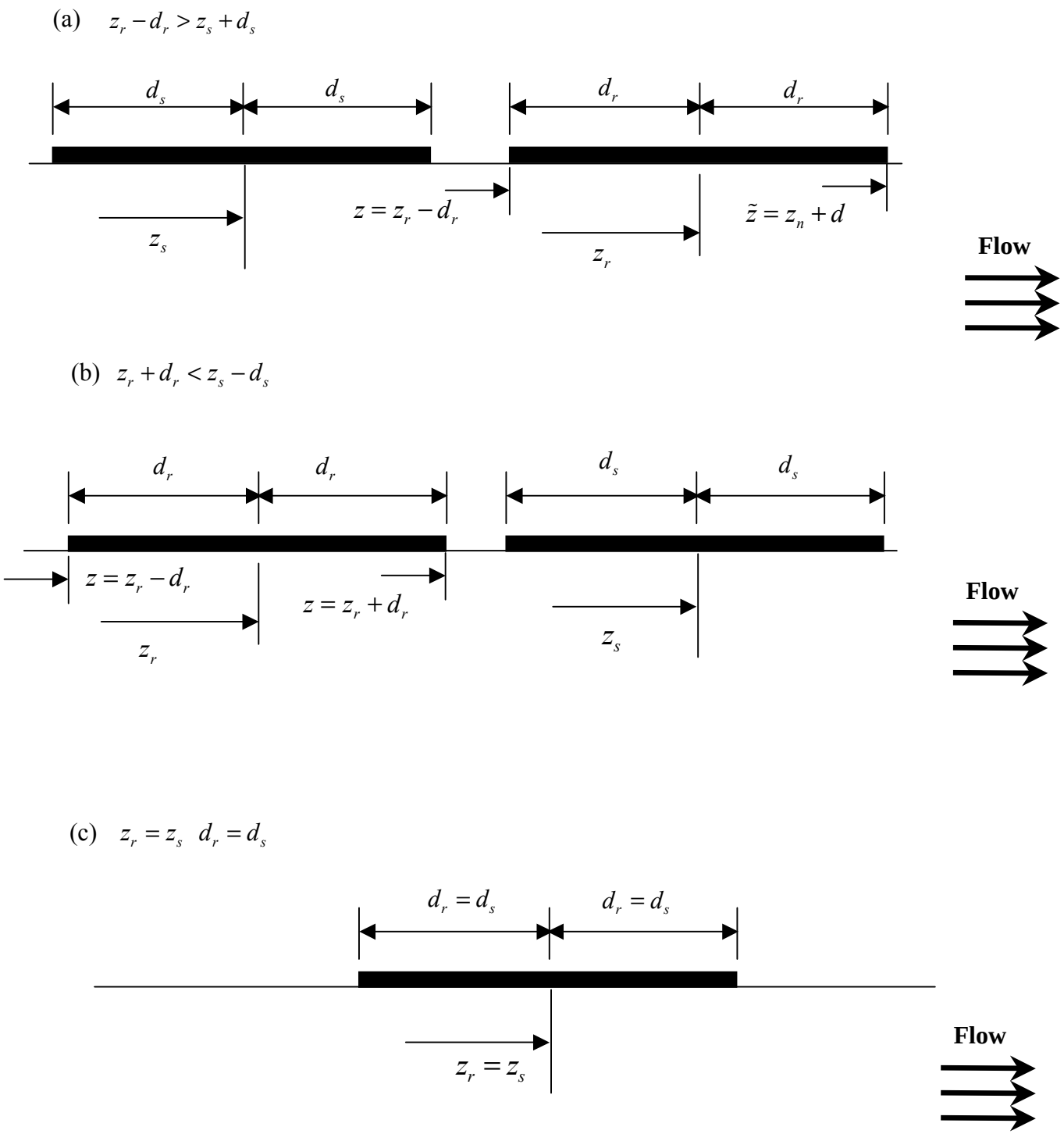

Figure 2-5: (a) observation source *"r"* is downstream of the source *"s"*, (b) observation source *"r"* is upstream of the source *"s"*, (c) observation source *"r"* and source *"s"* are at the same axial location.

CASE 1: The observation source "*r*" is downstream of source "*s*", i.e. $z_r - d_r > z_s + d_s$. In this case, equation (2.45) is replaced into (2.50) and the following integral is solved

$$\int_{z_r-d_r}^{z_r+d_r} e^{-ik_z^{(+)}(z-z_s)} \frac{\sin(k_z^{(+)}d_s)}{k_z^{(+)}d_s} 2d_s dz = e^{-ik_z^{(+)}(z_r-z_s)} \frac{\sin(k_z^{(+)}d_r)}{k_z^{(+)}d_r} 2d_r \frac{\sin(k_z^{(+)}d_s)}{k_z^{(+)}d_s} 2d_s \quad (2.52)$$

The impedance function in this case is

$$\begin{aligned} Z_{rs} = \frac{k_0\rho c}{S_r\pi a^2} \sum_m^{M_g} \sum_n^{N_g} & \frac{\kappa_\theta(\alpha_r)\kappa_\theta(\alpha_s)\cos m(\theta_r-\theta_s) J_m(k_{mn}a) J_m(k_{mn}a)}{\Lambda_{mn}(1-M^2)(k_z^{(+)}-k_z^{(-)})} \\ & \times e^{-ik_z^{(+)}(z_r-z_s)} \frac{\sin(k_z^{(+)}d_r)}{k_z^{(+)}d_r} 2d_r \frac{\sin(k_z^{(+)}d_s)}{k_z^{(+)}d_s} 2d_s \end{aligned} \quad (2.53)$$

CASE 2: The observation source "*r*" is upstream of source "*s*", i.e. $z_r + d_r < z_s - d_s$. In this case, equation (2.47) is replaced into (2.50) and the following integral is solved

$$\int_{z_r-d_r}^{z_r+d_r} e^{-ik_z^{(-)}(z-z_s)} \frac{\sin(k_z^{(-)}d_s)}{k_z^{(-)}d_s} 2d_s dz = e^{-ik_z^{(-)}(z_r-z_s)} \frac{\sin(k_z^{(-)}d_r)}{k_z^{(-)}d_r} 2d_r \frac{\sin(k_z^{(-)}d_s)}{k_z^{(-)}d_s} 2d_s \quad (2.54)$$

The impedance function in this case is

$$\begin{aligned} Z_{rs} = \frac{k_0\rho c}{S_r\pi a^2} \sum_m^{M_g} \sum_n^{N_g} & \frac{\kappa_\theta(\alpha_r)\kappa_\theta(\alpha_s)\cos m(\theta_r-\theta_s) J_m(k_{mn}a) J_m(k_{mn}a)}{\Lambda_{mn}(1-M^2)(k_z^{(+)}-k_z^{(-)})} \\ & \times e^{-ik_z^{(-)}(z_r-z_s)} \frac{\sin(k_z^{(-)}d_r)}{k_z^{(-)}d_r} 2d_r \frac{\sin(k_z^{(-)}d_s)}{k_z^{(-)}d_s} 2d_s \end{aligned} \quad (2.55)$$

CASE 3: The observation source "*r*" is at the same axial location as source "*s*". In addition, we assume they have the same dimensions, i.e. d_r=d_s. In this case, equation (2.49) is replaced into (2.50) and the following integral is solved

$$\int_{z_r-d_r}^{z_r+d_r} \left[\frac{1-e^{-ik_z^{(+)}(z-z_s+d_s)}}{ik_z^{(+)}} - \frac{1-e^{-ik_z^{(-)}(z-z_s-d_s)}}{ik_z^{(-)}} \right] dz = \frac{2d_r}{ik_z^{(+)}} - \frac{2d_r}{ik_z^{(-)}} + \frac{1-e^{-ik_z^{(+)}2d_r}}{\left(k_z^{(+)}\right)^2} + \frac{1-e^{ik_z^{(-)}2d_r}}{\left(k_z^{(-)}\right)^2} \quad (2.56)$$

Thus, the impedance function is

$$\begin{aligned} Z_{rs} = \frac{k_0\rho c}{S_r\pi a^2} \sum_m^{M_g} \sum_n^{N_g} & \frac{\kappa_\theta(\alpha_r)\kappa_\theta(\alpha_s)\cos m(\theta_r-\theta_s) J_m(k_{mn}a) J_m(k_{mn}a)}{\Lambda_{mn}(1-M^2)(k_z^{(+)}-k_z^{(-)})} \\ & \times \left[\frac{2d_r}{ik_z^{(+)}} - \frac{2d_r}{ik_z^{(-)}} + \frac{1-e^{-ik_z^{(+)}2d_r}}{\left(k_z^{(+)}\right)^2} + \frac{1-e^{ik_z^{(-)}2d_r}}{\left(k_z^{(-)}\right)^2} \right] \end{aligned} \quad (2.57)$$

2.1.3 Duct dynamics

The previous section allowed to find the expressions for the sound field in a rigid walled duct and the impedance of the piston sources on the duct wall. The model of the duct with HQ tubes will now be developed. The problem consists of a hard wall circular duct of radius a with one or several arrays of HQ tubes located around the wall of the duct as shown in Figure 2-6. A flow of Mach number M is assumed to travel in the duct in the positive z-direction and the disturbance noise field is also assumed to propagate within the duct in the positive z-direction.

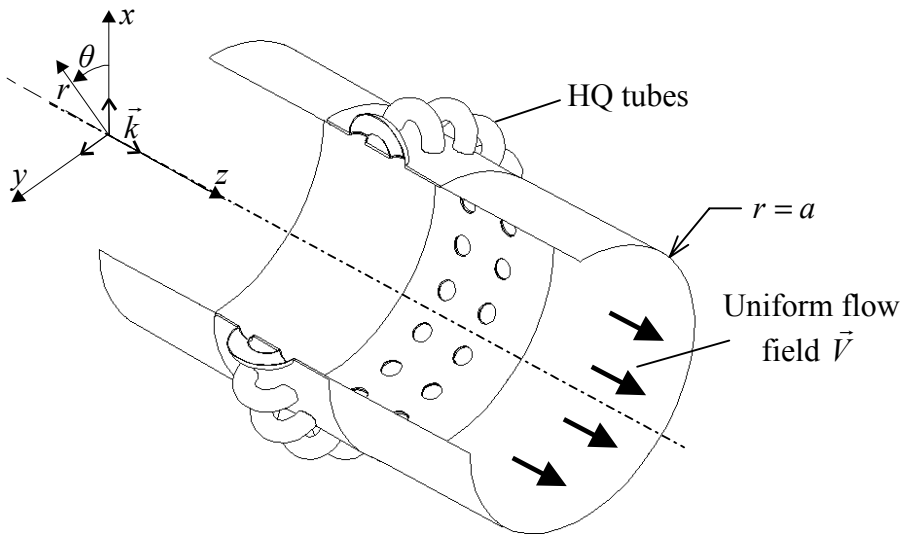

Figure 2-6: Circular duct model with HQ tubes.

The modeling of the HQ tube-duct system is carried out by first separating the HQ tubes from the duct at the interfaces. The models of the sound fields in the HQ tubes and in the main duct are developed independently. Then, these models are fully coupled by matching the acoustic pressure and particle velocity at the tube-duct interfaces. The effect of the tubes on the duct is modeled by considering the tube-duct interfaces as finite piston sources radiating into the duct as shown in Figure 2-7. Each piston source is assumed to have an unknown velocity v, which represents the particle velocity at the ends of the tubes. This section will concentrate on the model of the duct. The model of the tubes and the coupling between both systems are developed in the next sections.

The pressure due to the disturbance p_d, at any point in the duct can be expressed as the sum of a set of positive spinning modes traveling in the positive z-direction as

$$p_d(r,\theta,z) = \sum_{m=0}^{M_d} \sum_{n=0}^{N_d} A_{mn}^d J_m\left(k_{mn} r\right) e^{-im\theta} e^{-ik_z^{(+)} z} \tag{2.58}$$

where A_{mn}^d is the complex amplitude of the disturbance mode (m,n), $k_z^{(+)}$ is the axial wavenumber of a positive z-direction traveling or decaying wave, and M_d and N_d are the number of m and n modes included in the disturbance. The indexes m and n refer to circumferential and radial modes, respectively. The propagation characteristics of the modes are given by the axial wavenumber $k_z^{(+)}$ (see equations (2.21) and (2.22)).

The acoustic field inside the duct is obtained from the superposition of the sound pressure due to the disturbance and due to the N_s finite piston "sources" at the HQ tube ends. The number of piston sources is twice the number of tubes. The two piston sources corresponding to the ℓ^{th} tube will be identified by the subscripts "i" (input) and "o" (output) as shown in Figure 2-7.

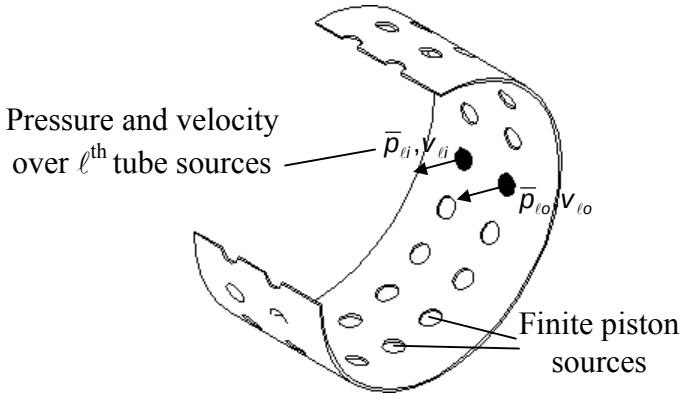

Figure 2-7: Duct with finite piston sources modeling the effect of HQ tubes on duct.

The average pressure over each source can be expressed in the following matrix form

$$\begin{Bmatrix} \overline{p}_{1i} \\ \overline{p}_{1o} \\ \vdots \\ \overline{p}_{\ell i} \\ \overline{p}_{\ell o} \\ \vdots \\ \overline{p}_{Ni} \\ \overline{p}_{No} \end{Bmatrix} = \begin{bmatrix} Z_{1i1i} & Z_{1i1o} & Z_{1i2i} & Z_{1i2o} & \cdots & Z_{1iNi} & Z_{1iNo} \\ Z_{1o1i} & Z_{1o1o} & Z_{1o2i} & Z_{1o2o} & \cdots & Z_{1oNi} & Z_{1oNo} \\ \vdots & \vdots & \ddots & & & \vdots & \vdots \\ & & & Z_{\ell i\ell i} & Z_{\ell i\ell o} & & \\ & & & Z_{\ell o\ell i} & Z_{\ell o\ell o} & & \\ \vdots & \vdots & & & \ddots & \vdots & \vdots \\ Z_{Ni1i} & Z_{Ni1o} & \cdots & & & Z_{NiNi} & Z_{NiNo} \\ Z_{No1i} & Z_{No1o} & \cdots & & & Z_{NoNi} & Z_{NoNo} \end{bmatrix} \begin{Bmatrix} v_{1i} \\ v_{1o} \\ \vdots \\ v_{\ell i} \\ v_{\ell o} \\ \vdots \\ v_{Ni} \\ v_{No} \end{Bmatrix} + \begin{Bmatrix} \overline{p}^{d}_{1i} \\ \overline{p}^{d}_{1o} \\ \vdots \\ \overline{p}^{d}_{\ell i} \\ \overline{p}^{d}_{\ell o} \\ \vdots \\ \overline{p}^{d}_{Ni} \\ \overline{p}^{d}_{No} \end{Bmatrix} \tag{2.59}$$

where $v_{\ell i}$ and $v_{\ell o}$ are the input and output velocities of the ℓ^{th} tube sources, respectively, $\overline{p}^{d}_{\ell i}$ and $\overline{p}^{d}_{\ell o}$ are the average pressure over the sources of the ℓ^{th} tube due to the disturbance, and N is the number of HQ tubes.

A general element Z_{rs} of the matrix in equation (2.59) represents the average pressure over the "r" piston source due to a unit velocity of the "s" piston source, i.e. impedance function. These impedance functions were derived previously and are given by equation (2.53), (2.55) or (2.57), depending on the relative positions of the sources.

The average pressure over the piston source located at (a,θ_n,z_n) due to the disturbance is given by

$$\overline{p}_d(a,\theta_{n,},z_n) = \frac{1}{S_n}\int_{z_n-d}^{z_n+d}\int_{\theta_n-\alpha}^{\theta_n+\alpha} p_d(a,\theta,z)\,ad\theta\,dz \tag{2.60}$$

Replacing equation (2.58) into (2.60) and solving the integral gives

$$\overline{p}_d\left(a,\theta_n,z_n\right) = \sum_{m=0}^{M_d}\sum_{n=0}^{N_d} A^d_{mn} J_m\left(k_{mn}a\right) e^{-ik_z^{(+)}z_n} \frac{\sin m\alpha}{m\alpha} e^{-im\theta_n} \frac{\sin\left(k_z^{(+)}d\right)}{k_z^{(+)}d} \tag{2.61}$$

2.1.4 HQ tubes dynamics

The dynamic model of the HQ tubes is developed in this section. The goal is to find an expression for the sound field inside each tube. The tube ends are considered to be piston sources with velocity v^t and pressure p^t, as shown in Figure 2-8. The model of the sound field in a single tube will first be developed and the sound fields for all tubes will then be assembled and written in matrix form.

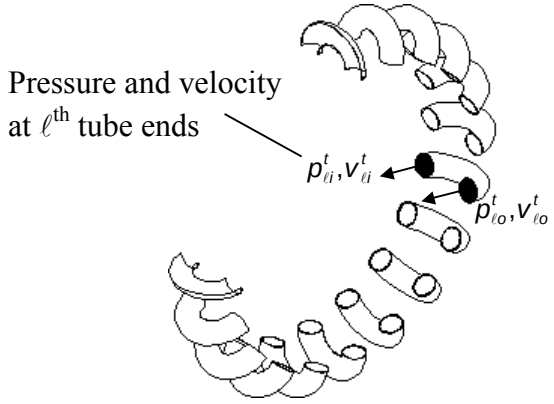

Figure 2-8: Model of the HQ tubes.

In practice, the HQ tubes are constructed as a semi-circle or other smooth shapes. However, for modeling purposes they are considered as straight tubes with uniform cross-section as shown in Figure 2-9. This assumption does not change the dynamic model of the tube since there are only plane waves propagating in the tube.

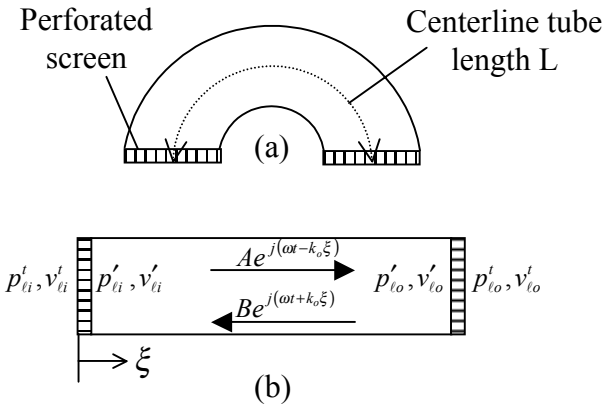

Figure 2-9: (a) HQ tube representation. (b) Simplified model.

The sound field inside a tube is assumed to consist of plane waves only, a valid assumption well below the first cut-off frequency of the tube. It is also assumed that there is no flow in the tube. The sound field inside a tube is expressed in terms of a positive and a negative traveling plane wave of amplitude A and B, respectively. If ξ is the local tube coordinate, the pressure and particle velocity inside the tube are given as

$$p'(\xi,t) = Ae^{-ik_o\xi} + Be^{+ik_o\xi} \tag{2.62}$$

$$v'(\xi,t) = \frac{Ae^{-ik_o\xi} - Be^{+ik_o\xi}}{\rho c} \tag{2.63}$$

The acoustic pressure and particle velocity at the ends of the ℓ^{th} tube are expressed in the following matrix form

$$\begin{Bmatrix} p'_{\ell i} \\ \rho c v'_{\ell i} \end{Bmatrix} = \left[T_t\right] \begin{Bmatrix} p'_{\ell o} \\ \rho c v'_{\ell o} \end{Bmatrix} = \begin{bmatrix} \cos(k_o L) & i\sin(k_o L) \\ i\sin(k_o L) & \cos(k_o L) \end{bmatrix} \begin{Bmatrix} p'_{\ell o} \\ \rho c v'_{\ell o} \end{Bmatrix} \tag{2.64}$$

where L is the centerline length of the tubes and subscripts "i" and "o" refer to tube input and output, respectively. In practice, the tube is connected to the main duct through a perforated screen. This screen minimizes the potential for flow distortion (vortex shedding) due to the tube opening, which could create additional noise. The effect of these perforated screens is included as

$$\begin{Bmatrix} p^t_{\ell i} \\ \rho c v^t_{\ell i} \end{Bmatrix} = \left[T_{ps}\right] \begin{Bmatrix} p'_{\ell i} \\ \rho c v'_{\ell i} \end{Bmatrix} \text{ and } \begin{Bmatrix} p'_{\ell o} \\ \rho c v'_{\ell o} \end{Bmatrix} = \left[T_{ps}\right] \begin{Bmatrix} p^t_{\ell o} \\ \rho c v^t_{\ell o} \end{Bmatrix} \tag{2.65}$$

where the transfer matrix of the perforated screen T_{ps} is

$$\left[T_{ps}\right] = \begin{bmatrix} 1 & \dfrac{Z_{ps}}{\rho c} \\ 0 & 1 \end{bmatrix} \tag{2.66}$$

Z_{ps} is the impedance of the perforated screen written as [16]

$$Z_{ps} = i\frac{\omega\rho}{\sigma}\left(t_{ps} + 2a_{orif}\frac{8}{3\pi}\right) + \begin{cases} \dfrac{\sqrt{8\mu\rho\omega}}{\sigma}\left(1 + \dfrac{t_{ps}}{2a_{orif}}\right) & \text{linear model} \\ \dfrac{\rho v_{orif}}{\sigma} & \text{non-linear model} \end{cases} \tag{2.67}$$

where t_{ps} is the thickness of the screen, a_{orif} is the orifice radius, σ is the screen open area ratio, v_{orif} is the orifice fluid velocity (acoustic particle velocity divided by σ), ρ is the

fluid density and μ is the viscosity coefficient. The linear model for the resistive part of the screen impedance is chosen for small orifice velocity, however if this velocity becomes higher than the critical value, a non-linear model has to be chosen. The critical value for the orifice velocity is given by the equation:

$$v_{orif} = \sqrt{\frac{f}{200}}\left(1+\frac{t_{ps}}{2a_{orif}}\right) \tag{2.68}$$

where f is the frequency. In the present study, only the linear model will be used for the impedance of the perforated screen since the orifice velocity is small. Including the effects of the perforated screens, the matrix that relates the pressure and particle velocity at the tube ends is thus

$$\begin{Bmatrix} p^t_{\ell i} \\ \rho c v^t_{\ell i} \end{Bmatrix} = \begin{bmatrix} T_{ps} \end{bmatrix}\ \begin{bmatrix} T_t \end{bmatrix}\ \begin{bmatrix} T_{ps} \end{bmatrix}\ \begin{Bmatrix} p^t_{\ell o} \\ \rho c v^t_{\ell o} \end{Bmatrix} = \begin{bmatrix} T_{11} & T_{12} \\ T_{21} & T_{22} \end{bmatrix} \begin{Bmatrix} p^t_{\ell o} \\ \rho c v^t_{\ell o} \end{Bmatrix} \tag{2.69}$$

Rearranging equation (2.69), the impedance matrix for the ℓ^{th} tube can be expressed as

$$\begin{Bmatrix} p^t_{\ell i} \\ p^t_{\ell o} \end{Bmatrix} = \rho c \begin{bmatrix} \dfrac{T_{11}}{T_{21}} & \dfrac{T_{12}T_{21}-T_{11}T_{22}}{T_{21}} \\ \dfrac{1}{T_{21}} & -\dfrac{T_{22}}{T_{21}} \end{bmatrix} \begin{Bmatrix} v^t_{\ell i} \\ v^t_{\ell o} \end{Bmatrix} = \begin{bmatrix} Z^{t\ell}_{ii} & Z^{t\ell}_{io} \\ Z^{t\ell}_{oi} & Z^{t\ell}_{oo} \end{bmatrix} \begin{Bmatrix} v^t_{\ell i} \\ v^t_{\ell o} \end{Bmatrix} \tag{2.70}$$

where the impedance matrix in (2.70) relates the pressure to the particle velocity at the two ends of the ℓ^{th} tube including the effect of the perforated screen.

It is important to note that in the process of matching the source velocity to the corresponding tube particle velocity, a consistent convention for the positive direction must be kept. To this end, the positive particle velocity in the entrance end of the tube at $\xi = 0$, which is opposite to the positive source velocity, is reversed by changing the sign of the first column of the matrix in (2.70). This will then yield

$$\begin{Bmatrix} p^t_{\ell i} \\ p^t_{\ell o} \end{Bmatrix} = \rho c \begin{bmatrix} -\dfrac{T_{11}}{T_{21}} & \dfrac{T_{12}T_{21}-T_{11}T_{22}}{T_{21}} \\ -\dfrac{1}{T_{21}} & -\dfrac{T_{22}}{T_{21}} \end{bmatrix} \begin{Bmatrix} v^t_{\ell i} \\ v^t_{\ell o} \end{Bmatrix} = \begin{bmatrix} Z^{t\ell}_{ii} & Z^{t\ell}_{io} \\ Z^{t\ell}_{oi} & Z^{t\ell}_{oo} \end{bmatrix} \begin{Bmatrix} v^t_{\ell i} \\ v^t_{\ell o} \end{Bmatrix} \tag{2.71}$$

Equation (2.71) gives the impedance matrix for the ℓ^{th} tube alone. Once the tubes are put together in a circumferential array around the duct, the average pressure over each source is written in matrix form as

$$\begin{Bmatrix} \overline{p}^t_{1i} \\ \overline{p}^t_{1o} \\ \vdots \\ \overline{p}^t_{\ell i} \\ \overline{p}^t_{\ell o} \\ \vdots \\ \overline{p}^t_{Ni} \\ \overline{p}^t_{No} \end{Bmatrix} = \begin{bmatrix} Z^{t1}_{ii} & Z^{t1}_{io} & 0 & 0 & \cdots & 0 & 0 \\ Z^{t1}_{oi} & Z^{t1}_{oo} & 0 & 0 & \cdots & 0 & 0 \\ 0 & 0 & & & & & \\ 0 & 0 & & & & & \\ \vdots & \vdots & & Z^{t\ell}_{ii} \; Z^{t\ell}_{io} & & \vdots & \\ & & & Z^{t\ell}_{oi} \; Z^{t\ell}_{oo} & & & \\ 0 & 0 & & & & Z^{tN}_{ii} & Z^{tN}_{io} \\ 0 & 0 & \cdots & & & Z^{tN}_{oi} & Z^{tN}_{oo} \end{bmatrix} \begin{Bmatrix} v^t_{1i} \\ v^t_{1o} \\ \vdots \\ v^t_{\ell i} \\ v^t_{\ell o} \\ \vdots \\ v^t_{Ni} \\ v^t_{No} \end{Bmatrix} \tag{2.72}$$

The main impedance matrix consists of the impedance matrices of each HQ tube on its diagonal and of zeros everywhere else since there is no connection between the tubes.

2.1.5 Coupled tube-duct system

The sound fields inside the duct (see Figure 2-7) and inside the HQ tubes (see Figure 2-8) were developed individually in the previous sections. Now, both systems will be assembled to find an expression for the particle velocity at the ends of each tube. The model for the coupled tube-duct system is obtained by matching: (i) the average pressure on the surface of the source to the pressure in the tube, i.e. $\overline{p}_{\ell i} = p^t_{\ell i}$ and $\overline{p}_{\ell o} = p^t_{\ell o}$, and (ii) the source velocity to the particle velocity in the tube, $v_{\ell i} = v^t_{\ell i}$ and $v_{\ell o} = v^t_{\ell o}$. Thus, replacing equation (2.72) into the left-hand side of equation (2.59) the unknown source velocities are written in terms of the impedance functions and of the pressure due to the disturbance as

$$\begin{Bmatrix} v_{1i} \\ v_{1o} \\ \vdots \\ v_{\ell i} \\ v_{\ell o} \\ \vdots \\ v_{Ni} \\ v_{No} \end{Bmatrix} = \left(\begin{bmatrix} Z_{ii}^{t1} & Z_{io}^{t1} & 0 & 0 & \cdots & 0 & 0 \\ Z_{oi}^{t1} & Z_{oo}^{t1} & 0 & 0 & & 0 & 0 \\ 0 & 0 & & & & & \\ 0 & 0 & & & Z_{ii}^{t\ell} \; Z_{io}^{t\ell} & & \\ \vdots & & & & Z_{oi}^{t\ell} \; Z_{oo}^{t\ell} & & \vdots \\ & & & & & & \\ 0 & 0 & \cdots & & & Z_{ii}^{tN} & Z_{io}^{tN} \\ 0 & 0 & & & & Z_{oi}^{tN} & Z_{oo}^{tN} \end{bmatrix} - \begin{bmatrix} Z_{1i1i} & Z_{1i1o} & Z_{1i2i} & Z_{1i2o} & \cdots & Z_{1iNi} & Z_{1iNo} \\ Z_{1o1i} & Z_{1o1o} & Z_{1o2i} & Z_{1o2o} & & Z_{1oNi} & Z_{1oNo} \\ & & & & & & \\ & & & & Z_{\ell i\ell i} \; Z_{\ell i\ell o} & & \\ \vdots & & & & Z_{\ell o\ell i} \; Z_{\ell o\ell o} & & \vdots \\ & & & & & & \\ Z_{Ni1i} & Z_{Ni1o} & \cdots & & & Z_{NiNi} & Z_{NiNo} \\ Z_{No1i} & Z_{No1o} & & & & Z_{NoNi} & Z_{NoNo} \end{bmatrix}^{-1} \begin{Bmatrix} \overline{p}_{1i}^{d} \\ \overline{p}_{1o}^{d} \\ \vdots \\ \overline{p}_{\ell i}^{d} \\ \overline{p}_{\ell o}^{d} \\ \vdots \\ \overline{p}_{Ni}^{d} \\ \overline{p}_{No}^{d} \end{Bmatrix} \right) \tag{2.73}$$

Once the velocity of each source is found, the pressure at any point in the duct can easily be calculated using the Green's function. An expression for the sound power radiated at the end of the duct will then found as shown in the following section.

2.1.6 Modal amplitudes and sound power radiation

The pressure field in the duct downstream of the HQ tubes, i.e. transmitted field, is computed by adding the pressure due to each piston source and due to the incident disturbance. That is

$$p_{trans}(r,\theta,z) = p_d(r,\theta,z) + \sum_{r=1}^{N_s} p\ (r,\theta,z|r_r,\theta_r,z_r) \tag{2.74}$$

where the pressure due to the disturbance $p_d(r,\theta,z)$ is given in (2.58) and the pressure due to a unit velocity of the r^{th} source is obtained from equation (2.45) as

$$p\ (r,\theta,z|r_r,\theta_r,z_r) = \sum_{m=0}^{M_g}\sum_{n=0}^{N_g}(A_{mn}^{(+)})_r \cos m(\theta-\theta_r) J_m(k_{mn}r)\ e^{-ik_z^{(+)}z} \tag{2.75}$$

The sound field created by the r^{th} piston source is non-spinning and symmetric with respect to $\theta=\theta_r$. However, it can be written as a set of positive and negative spinning modes by using the following trigonometric relationship

$$\cos m(\theta-\theta_r) = e^{-im\theta}\left(\frac{e^{im\theta_r}}{2}\right)+e^{im\theta}\left(\frac{e^{-im\theta_r}}{2}\right) \tag{2.76}$$

Thus, equation (2.75) is written as

$$\begin{aligned} p\ (r,\theta,z|r_r,\theta_r,z_r) = &\sum_{m=0}^{M_g}\sum_{n=0}^{N_g}(A_{mn}^{(+)})_r^{pos} J_m(k_{mn}r)\ e^{-im\theta}e^{-ik_z^{(+)}z} \\ &+\sum_{m=0}^{M_g}\sum_{n=0}^{N_g}(A_{mn}^{(+)})_r^{neg} J_m(k_{mn}r)\ e^{+im\theta}e^{-ik_z^{(+)}z} \end{aligned} \tag{2.77}$$

where $\left(A_{mn}^{(+)}\right)_r^{pos}$ and $\left(A_{mn}^{(+)}\right)_r^{neg}$ are the complex amplitude of transmitted modes spinning in the positive and negative direction, respectively, due to source "*r*". These amplitudes are given as

$$(A_{mn}^{(+)})_r^{pos} = \frac{v_r k_o \rho c}{\pi a^2}\frac{J_m(k_{mn}a)}{\Lambda_{mn}(1-M^2)(k_z^{(+)}-k_z^{(-)})}\frac{2a\alpha_r\sin(m\alpha_r)}{m\alpha_r}\frac{2d_r\sin(k_z^{(+)}d_r)}{k_z^{(+)}d_r}e^{ik_z^{(+)}z_r}\frac{e^{+im\theta_r}}{2} \tag{2.78}$$

$$(A_{mn}^{(+)})_r^{neg} = \frac{v_r k_o \rho c}{\pi a^2}\frac{J_m(k_{mn}a)}{\Lambda_{mn}(1-M^2)(k_z^{(+)}-k_z^{(-)})}\frac{2a\alpha_r\sin(m\alpha_r)}{m\alpha_r}\frac{2d_r\sin(k_z^{(+)}d_r)}{k_z^{(+)}d_r}e^{ik_z^{(+)}z_r}\frac{e^{-im\theta_r}}{2} \tag{2.79}$$

The mode of circumferential order $m=0$ is not spinning; therefore, there is no use of defining positive and negative spinning amplitudes for this mode. However, in order to stay consistent with the previous notations and avoid presenting too many equations, it can simply be assumed that, for mode m=0, $(A_{0n}^{(+)})_r^{neg}$ is equal to zero and $(A_{0n}^{(+)})_r^{pos}$ is given by the equation

$$(A_{0n}^{(+)})_r^{pos} = \frac{v_r k_o \rho c}{\pi a^2}\frac{J_0(k_{0n}a)}{\Lambda_{0n}(1-M^2)(k_z^{(+)}-k_z^{(-)})}2a\alpha_r\frac{2d_r\sin(k_z^{(+)}d_r)}{k_z^{(+)}d_r}e^{ik_z^{(+)}z_r} \tag{2.80}$$

The source velocity v_r in the previous equations (2.78), (2.79) and (2.80) is obtained from the solution of the system of equations in (2.73). Replacing (2.58) and (2.77) into (2.74), the transmitted pressure upstream of the tubes can be written as

$$p_{trans}(r,\theta,z)=\sum_{m=0}^{M_g}\sum_{n=0}^{N_g}(A_{mn}^{(+)})_{hq}^{pos}J_m\left(k_{mn}r\right)e^{-im\theta}e^{-ik_z^{(+)}z}+\sum_{m=0}^{M_g}\sum_{n=0}^{N_g}(A_{mn}^{(+)})_{hq}^{neg}J_m\left(k_{mn}r\right)e^{+im\theta}e^{-ik_z^{(+)}z} \quad (2.81)$$

where

$$(A_{mn}^{(+)})_{hq}^{pos}=A_{mn}^{d}+\sum_{r=1}^{N_s}(A_{mn}^{(+)})_{r}^{pos} \quad (2.82)$$

$$(A_{mn}^{(+)})_{hq}^{neg}=\sum_{r=1}^{N_s}(A_{mn}^{(+)})_{r}^{neg} \quad (2.83)$$

are the modal amplitudes of the transmitted mode (*m,n*) spinning in positive and negative direction, respectively, due to all sources and A_{mn}^{d} is the amplitude of the modes included in the disturbance (only positive spinning modes). The pressure reflected downstream of the HQ tubes can be similarly computed to give

$$p_{ref}(r,\theta,z)=\sum_{m=0}^{M_g}\sum_{n=0}^{N_g}(A_{mn}^{(-)})_{hq}^{pos}J_m\left(k_{mn}r\right)e^{-im\theta}e^{-ik_z^{(-)}z}+\sum_{m=0}^{M_g}\sum_{n=0}^{N_g}(A_{mn}^{(-)})_{hq}^{neg}J_m\left(k_{mn}r\right)e^{+im\theta}e^{-ik_z^{(-)}z} \quad (2.84)$$

where

$$(A_{mn}^{(-)})_{hq}^{pos}=\sum_{r=1}^{N_s}(A_{mn}^{(-)})_{r}^{pos} \quad (2.85)$$

$$(A_{mn}^{(-)})_{hq}^{neg}=\sum_{r=1}^{N_s}(A_{mn}^{(-)})_{r}^{neg} \quad (2.86)$$

are the amplitudes of the reflected mode (*m,n*), spinning in the positive and negative direction, respectively, due to the radiation of all sources. $\left(A_{mn}^{(-)}\right)_r^{pos}$ and $\left(A_{mn}^{(-)}\right)_r^{neg}$ are the amplitudes of mode (*m,n*) spinning in the positive and negative direction, respectively, due to an individual source "*r*" given as

$$(A_{mn}^{(-)})_{r}^{pos}=\frac{v_r k_o \rho c}{\pi a^2}\frac{J_m\left(k_{mn}a\right)}{\Lambda_{mn}(1-M^2)(k_z^{(+)}-k_z^{(-)})}\frac{2a\alpha_r\sin\left(m\alpha_r\right)}{m\alpha_r}\frac{2d_r\sin(k_z^{(-)}d_r)}{k_z^{(-)}d_r}e^{ik_z^{(-)}z_r}\frac{e^{+im\theta_r}}{2} \quad (2.87)$$

$$(A_{mn}^{(-)})_{r}^{neg}=\frac{v_r k_o \rho c}{\pi a^2}\frac{J_m\left(k_{mn}a\right)}{\Lambda_{mn}(1-M^2)(k_z^{(+)}-k_z^{(-)})}\frac{2a\alpha_r\sin\left(m\alpha_r\right)}{m\alpha_r}\frac{2d_r\sin(k_z^{(-)}d_r)}{k_z^{(-)}d_r}e^{ik_z^{(-)}z_r}\frac{e^{-im\theta_r}}{2} \quad (2.88)$$

The radiated sound power can now be computed. To this end, the acoustic intensity in the z-direction is written as

$$I_z = \frac{1}{2} Real\left[pv_z^* + \rho c \left|v_z\right|^2 M + \frac{\left|p\right|^2}{\rho c} M + v_z p^* M^2 \right] \tag{2.89}$$

or

$$I_z = \frac{1}{2}\left\{ Real\left[pv_z^* \right](1+M^2) + \rho c M \left|v_z\right|^2 + \frac{M}{\rho c}\left|p\right|^2 \right\} \tag{2.90}$$

where v_z is the particle velocity in the z-direction and asterisk (*) denotes complex conjugate. To compute the intensity, the particle velocity in the z-direction is obtained from Euler's equation as

$$-\frac{\partial p}{\partial z} = i\omega\rho v_z + \rho c M \frac{\partial v_z}{\partial z} \tag{2.91}$$

Since, the particle velocity is given as

$$v_z\left(r,\theta,z\right) = v_z\left(r,\theta\right) e^{-ik_z^{(+)}z} \tag{2.92}$$

equation (2.91) becomes

$$-\frac{\partial p}{\partial z} = i\rho c\left(k_o - k_z^{(+)} M\right) v_z\left(r,\theta\right) e^{-ik_z^{(+)}z} \tag{2.93}$$

that can be solved for the particle velocity as

$$v_z\left(r,\theta,z\right) = -\frac{1}{i\rho c\left(k_o - k_z^{(+)} M\right)} \frac{\partial p}{\partial z} \tag{2.94}$$

Replacing the transmitted pressure from (2.81) into (2.94) results

$$\begin{aligned} v_z\left(r,\theta,z\right) = & \sum_{m=0}^{M_g}\sum_{n=0}^{N_g} \frac{\left(A_{mn}^{(+)}\right)_{hq}^{pos} J_m\left(k_{mn} r\right) e^{-im\theta} k_z^{(+)} e^{-ik_z^{(+)}z}}{\rho c\left(k_o - k_z^{(+)} M\right)} \\ & + \sum_{m=0}^{M_g}\sum_{n=0}^{N_g} \frac{\left(A_{mn}^{(+)}\right)_{hq}^{neg} J_m\left(k_{mn} r\right) e^{+im\theta} k_z^{(+)} e^{-ik_z^{(+)}z}}{\rho c\left(k_o - k_z^{(+)} M\right)} \end{aligned} \tag{2.95}$$

The acoustic power is obtained by integrating the intensity over the cross sectional area of the duct as

$$W = \int_0^a \int_0^{2\pi} I_z r dr d\theta \tag{2.96}$$

Replacing (2.81) and (2.95) into (2.90) and this into (2.96) and considering the orthogonality condition of the modes

$$\int_0^{2\pi}\int_0^{a} J_m^2\left(k_{mn}r\right) r dr d\theta = 2\pi a^2 \Lambda_{mn} \tag{2.97}$$

$$\Lambda_{mn} = \begin{cases} \dfrac{1}{2} J_m^2\left(k_{mn}a\right) & \text{if} \quad m = 0 \\ \dfrac{1}{2}\left[1 - \dfrac{m^2}{\left(k_{mn}a\right)^2}\right] J_m^2\left(k_{mn}a\right) & \text{if} \quad m \neq 0 \end{cases} \tag{2.98}$$

results in the total transmitted power to be given as

$$W = \sum_{m=0}^{M_g}\sum_{n=0}^{N_g} W_{mn}^T \tag{2.99}$$

Therefore, the total sound power transmitted upstream of the HQ system is expressed in terms of the modal amplitudes as

$$\begin{aligned} W_{mn}^T = {} & \frac{\pi a^2 \Lambda_{mn}}{\rho c}\left(\left|\left(A_{mn}^{(+)}\right)_{hq}^{pos}\right|^2 + \left|\left(A_{mn}^{(+)}\right)_{hq}^{neg}\right|^2\right) \\ & \times\left\{\left(1+M^2\right) Real\left[\frac{\left(k_z^{(+)}\right)}{\left(k_o - k_z^{(+)}M\right)}\right] + \frac{M\left|k_z^{(+)}\right|^2}{\left|k_o - k_z^{(+)}M\right|^2} + M\right\} \end{aligned} \tag{2.100}$$

Based on the previous modeling approach, a computer code was developed. This computer code is presented in Appendix A.

2.2 Optimization technique using genetic algorithms

In the previous section, the modeling technique was presented. The model allows to predict the sound power reduction provided by the HQ system. However, since the performance of the HQ tube system depends on several parameters, it would be useful to develop an optimization technique to find the set of parameters that gives the best noise reduction. This technique will be based on the genetic algorithms (GA) and is presented in this section. Genetic algorithms use probabilistic search methods to minimize a specified cost or fitness function. The method is based upon an abstraction of the process of natural selection and was developed by Goldberg in 1989 [17]. The main advantage of the genetic algorithm is that it allows to seek for the global optimum, whereas traditional optimization methods can converge toward a local minimum, and miss the global optimum. Genetic algorithms are used here to find the optimal set of parameters that will minimize the cost function. In our case, this function is the radiated sound power upstream of the HQ system and the parameters to optimize are the dimensions of the HQ system such as centerline tube length, tube cross sectional area, axial location and so forth.

The fundamental characteristics of this optimization technique is that (i) the algorithm does not work with the parameters themselves but with a coding of them, (ii) the optimum search operates on a population of solution points, (iii) there is no need of knowing the derivatives of the fitness function and (iv) the algorithm uses probabilistic transition rules rather than deterministic ones. The optimization process used by the GA is illustrated in the flow chart, Figure 2-10. The main steps are explained in the following sections.

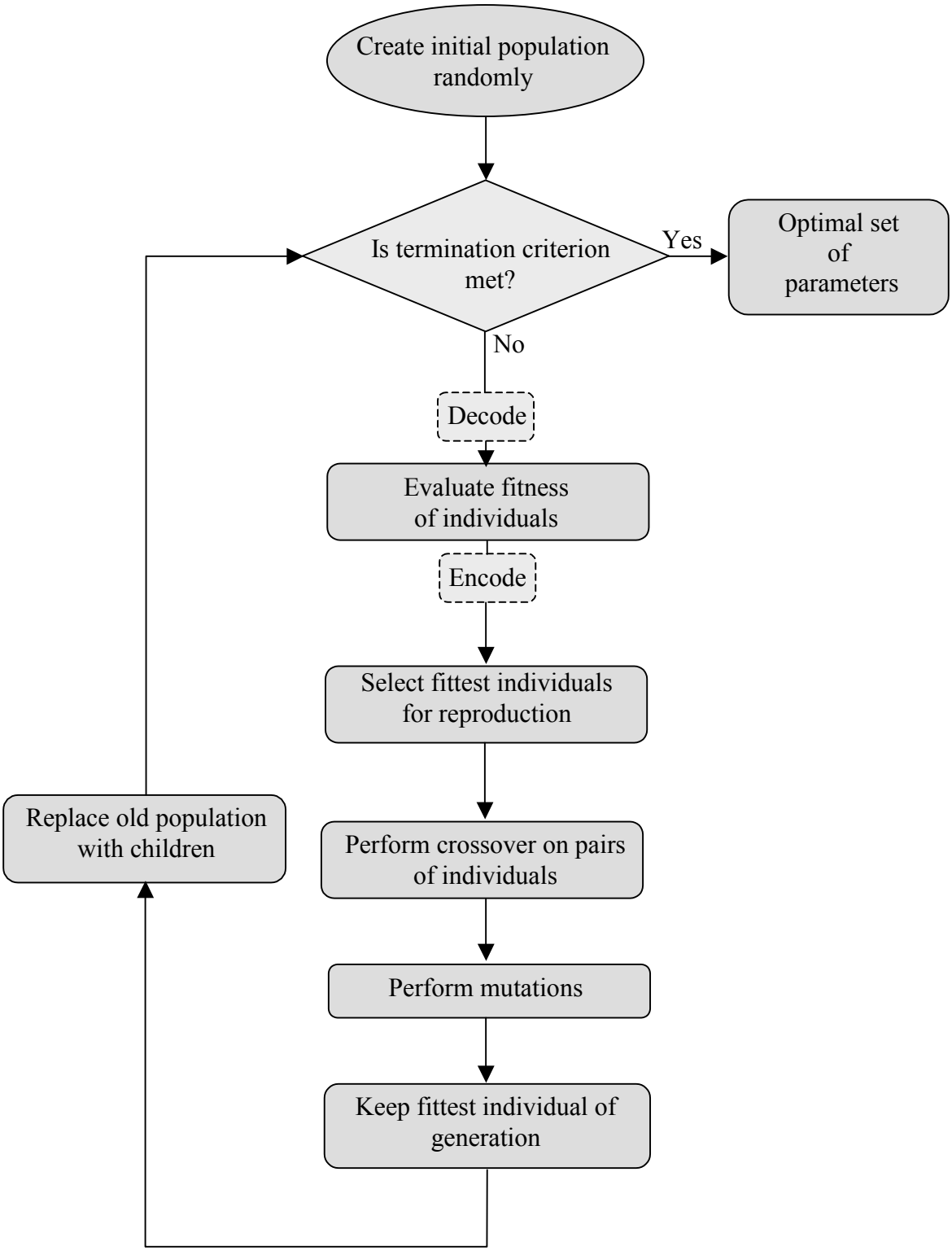

Figure 2-10: Main steps of the optimization process using genetic algorithms.

2.2.1 Encoding

The main idea of the GA consists of representing the input parameters by a binary string and manipulating this string until the optimal value is found. Each parameter to be optimized is discretized using a set of possible values within a specified range. The chosen parameter value is then written as a binary number coded on n bits. Thus, the total number of possible values is 2^n. The same principle is applied to each parameter and by concatenating the binary strings corresponding to a set of parameter values, an individual or chromosome is formed. Each binary number 0 or 1 is called gene. Figure 2-11 illustrates this mechanism where 2 parameters are to be optimized and each parameter is encoded on 4 bits. Therefore, there are 2^4=16 possible discrete values for each parameter. A particular value is chosen for each of these two parameters and the two corresponding binary strings are concatenated producing an individual of 2x4=8 bits. Therefore, the total possible number of individuals that can be created is $2^{(2x4)}$=256 individuals.

Each individual has to be encoded for genetic manipulations such as selection, crossover and mutations. The binary string is then decoded to find the value of the corresponding parameters and to evaluate the corresponding fitness.

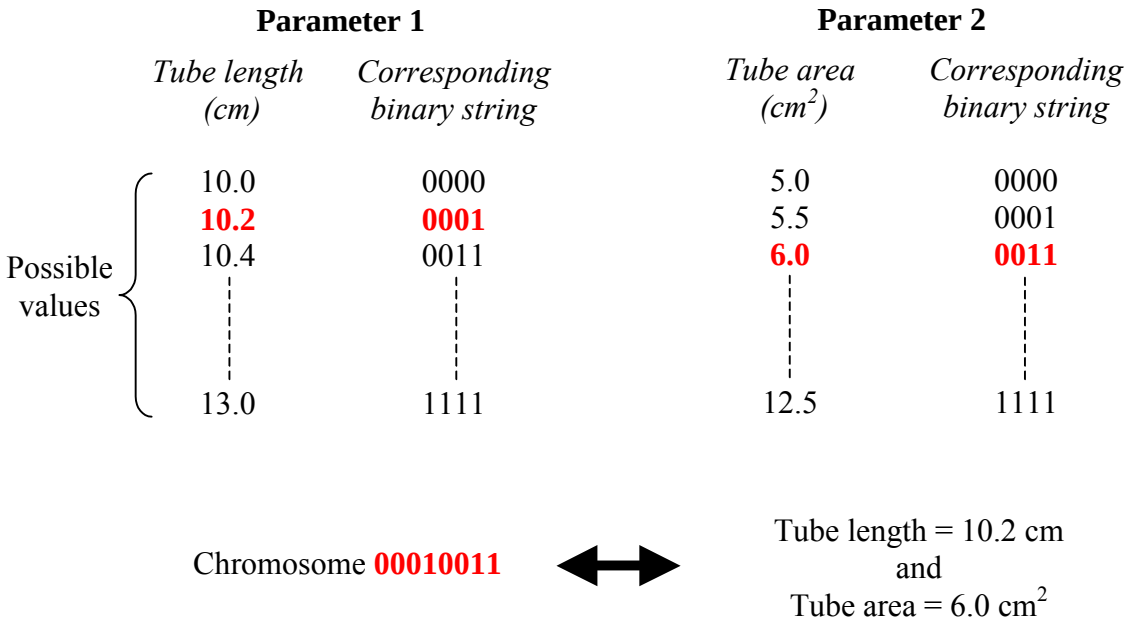

Figure 2-11: Encoding of parameters into chromosomes.

2.2.2 Fitness function

The fitness function is the link between the genetic algorithm and the system. It gives the information on how suitable an individual is for the goal of the optimization. In our case, the fitness function will be the sound power radiated at the end of the engine inlet and the goal of the optimization is to minimize its value. The key advantage of the GA is that it does not require information about the fitness function (such as derivatives like in the typical optimization techniques). The only required information is the fitness value associated with an individual. The fitness of a chromosome is a determinant criterion for the selection process.

2.2.3 Selection

The initial population is chosen such that each parameter takes a random value in a specified range. In this study, the range of each parameter is selected such that unrealistic tubes cannot be generated (i.e. for instance tubes with centerline length smaller than the distance between tube ends). Whereas the initial population is chosen randomly, one needs to find a way to decide which of the individuals in the current population will be allowed to pass their genetic material to the following generations. This is the role of the selection process. The key assumption is to give preference to fitter individuals. In our case, the tournament selection will be used. Two chromosomes are selected randomly from the current population, but only the one with the higher fitness value is inserted into the mating pool. The mating pool constitutes the group of individuals that will be mated to create the new generation. This process is repeated until the number of chromosome chosen for reproduction is the same as the initial number of individuals in the population.

2.2.4 Crossover

The crossover operator is the key operator to generate new individuals. This operator is applied to each pair of the mating pool to produce one or two children. The pairs of parent chromosomes, which the crossover applies on, are chosen randomly

among the mating pool. In our case, the uniform crossover technique will be applied. Therefore, every gene will exchange genetic material with the other parent's gene of the same location with a probability p_c (p_c is equal to 0.5 here). This process is illustrated in the following example, Figure 2-12. For each gene of the parent chromosomes, a random number is chosen between 0 and 1 and if this number is higher than p_c, the gene is exchanged with the gene from the other parent. This happens on the genes at position 1, 4, 5 and 7 in the example. This way, the children receive genetic information coming from their two parents.

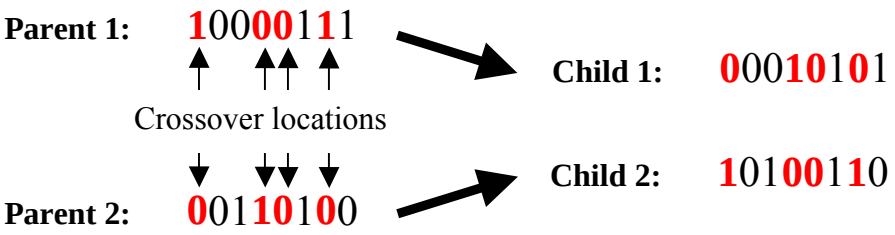

Figure 2-12: Example of uniform crossover.

2.2.5 Mutation

The final operation of the mating process is the mutation and is applied to the generation produced after the crossover. This process should allow to find solutions which contain genes that are nonexistent in the initial population. There are two kinds of mutation. First of all, the **jump** mutation directly acts on the chromosome and consists of changing the value of a gene, i.e. 0 is changed to 1 or vice-versa. On the other hand, the **creep** mutation consists of decoding the value of the chromosome and changing it by a small discrete increment (range of the parameter value divided by the number of possible values). This last type of mutation directly acts on the discrete value of the parameter (decimal value). The mutation process is illustrated in Figure 2-13. The chance that a creep or jump mutation will occur is determined by the mutation probability. While a high probability can transform the GA into a kind of random search algorithm, it has to be kept high enough to avoid premature convergence into a non-optimum zone. Here, the jump and creep mutation probability will both be kept under 0.05.

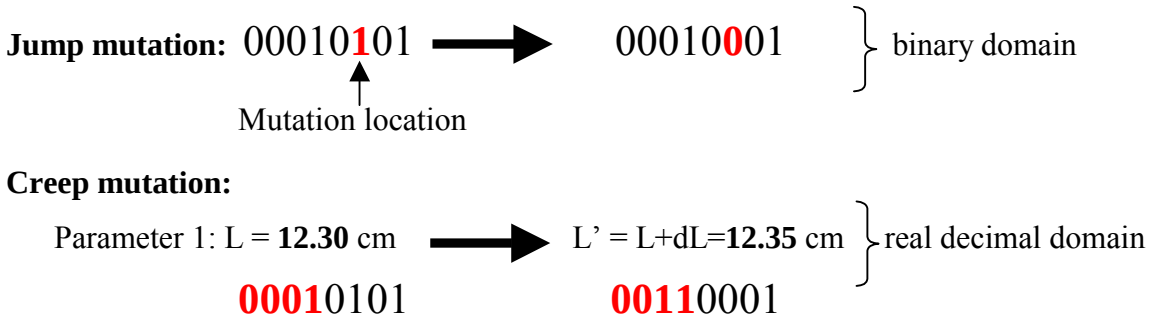

Figure 2-13: Example of jump and creep of mutation.

2.2.6 Replacement strategy

Once the operations of selection, crossover and mutation are completed, the current population is replaced with the children just created. However, an elitist strategy will be used here, therefore, all but one individuals are replaced by children. The individual from the old generation with the highest fitness value is directly transferred to the new generation. This way, the best genetic information of a population is maintained through the generations.

The creation of new individuals and replacement of the old population process will continue until the termination criterion is met. In our case, this criterion will be the maximum number of generation (usually set to 100), which is limited mainly for a computation time reason.

Chapter 3. Numerical analysis

In the previous chapter, a modeling technique was developed to predict the effect of the HQ tubes applied to the inlet of an engine. In order to validate this analytical approach, the predicted results will be compared to experimental data measured on real engines. In the first section both engines, a Pratt and Whittney JT15D and an AlliedSignal TFE731-60, will be described. A circumferential array of 20 and 27 tubes were used on these engines, respectively. Analytical and experimental results will be compared for the blade passage frequency reduction and then for the broadband reduction. Finally, a convergence study will be done in the case of the JT15D engine. This study will show the number of modes to include in the calculations in order to have some accurate predictions.

3.1 Test setup

The computer code presented previously allows to investigate the effect of HQ tubes applied to any kind of circular inlets, however, the study will be limited here to two systems. These systems are two real engines, on which the HQ tube concept was applied and actual measurements taken. This will allow to compare the predicted results with the experimental data and to validate the modeling approach. The two systems, a JT15D engine and a TFE 731-60 engine are described in the following sections.

3.1.1 JT15D turbofan engine

The Pratt and Whitney JT15D turbofan engine is a twin spool turbofan engine with a full-length bypass duct and a maximum bypass ratio of 2.7 (the bypass ratio is the ratio of air ducted around the core of the engine to the air that passes through the core). The thrust for this engine ranges from 2200 to 3350 lbs. There is a single-stage axial flow fan with 28 blades and a centrifugal high-pressure compressor with 16 full vanes and 16 splitter vanes. There are 33 exit guide vanes (EGV) and no inlet vanes. The diameter at the fan stage location is *0.53 m*. The length of the inlet in the axial direction is *0.46 m*. Experimental results were obtained by operating the engine at various speeds near idle condition yielding a BPF ranging from 2260 to 2420 Hz. However, the design speed for the HQ system tested on this engine corresponds to a BPF of about 2320 Hz. Near this condition, the inlet intake flow speed is about *42.5 m/s* which yields a Mach number of *M=-0.12*. Given these dimensions and Mach number, a large number of modes are in cut-on condition near the BPF range. The cut-off frequency for each mode is calculated with the following equation

$$f_{cut-off} = \frac{ck_{mn}}{2\pi}\sqrt{1-M^2} \tag{3.1}$$

where c is the sound velocity, k_{mn} are the eigenvalues, and M is the flow Mach number. The cut-off frequencies of the lower modes existing in this inlet are shown in Table 3-1 (as an illustration, modes cut-on at a BPF of 2320 Hz are written in bold in the table). The indexes m and n correspond to the circumferential and radial order of the modes, respectively.

		Radial order *n*				
		0	**1**	**2**	**3**	**4**
Circumferential order *m*	**0**	**0**	**779**	**1427**	**2069**	2710
	1	**374**	**1084**	**1736**	2381	3023
	2	**621**	**1364**	**2027**	2678	3324
	3	**854**	**1630**	**2307**	2966	3618
	4	**1081**	**1888**	2579	3246	3904
	5	**1305**	**2139**	2844	3521	4184
	6	**1525**	2386	3105	3790	4460
	7	**1744**	2630	3361	4055	4732
	8	**1962**	2871	3615	4317	5000
	9	**2178**	3109	3865	4576	5265
	10	2394	3345	4113	4832	5528

Table 3-1: Inlet mode analytical cut-off frequencies in Hertz for the JT15D engine.

To enhance the tonal nature of the inlet radiated sound and to excite the *m=1* modes to dominance, a set of 27 exciter rods are mounted upstream of the fan stage. The wakes from the rods interact with the fan blades to produce tones which are significantly higher in sound level than without the rod interactions, and thus emulate strong wake-stator interactions. The modes generated by the fan-EGV are cut-off at the BPF frequencies considered. The modal amplitudes of these dominant modes were measured at a BPF of 2320 Hz and are shown in Table 3-2. For the sake of simplicity, these modal amplitudes are assumed to remain constant over the BPF range from 2260 up to 2381 Hz. This last frequency corresponds to the cut-off frequency of the next radial mode of order (1,3).

Fan mode	Amplitude (Pa)
(1,0)	56.3
(1,1)	$55.5e^{-4.9i}$
(1,2)	$111.0e^{0.1i}$

Table 3-2: Inlet fan mode amplitudes for the JT15D engine.

As an illustration, pictures of the inlet of the engine mounted with two arrays of tubes are shown in Figure 3-1.

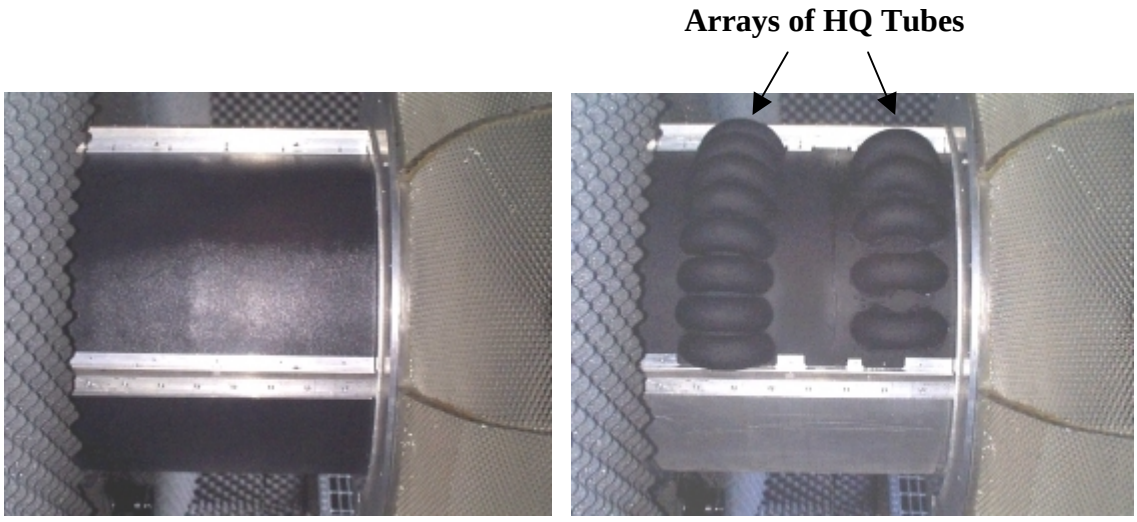

Figure 3-1: Pictures of the JT15D inlet configured (a) as a hard wall and (b) with two arrays of HQ tubes.

3.1.2 TFE 731-60 engine

The AlliedSignal TFE 731-60 turbofan engine has a 4-stage axial compressor, and a centrifugal high-pressure compressor. The maximum bypass ratio of 3.9. There is a single-stage axial flow fan with 22 blades and 10 bypass struts. The diameter at the fan stage location is *0.787 m* and the length of the inlet in the axial direction is *0.51 m*. The thrust for this engine ranges from 3500 to 5000 lbs. Experimental results were obtained by operating the engine at various power settings (60, 81, 88, 92, 98 %) yielding a BPF ranging from 2250-3730 Hz. The power setting selected for the design of the HQ tube system was 60% corresponding to a BPF of 2250 Hz. Near this condition, the inlet intake flow speed is about *42.5 m/s* which yields a Mach number of *M=-0.12*. The cut-off frequencies of the lower modes existing in this inlet are shown in Table 3-3 (as an illustration, modes cut-on at a BPF of 2250 Hz are written in bold in the table).

		Radial order *n*					
		0	**1**	**2**	**3**	**4**	**5**
Circumferential order *m*	**0**	**0**	**527**	**965**	**1400**	**1833**	2266
	1	**253**	**734**	**1175**	**1611**	**2045**	2479
	2	**420**	**923**	**1372**	**1812**	**2249**	2685
	3	**578**	**1103**	**1561**	**2007**	2448	2886
	4	**732**	**1277**	**1745**	**2197**	2641	3082
	5	**883**	**1448**	**1925**	2382	2831	3275
	6	**1032**	**1615**	**2101**	2565	3018	3465
	7	**1180**	**1780**	2274	2744	3202	3653
	8	**1327**	**1942**	2446	2921	3383	3838
	9	**1474**	**2103**	2615	3096	3563	4021
	10	**1620**	2263	2783	3270	3740	4202
	11	**1765**	2422	2949	3441	3916	4381
	12	**1910**	2579	3114	3612	4091	4559
	13	**2054**	2736	3278	3781	4264	4736
	14	**2198**	2892	3440	3948	4436	4911
	15	2342	3047	3602	4115	4607	5085

Table 3-3: Inlet mode analytical cut-off frequencies in Hertz for the TFE731 engine.

This particular engine has characteristics which make it very interesting for the present study. The rotor-strut interaction is such that the dominant modes propagating at the BPF frequency are of different circumferential order, i.e. m=-8, 2 and 12. Again the rotor-EGV interaction results in cut-off modes. The modal amplitudes of the dominant modes at a BPF of 2250 Hz were measured and are shown in Table 3-4.

Fan mode	Amplitude (Pa)
(-8,0)	1.2
(-8,1)	$1.0^{e-2.4i}$
(2.0)	$1.9\ ^{e-1.0i}$
(2.1)	$0.8\ ^{e0.4i}$
(2.2)	$3.3\ ^{e-4.6i}$
(2.3)	$0.5\ ^{e-4.0i}$
(12,0)	$3.2\ ^{e1.2i}$

Table 3-4: Inlet fan mode amplitudes for the TFE731 engine.

Pictures of the TFE 731 inlet mounted with 2 arrays of HQ tubes are shown in Figure 3-2.

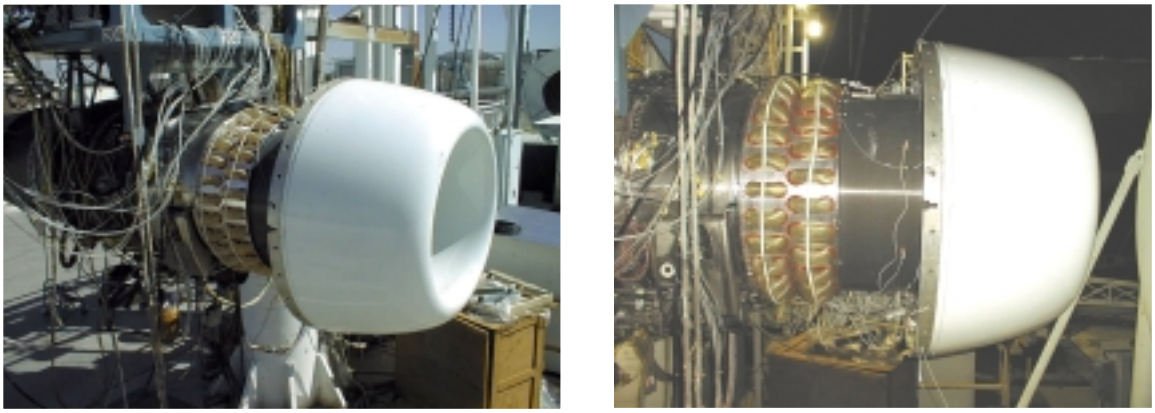

Figure 3-2: Pictures of the TFE731 inlet configured with two arrays of HQ tubes.

3.2 Blade passage frequency results

3.2.1 JT15D engine

In order to investigate the validity of the model, results predicted by the computer code will be compared to experimental results measured on the real engine. The comparison will first be done on the JT15D turbofan engine.

For these experiments, the HQ tube system consists of a single array of 20 tubes positioned at *0.35 m* upstream from the fan. The HQ tubes were designed to provide an optimal reduction at 2320 Hz, which is near the tube second resonance frequency. That is, the centerline tube length and distance between tube ends were chosen using the modeling technique such that the HQ system provides reduction at 2320 Hz The centerline tube length is *0.118 m*. The distance between the two tube ends is *0.092 m* and the tube diameter is *0.038 m*. A perforated screen is placed at the ends of the tubes to minimize the undesirable flow separation at the tubes-inlet interfaces. The parameters of the screen are given by the thickness t_{ps}*=0.00075 m,* the orifice radius a_{orif}*=0.00075 m*, and the screen open area ratio σ*=25%.*

The experimentally measured power attenuation of the BPF tone is presented in Figure 3-3 for a range of BPF tone frequencies from 2240 to 2380 Hz. Three different measurements for the same system are shown on this plot. Although the test setup is the same for the three cases, the radiated sound power is not exactly the same because the engine rotation speed is fluctuating. The HQ tube system is very efficient at these BPF frequencies and provides a maximum power level reduction of 6.0 dB at 2312 Hz.

Using the parameters from the experiment, the predicted sound power reduction is also computed to validate the accuracy of the model. The cut-off frequencies of the first radial modes ($m=1$, $\mu=0,1,2,3$) are 374, 1084, 1736, and 2381 Hz, respectively. Therefore, there are 3 propagating modes at a BPF lower than 2381 Hz. The amplitudes of these first three fan modes have been experimentally determined for a BPF of 2320 Hz, as explained in the previous section. These amplitudes were used in the model for a frequency range from 2240 to 2380 Hz. Since the amplitude of the fourth radial mode, cut-on at 2381 Hz, is unknown, the analysis was not performed above this frequency.

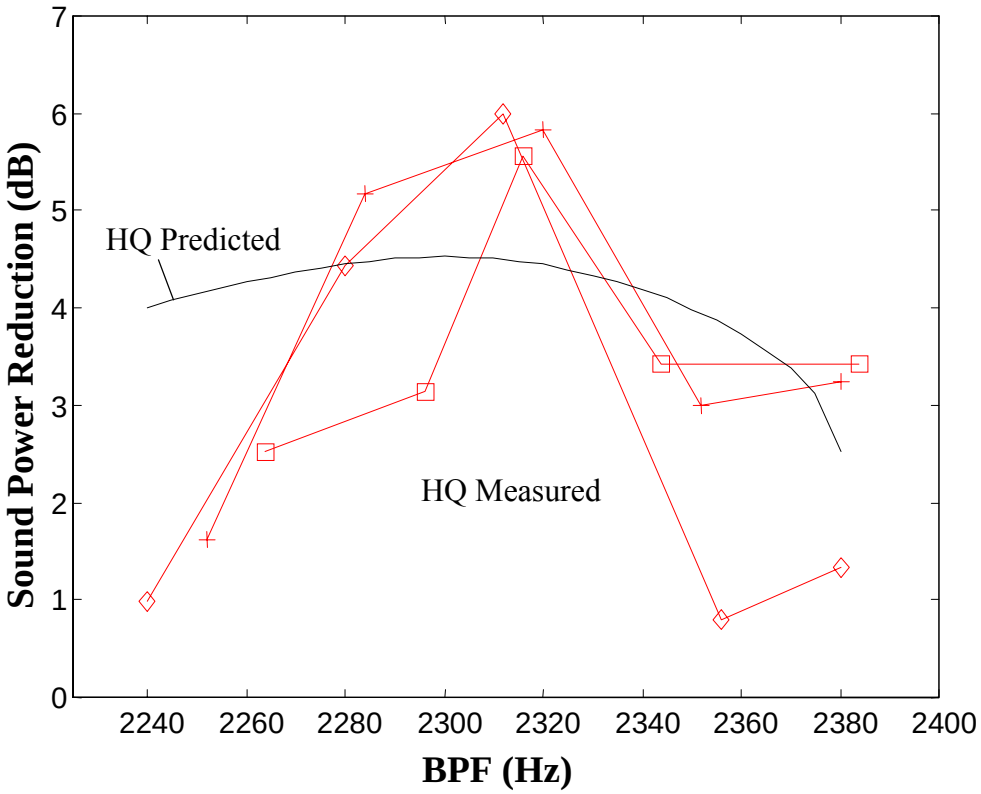

Figure 3-3: Comparison of the predicted and measured BPF sound power reduction level with one array of 20 tubes mounted on the inlet of the JT15D engine.

The predicted sound power reduction shows that there is an optimal frequency of attenuation at about 2300 Hz with a power reduction of about 4.5 dB. The analytical and experimental results show good agreement in both the optimum frequency of attenuation and the level of sound power reduction. However, the model predicts good attenuation over a wider frequency range than the experiments. This is probably due to the fact that the mode amplitudes are assumed to remain constant over the BPF range, which is probably not the case in reality.

3.2.2 TFE731-60 engine

The experiments run on the TFE731 were slightly different from the previous ones. Here, an array of 27 HQ tubes is mounted on the inlet of the engine. The array is positioned at *0.30 m* upstream from the fan. The centerline tube length is *0.135 m*. The

distance between the two tube ends is *0.104 m* and the tube diameter is *0.042 m*. The parameters of the perforated screen are given by the thickness t_{ps}*= 0.0015 m,* the orifice radius a_{orif}*=0.0016 m*, and the screen open area ratio σ*=21%.* The sound power reduction provided by the HQ tubes was experimentally measured at three different BPF: 2250, 2512 and 3038 Hz. These results as well as the predicted sound power reduction at these frequencies are shown in Table 3-5.

BPF (Hz)	Measured sound power level (dB)	Predicted sound power level (dB)
2250	2.7	0.4
2512	0.2	0.1
3038	2.3	0.8

Table 3-5: Comparison of the predicted and measured BPF sound power reduction level with one array of 27 tubes mounted on the inlet of the TFE731 engine.

Although the HQ tube system was designed to provide optimal reduction at a BPF of 2250 Hz, Table 3-5 shows that the HQ system is also efficient at a BPF of 3038 Hz. The measured sound power reduction at these frequencies is 2.7 and 2.3 dB, respectively. It is clear in Table 3-5 that the model underestimates the sound power reduction in these cases. This divergence between the experimental and predicted results is probably due to inaccurate measurements of the mode amplitudes present on the real engine.

3.3 Broadband results

The HQ concept applied to turbofan engine noise was primarily envisioned as a tonal noise reduction strategy, with the intent that the HQ inlet could be designed so that the frequencies at which reduction is achieved correspond to the BPF tone and harmonics. However, the HQ inlet also results in significant attenuation in the broadband noise levels radiated from the engine inlet. In this section, the predicted results will be compared to the measured data for both engines.

In the case of a BPF analysis, the complex amplitudes of the few dominant modes propagating at the BPF frequency could be measured and used as input in the model. However, in the case of a broadband study, the amplitudes of all the propagating modes are not available. Therefore, there are usually two kinds of assumptions that can be made to find the modal amplitudes. Either, it is assumed that, for each frequency, all cut-on modes have the same amplitude, or each mode will equally contribute to the total sound power. In this last case, the amplitudes of modes included in the disturbance are chosen such that all cut-on modes generate equal sound power at each frequency while the phase of the modes is chosen randomly. Results for both approaches will be shown in this section.

3.3.1 JT15D engine

The experimentally measured inlet broadband sound power for both the rigid wall inlet and the inlet with a single array of 20 HQ tubes is shown in Figure 3-4a) for a BPF at 2320 Hz. Figure 3-4a) also shows the analytical broadband prediction using the equal modal amplitude approach. The prediction based on the equal modal power technique is shown in Figure 3-4b). In both prediction results, the phase of the modes was chosen randomly. However, since the phase of the modes does not affect significantly the sound power level, the results are shown here only for one case of random phase.

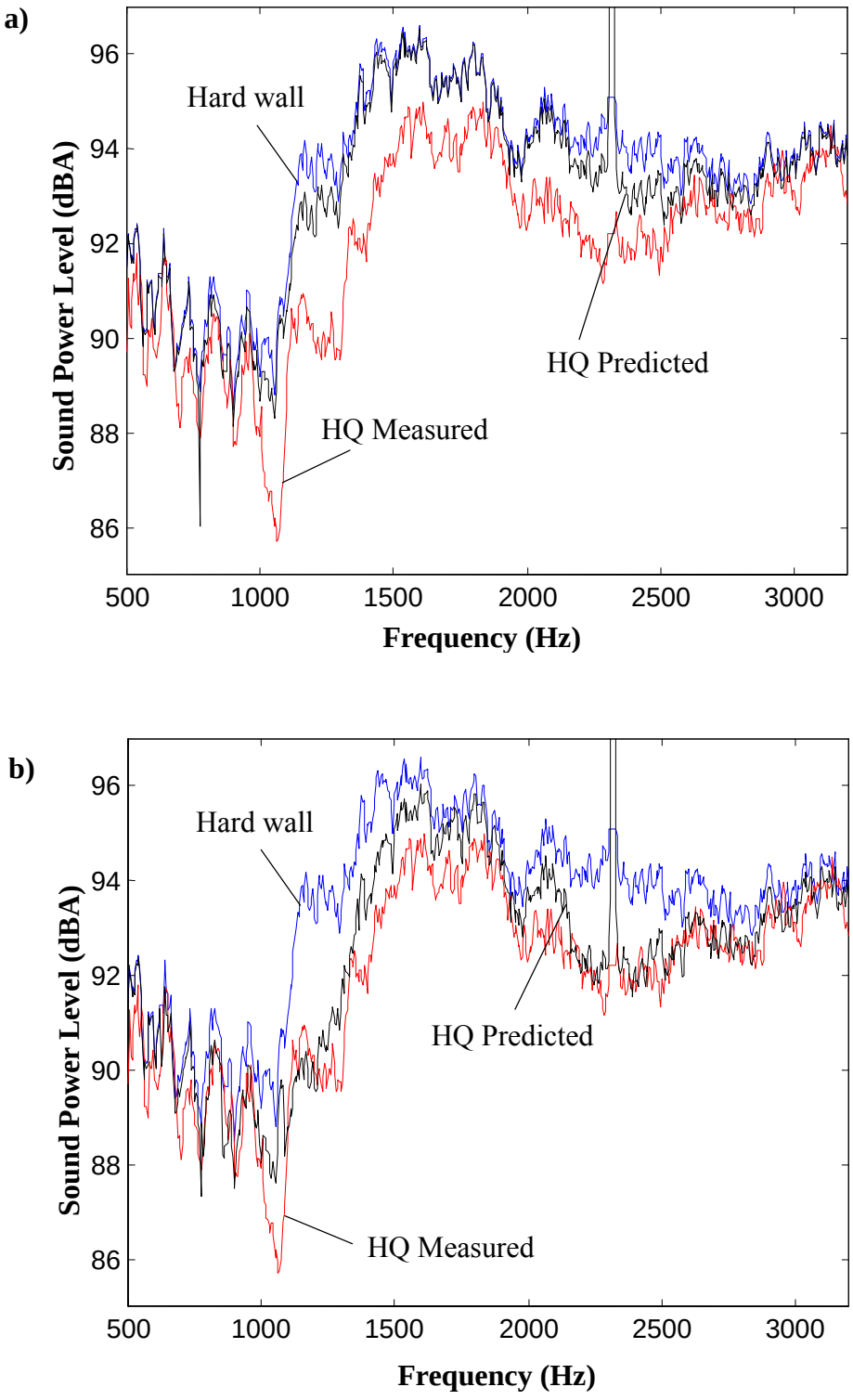

Figure 3-4: Comparison of the predicted and measured sound power levels with one array of 20 tubes mounted on the inlet of the JT15D engine a) equal modal amplitudes approach b) equal modal power approach.

The HQ array results in significant broadband reduction, primarily in the vicinity of the first and second resonances of system (i.e., approximately 1200 and 2400 Hz). It is also clear in Figure 3-4 that the predicted results using the equal modal power approach are closer to the experimental data than the predictions using equal modal amplitudes. The overall A-weighted measured sound power reduction over the frequency range from 500 to 3200 Hz is 1.5 dB. The overall predicted reductions are 0.3 dB and 1.0 dB for the equal amplitude and equal power approach, respectively. In the case of the equal modal power, the model predicts the broadband reduction very well, however, the analytical results seem to underpredict the reduction, especially in the frequency range from 1200 to 1800 Hz.

It is important to notice that the previous plots show the broadband sound power levels and are to be differentiated from the BPF plots in the previous section. When the broadband noise is considered, it is assumed that all cut-on modes (21 modes) are present in the disturbance and contribute to the propagation of acoustic energy with a relatively equal influence (modes have same amplitudes or generate same power). However, in the case of a BPF or tone analysis, most of the acoustic energy is propagated through a few dominant modes, whose amplitudes are much higher than the amplitudes of the rest of the cut-on modes. This is the reason why the plots in Figure 3-4 should not be considered at the frequency of the BPF, i.e. 2320 Hz here.

3.3.2 TFE 731 engine

The broadband sound power levels were also measured for the TFE731 engine at a BPF of 2560 Hz of. In this case, there is a single array of 27 tubes mounted on the inlet of the engine. Figure 3-5a) shows these experimental results. Once again, the predicted results using the equal amplitudes and equal modal power approach will be used here. They are shown in Figure 3-5 a) and b), respectively.

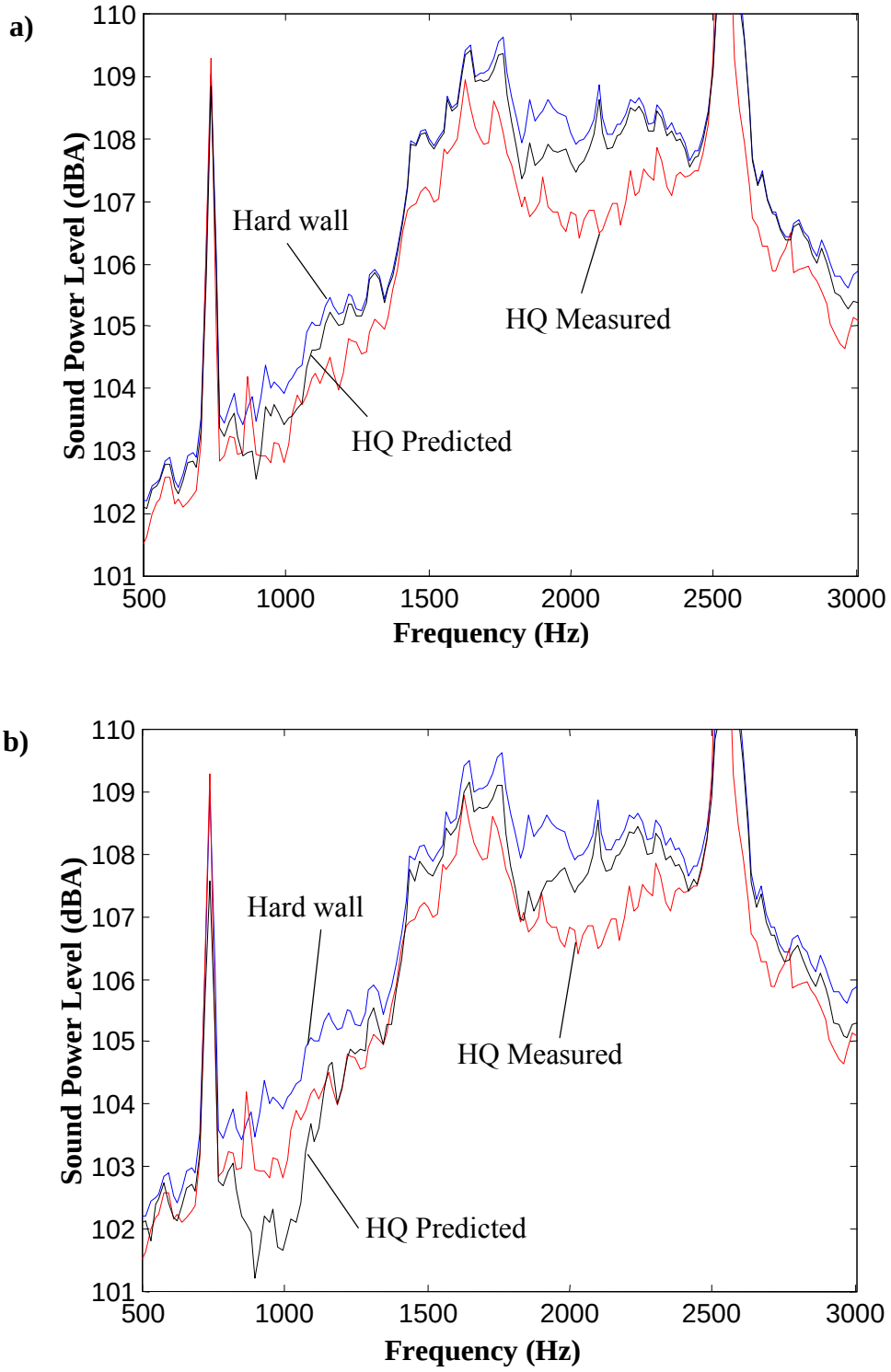

Figure 3-5: Comparison of the predicted and measured sound power levels with one array of 27 tubes mounted on the inlet of the TFE731 engine a) equal modal amplitudes approach b) equal modal power approach.

Figure 3-5 shows that, again, the equal modal power approach provides results, which are closer to the experimental data. The overall A-weighted measured sound power reduction over the frequency range from 500 to 3000 Hz is 0.8 dB. The overall predicted reductions are 0.2 dB and 0.5 dB for the equal amplitude and equal power approach, respectively.

The previous comparisons showed that the experimental and predicted results were in good agreement, allowing to validate the model, although, the code seems to underpredict slightly the reduction provided by the HQ tube system. Thus, the model will be used in the next chapter to study the noise control mechanisms involved in the HQ tube system.

3.4 Convergence of the predicted results

In the modeling technique presented in Chapter 2, the model of the HQ tube in the duct was based on the Green's function. This function actually corresponds to the radiation of a point source on the duct wall. Theoretically, the Green's function is written as an infinite series where each radial and circumferential mode contributes to the total expression of the function. In practice, a finite number of modes included in the calculations has to be chosen to be able to run the simulation in a finite amount of time. Moreover, the computing time will increase as more and more modes are included but the results will become more accurate. Therefore, there is a tradeoff between the desired accuracy of the results and the speed of computation. The aim of this study is to help choosing an appropriate number of modes to include in the computations.

In the case of the HQ system, the source is not a point source but a piston source located on the duct wall at each end of the tubes. Therefore, the influence of the number of modes on the impedance function of a piston source viewed by another piston source will be investigated here, rather than the Green's function. This impedance function is simply the average sound pressure over the surface of an observer source due to another piston source with unit velocity and is expressed in equation (2.53) for an observer source placed upstream. The contribution of each mode to the impedance function will first be

studied for different positions of the observer source. Then, the influence of the number of modes in terms of sound power level will be investigated.

The impedance of a piston source viewed by another source located upstream at 9.2 cm is first shown in Figure 3-6 at a frequency of 2320 Hz and in the configuration of the JT15D engine. This figure shows the total magnitude of the impedance function as a function of the radial and circumferential modes included in the computation. It is important to keep in mind that this figure does not show the individual contributions of each mode to the impedance. For a given number of radial N and circumferential modes M, the corresponding value of the impedance shown in the figure is the sum of the contributions due to all modes (m,n) for $n \leq N$ and $m \leq M$. Therefore, the magnitude of the impedance is expected to converge towards a limit value, as more and more modes are included. The indexes m and n refer to circumferential and radial order mode, respectively.

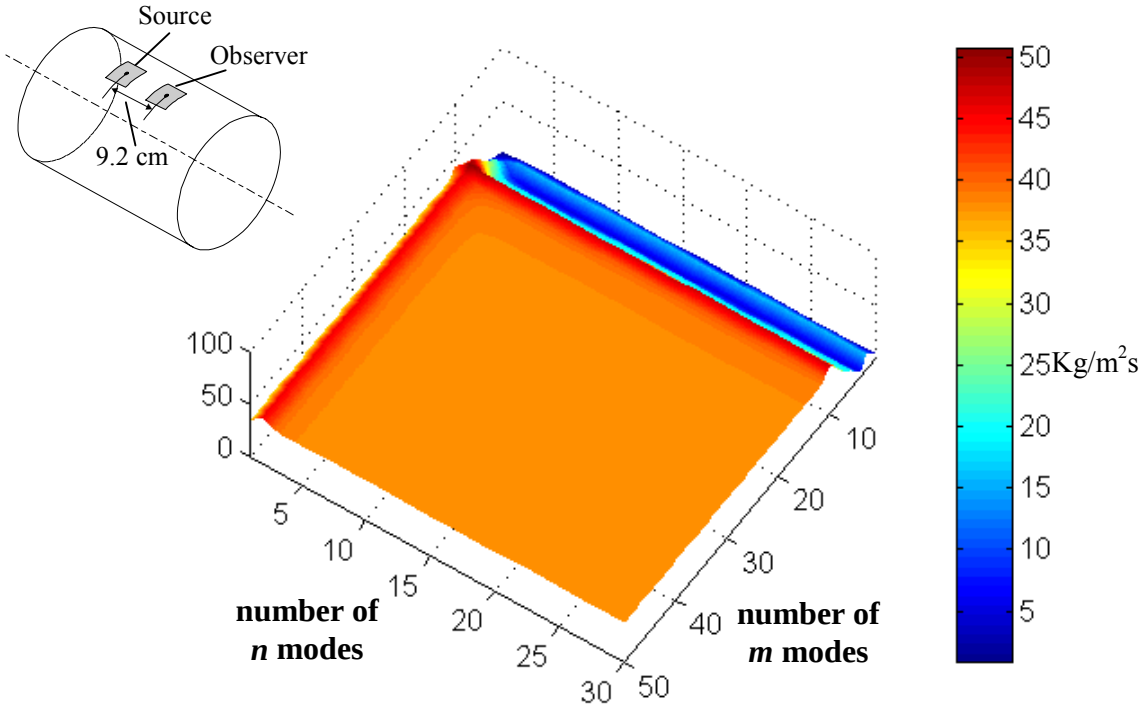

Figure 3-6: Total magnitude of the impedance function of a piston source viewed by another source located upstream at 9.2 cm – BPF frequency is 2320 Hz.

As seen in Figure 3-6, the impedance function rapidly converges, as more radial and circumferential modes are included in the calculation. A steady value is reached when more than 5 radial and 15 circumferential modes are included. In this configuration, the cut-on modes and modes that are just cut-off have a significant contribution to the impedance function. However, modes that are well cut-off rapidly vanish and their effect on the observer source 9.2 cm further upstream is negligible.

The same study will now be done for an observer source at the same axial location as the "source" piston source but at an angle of 18° relative to the position of the "source" piston. This angle corresponds to the distance between to tubes in the circumference for an array of 20 tubes. The magnitude of the impedance in this case is shown in Figure 3-7, as a function of the number of modes included in the calculation.

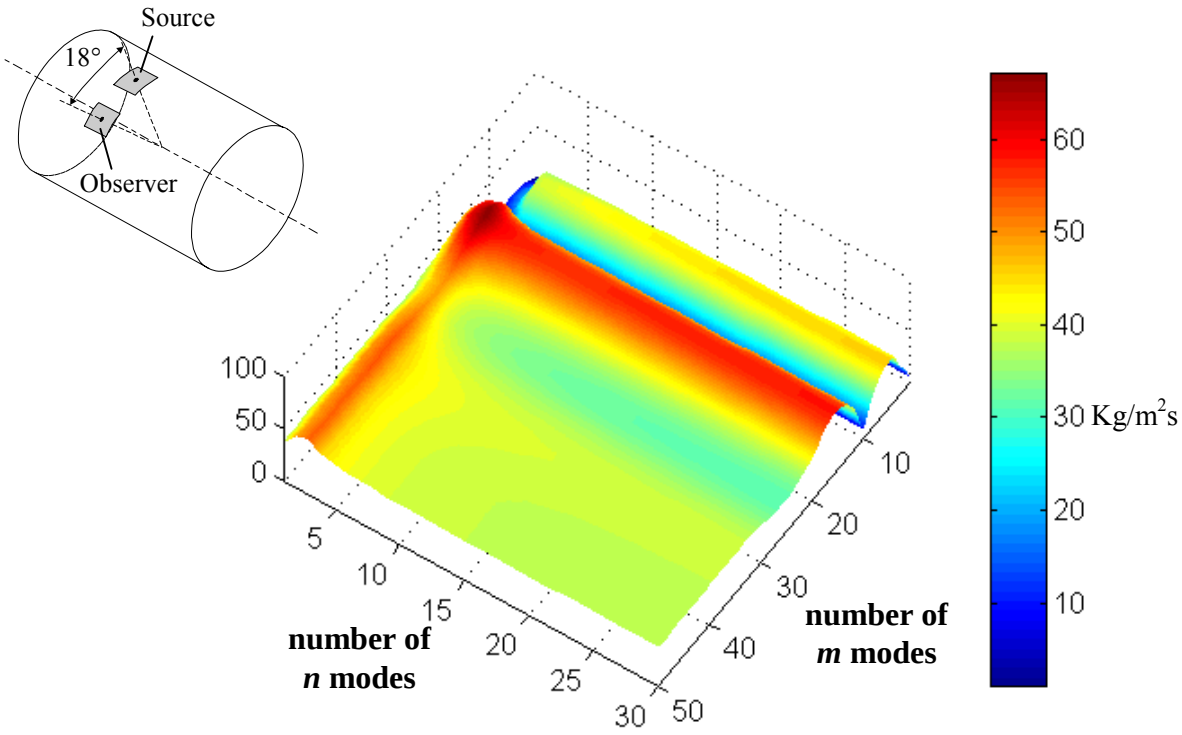

Figure 3-7: Total magnitude of the impedance function of a piston source viewed by another source at 18° in the same cross-sectional plane.

As seen in Figure 3-7, when the sources are in the same the cross-sectional plane, the number of circumferential modes that need to be included in the calculation to reach convergence is very large. Even if 50 circumferential modes are included, the impedance

value is not constant. This is due to the fact that cut-off modes have a great influence in this case. Cut-off modes actually decay as they travel along the duct axis; however, these modes do not have a decay characteristic along the circumference. This suggests that a very large number of circumferential modes would need to be included to obtain accurate results. It is interesting to look at the impedance of a piston viewed by another piston on the circumference at higher angles. This is shown in Figure 3-8a and b, where the observer source is located at 54° and 90°, respectively. These two angles correspond to the position of the third and fifth tube in an array of 20 tubes.

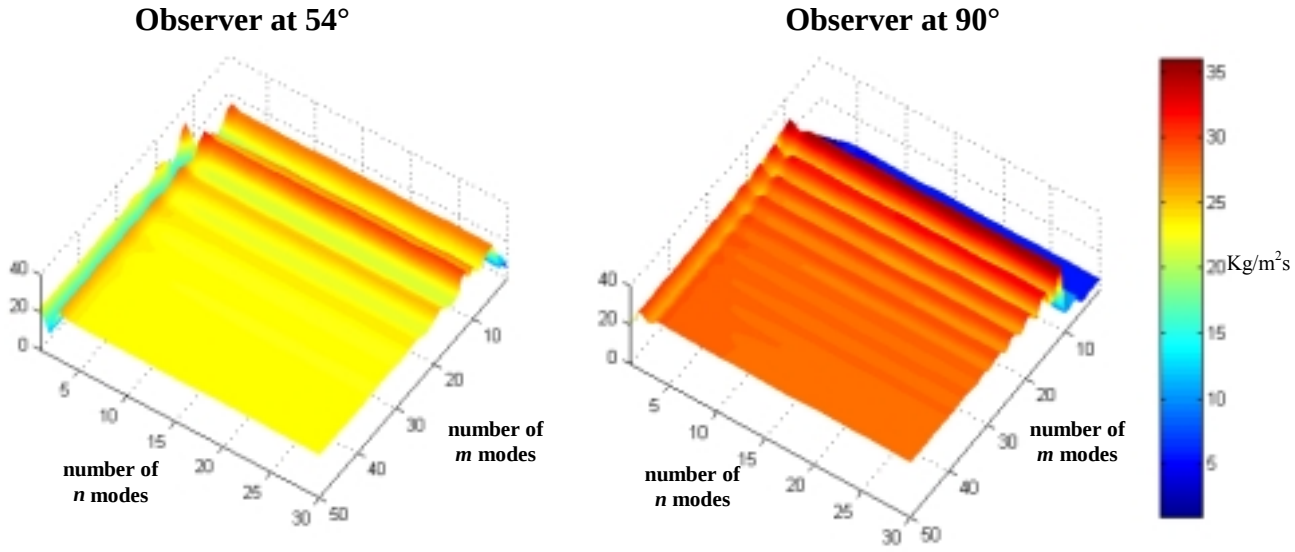

Figure 3-8: Total magnitude of the impedance function of a piston source viewed by another source in the same cross-sectional plane at a) 54° b) 90° apart.

Figure 3-8a and b show that even when the spacing between the sources increases, the influence of the cut-off modes remains significant and causes the impedance function to oscillate. However, the magnitude of the impedance clearly convergences towards a constant value when the number of modes increases. Moreover, including a low number of radial modes is enough to reach the convergence.

This study allowed to show that when tubes are placed in a circumferential array, the number of circumferential modes needed to reach a steady value of the impedance is

relatively high. However, the influence of cut-off radial modes on the impedance value seems to be negligible. Therefore, in order to limit the computing time and to get accurate results, it is important to choose a high number of circumferential modes to the detriment of the radial modes.

The influence of the number of modes will now be investigated by looking directly at the predicted sound power level. For this study, the HQ system is made of a circumferential array of 20 tubes. The centerline tube length is 11.8 cm and the disturbance is made of three incident mode of order (1,0), (1,1) and (1,2). The effect of the number of modes included in the calculations will be studied individually for radial and circumferential modes. In the first example, the number of circumferential modes is chosen to be very high and the effect of radial modes will be studied. Then, the influence of the circumferential modes will be shown while a high number of radial modes is chosen.

The results of the first study are presented in Figure 3-9 where the sound power reduction is plotted as a function of BPF frequency. There are 40 circumferential modes included in the calculation of the impedance function and the number of radial modes changes from 6 to 40.

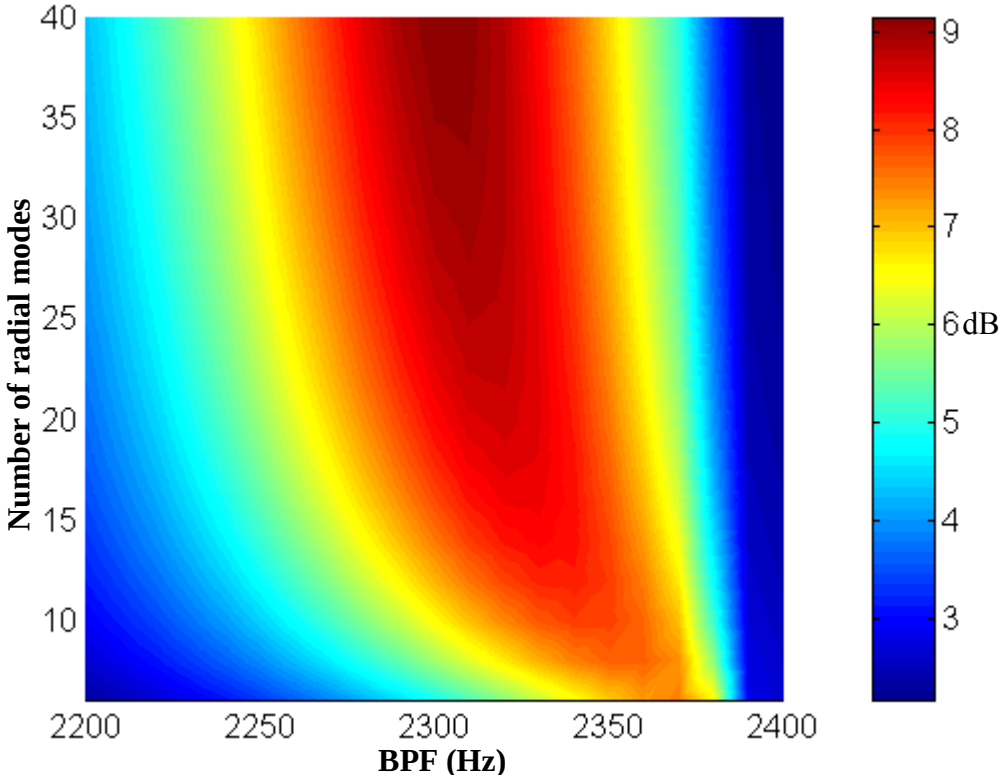

Figure 3-9: Influence of number of radial modes on the sound power reduction when 40 circumferential modes are included in the calculations.

As seen in Figure 3-9, the number of radial modes included in the calculation does not seem to affect dramatically the sound power reduction level. However, it can be noticed that the optimum frequency of attenuation is slightly shifted down as the number of radial modes increases. In this case, choosing a number of radial modes higher than 20 seems to give reasonably accurate results.

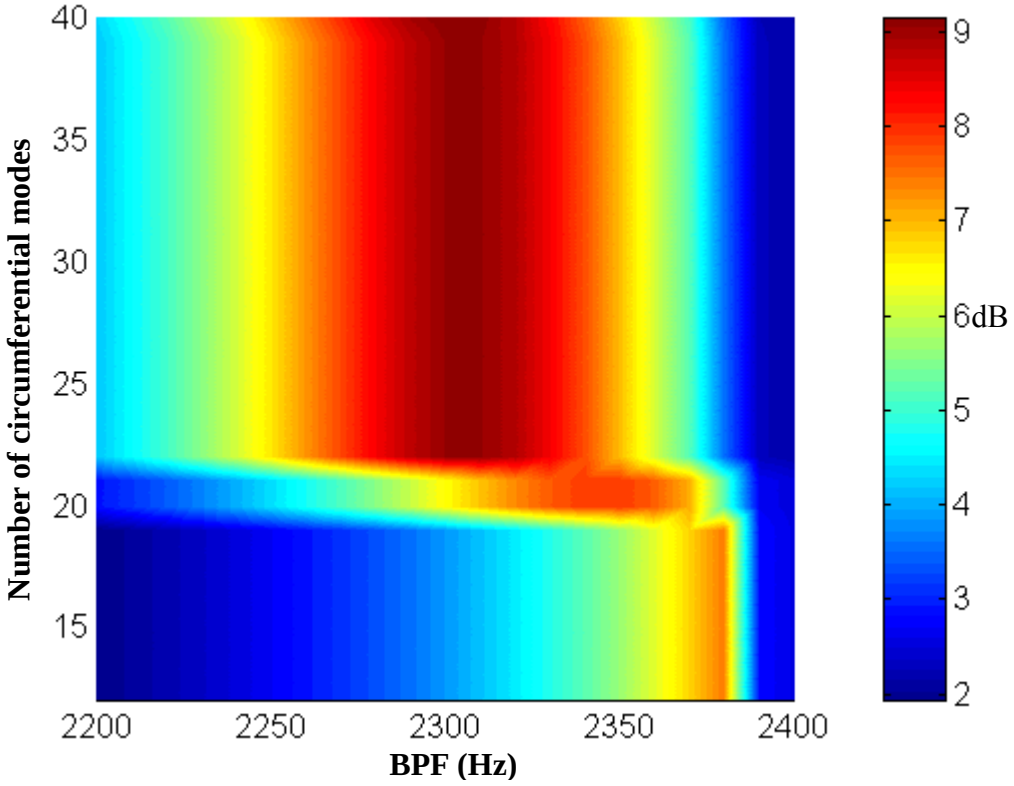

Figure 3-10: Influence of number of circumferential modes on the sound power reduction when 40 radial modes are included in the calculations.

The influence of the total number of circumferential modes is shown in Figure 3-10 where 40 radial modes are included in the computations. Figure 3-10 clearly shows that the sound power reduction level reaches a steady value when more than 22 circumferential modes are included in the computation. Although the contributions of higher-order modes to the impedance function previously studied was noticeable, including more than 22 circumferential modes does not seem to affect the sound power reduction.

In order to limit the computing time and obtain accurate results, the number of modes included in the calculations in the case of an array of 20 tubes will be chosen as 25 circumferential and 20 radial modes unless otherwise specified.

Chapter 4. Noise control mechanisms

In the previous chapter, the HQ system was shown to be very efficient at reducing BPF tones. Moreover, the modeling approach seems to predict to reasonable accurately the noise reduction. Therefore, the model will now be used to try understanding the attenuation mechanisms involved in the HQ tubes system.

An impedance study is first performed, where the dynamics of the HQ system is analyzed as a function of the frequency and the resonances of the system will be identified. A study of the incident and transmitted modal amplitudes will then illustrate the scattering mechanisms. A HQ system with 20 tubes applied to the JT15D engine first introduces the scattering effect of incident energy between radial modes. The effects of the system parameters on this scattering mechanism will then be shown. In particular, the influence of the centerline tube length and distance between tube ends is investigated. A different HQ system with only 10 tubes is studied next. This system shows that the scattering mechanism not only occurs between radial modes but also among circumferential modes. The HQ system is then applied to a more complex engine and two design strategies are compared to investigate the effect of the number of tubes on the efficiency of the system.

The next section shows the effect of each parameter of the HQ system on the sound power reduction. This parametric study shows the variation of the sound power reduction for a range of frequencies from 2200 to 2400 Hz. This study concerns the intrinsic parameters of the HQ system such as tube length, number of tubes, and so forth, as well as the external parameters such as uniform flow velocity. Then, the performance of the

HQ system is investigated for different incident modal contents and the effect of the incident mode order is investigated.

In the previous sections, the HQ tube system investigated consists of a circumferential array of tubes placed uniformly around the circumference. The next section proposes to investigate the performance of new geometries for the tubes. These geometries are based on the idea that modes are propagating in the inlet along helixes. Therefore, in the first system, the tubes are placed in arrays forming a helix while tubes are kept parallel to the inlet axis. The next system investigates the case of a circumferential array where tubes are rotated at an angle with respect to the engine axis. Finally, both systems are combined and arrays are placed in helix with tubes rotated at the same angle as the helix. The aim of this section is to show if there is any improvement in the performance of the system and if there is any relation between the shape of the HQ system and the propagation patterns of the modes.

4.1 Impedance analysis

In this section, an impedance analysis will be performed to have a better understanding of the mechanisms involved in the HQ system. The aim of this study is to look at the dynamics of the inlet duct and of the tubes and analyze their interaction in the frequency domain. In this study, the HQ tube system consists of a circumferential array of 20 tubes with centerline length 11.8 cm and distance between tube ends 9.2 cm. The engine inlet has a diameter of 0.533 m and the disturbance contains the three modes (1,0), (1,1) and (1,2).

The dynamic of the tubes with perforated screens will first be studied when they are placed in free field conditions. At both ends of the tube, the positive and negative propagating plane waves will be reflected and this reflection mechanism will generate standing waves in the tube. Thus, the HQ tube will exhibit some resonances at discrete frequencies. These resonant frequencies can be computed using the tube impedance matrix in equation (2.70). Due to the pressure release condition at tube ends, the resonant frequencies are the frequencies satisfying the equation:

$$\det\begin{bmatrix} Z_{ii}^{t\ell} & Z_{io}^{t\ell} \\ Z_{oi}^{t\ell} & Z_{oo}^{t\ell} \end{bmatrix} = 0 \tag{4.1}$$

The first two resonance frequencies of the tube with a perforated screen at both ends are found to be 1370 and 2740 Hz. However, these resonance frequencies are those of a tube placed in free field. In order to investigate the effect of the inlet duct on the tube dynamics, the impedance of the tube placed in the inlet duct was calculated. The following equations allow to compute the impedance at the input and output ends of the ℓ^{th} tube as

$$Z_{\ell i} = \frac{p_{\ell i}^{t}}{v_{\ell i}^{t}} = Z_{ii}^{t\ell} + Z_{io}^{t\ell}\frac{v_{\ell o}^{t}}{v_{\ell i}^{t}} \tag{4.2}$$

$$Z_{\ell o} = \frac{p_{\ell o}^{t}}{v_{\ell o}^{t}} = Z_{oi}^{t\ell}\frac{v_{\ell i}^{t}}{v_{\ell o}^{t}} + Z_{oo}^{t\ell} \tag{4.3}$$

where $Z_{ii}^{t\ell}$, $Z_{io}^{t\ell}$, $Z_{oi}^{t\ell}$ and $Z_{oo}^{t\ell}$ are expressed in equation (2.71) and the source velocities $v_{\ell i}^{t}$ and $v_{\ell o}^{t}$ are computed from equation (2.73). The tube input impedance is shown in Figure 4-1a as a function of the frequency from 500 to 3500 Hz (the tube output impedance looks very similar). The piston source velocity at this tube end due to the incident modes (1,0), (1,1) and (1,2) is also shown in Figure 4-1b.

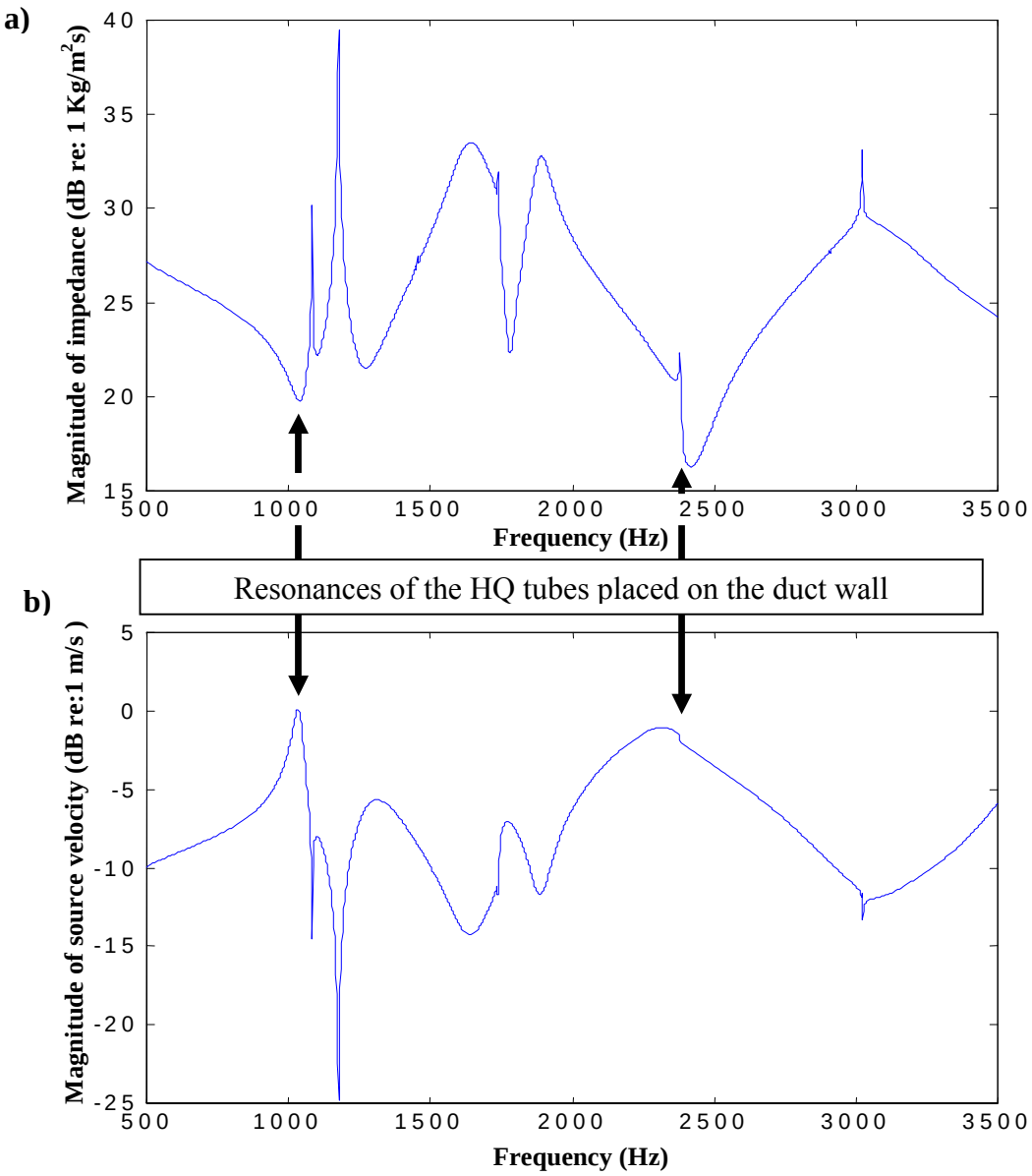

Figure 4-1: a) Input impedance of an 11.8 cm long HQ tube end placed on the duct wall and b) particle velocity of source.

As seen in Figure 4-1a, the impedance of the piston source drops out at two specific frequencies, at 1040 Hz and 2420 Hz. These frequencies correspond to the resonance of the HQ tube placed in the duct. It can be noticed that the resonant frequencies of this system are different from those of the tube placed in free field (1370 and 2740 Hz). The dynamics of the inlet duct actually changes the dynamic of the tube, whose resonance frequencies are shifted down. It is clear in Figure 4-1b that the source velocity increases

at the resonant frequencies, where the impedance exhibits minimum values. It is important how these resonances are affecting the performance of the HQ system. To investigate this, the total sound power reduction provided with 20 HQ tubes was computed and is shown in Figure 4-2.

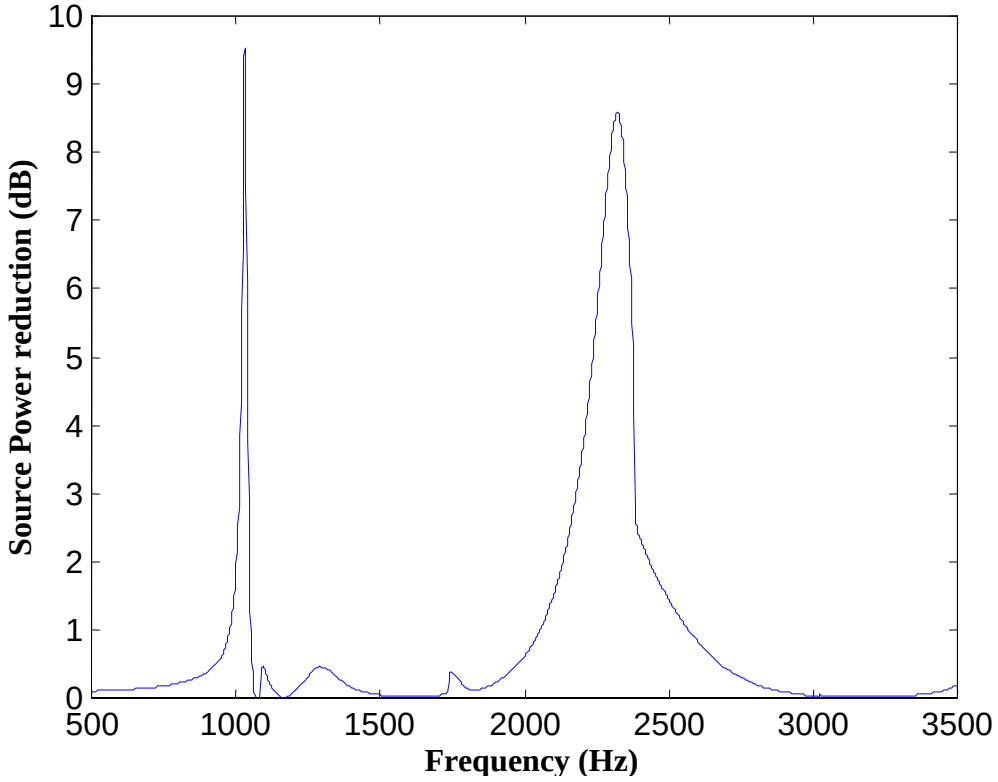

Figure 4-2: Total sound power reduction due to a circumferential array of 20 tubes with three incident modes.

It is interesting to notice in Figure 4-2 that the maximum sound reduction provided by the HQ tube occurs at the frequencies where the source velocity, at the ends of the tubes, was maximal, i.e. at 1030 and 2320 Hz. The sound power reduction provided by the HQ tube is 9.5 and 8.6 dB at these two frequencies, respectively. The key idea here is that the HQ system will show good performance at frequencies where the source velocity at the end of the tubes is high, i.e. at the resonant frequencies of the coupled tube-duct system.

4.2 Radial scattering

Previous studies on the control of plane waves with HQ tubes showed that the only attenuation mechanism happening was reflection of the incident energy [11]. The present study focuses on a cylindrical inlet duct in the presence of higher-order modes. Therefore, one can wonder if the attenuation mechanisms are different in this case. In order to have insight into the noise control mechanisms in this case, the modal amplitudes of the incident, reflected and transmitted modes will be investigated.

In this first study, the HQ system consists of a circumferential array of 20 tubes placed 0.4 m upstream from the fan. The incident disturbance is composed of the modes (1,0), (1,1) and (1,2), i.e. all of the same circumferential order m=1, whose complex amplitudes correspond to those measured on the JT15D engine. The effect of the array of 20 tubes on the sound field in the inlet will be investigated here at a BPF frequency of 2320 Hz. The pressure mode amplitudes in Pa are plotted in the complex plane. For the sake of clarity, in the figures showing the modal amplitudes, the black, red and blue colors are used for the (1,0), (1,1) and (1,2) modes, respectively. These plots allow to see both the magnitude and phase of the modal amplitudes. Figure 4-3a first shows the amplitudes of the incident fan modes. The transmitted and reflected mode amplitudes due to the HQ system are shown in Figure 4-3b and c, respectively.

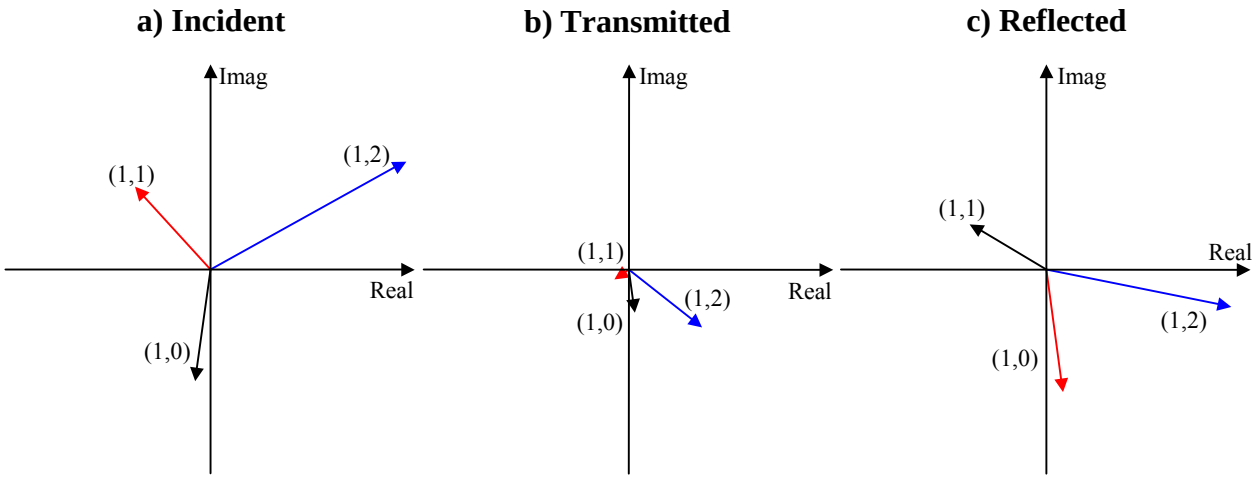

Figure 4-3: Incident, transmitted and reflected modal amplitudes in the case of 20 HQ tubes applied to the inlet of the JT15D engine.

As seen in Figure 4-3b, the amplitudes of the transmitted modes are reduced as compared to the incident amplitudes in Figure 4-3a. This leads to the reduction of the sound power radiated at the end of the inlet. Since the transmitted mode amplitudes are small, the amount of energy reflected back to the fan is important, as seen in Figure 4-3c. In this case, the HQ tube system is very efficient and provides significant reduction in the sound power. However, an important issue is to investigate how the array of HQ tubes produces the significant reflection of the incident disturbance modes and provides such a good sound reduction. To this end, a modal breakdown is carried out where the transmitted and reflected mode amplitudes are computed for each of the incident modes propagating individually. The modal breakdowns for each incident mode (1,0), (1,1) and (1,2) are shown in Figure 4-4 a, b and c, respectively.

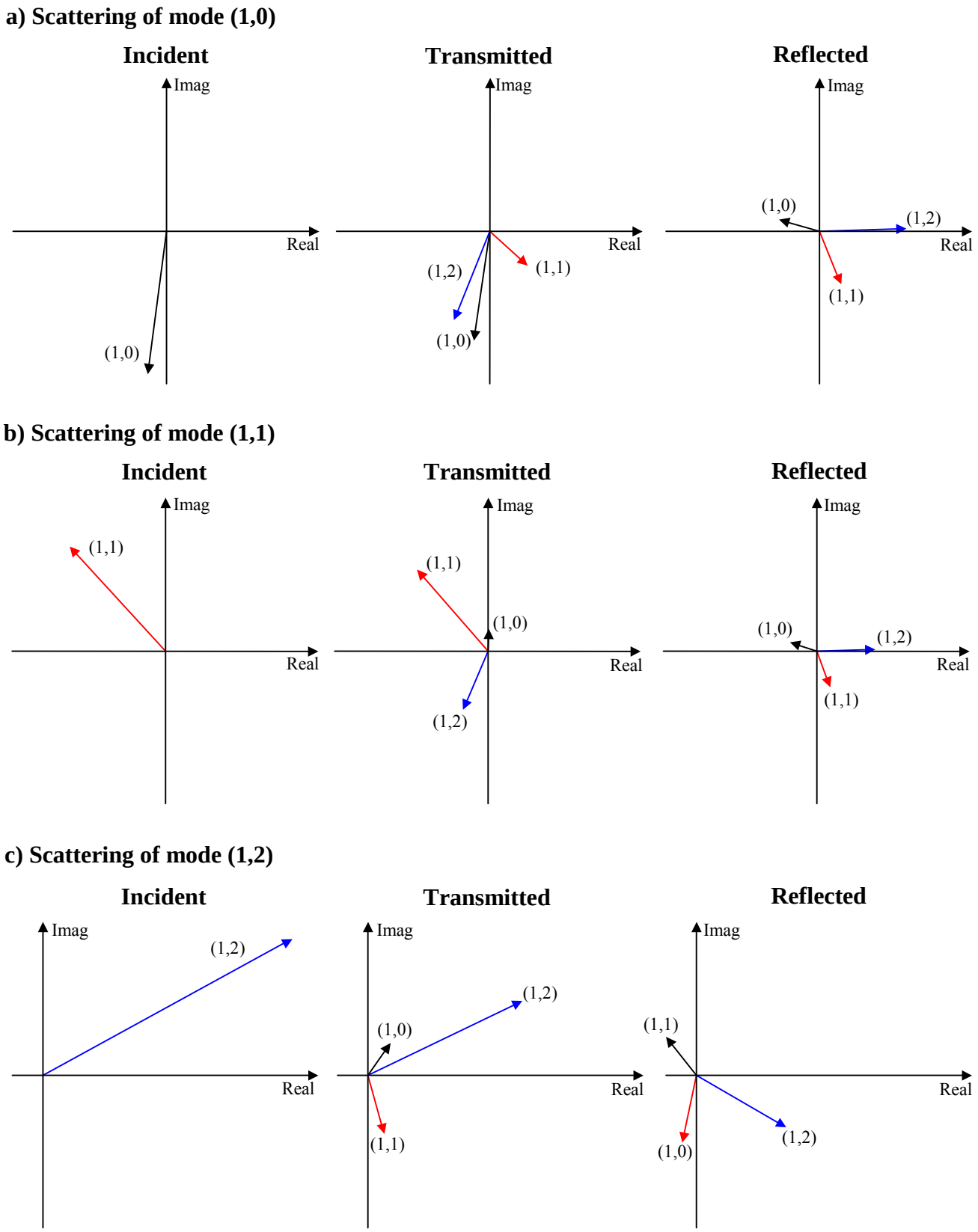

Figure 4-4: Modal breakdown for each incident mode in the case of 20 HQ tubes applied to the inlet of the JT15D engine.

Figure 4-4a shows the incident (1,0) mode amplitude and the resulting transmitted and reflected (1,0), (1,1) and (1,2) mode amplitudes. Figure 4-4b and c show the same breakdown mechanism for incident modes (1,1) and (1,2), respectively. These plots clearly demonstrate that the HQ tube array allows energy in an incident radial mode to be spilled over other radial modes of the same circumferential order. This behavior is referred here as radial scattering effect. These results also demonstrate that there are two mechanisms involved in the reduction of the incident mode. Firstly, the energy in an incident mode is in part reflected back to the fan, and secondly there is some energy scattered into the other radial modes. Figure 4-4 also suggests that there is more energy scattered from the low order into the higher order radial modes than vice versa.

When the three incident modes propagate simultaneously in the inlet duct, the previous scattering effects will happen for each mode and the transmitted and scattered amplitudes will recombine in each mode. Therefore, the suppression of a particular mode is due to the contribution of the scattered energy from other modes. As an example of this mechanism, Figure 4-5 illustrates the suppression of mode (1,1). As shown in Figure 4-5 (enlarged scale), the transmitted component in mode (1,1) recombines with the scattered components from modes (1,0) and (1,2). The total transmitted amplitude in mode (1,1) is simply due to the vector summation of all these components. Therefore, it can be noticed that this recombination occurs in an optimal way and provides large reduction of the incident mode amplitudes.

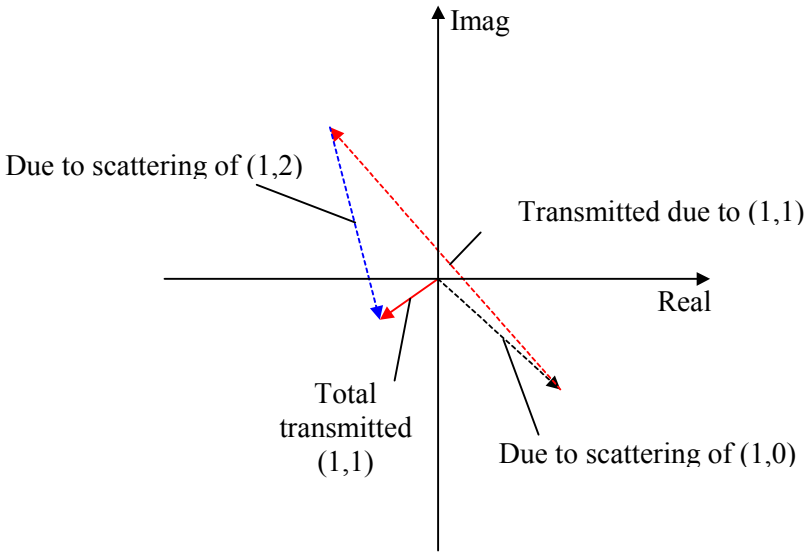

Figure 4-5: Suppression of mode (1,1).

This study allows to show that the main noise control mechanisms involved in the HQ system with 20 tubes are reflection of incident energy and recombination of scattered energy in each radial mode. This behavior should be contrasted to the traditional analysis of the HQ tube to the plane wave where the only noise reduction mechanism that takes place is reflection of the incident wave. Thus, the scattering effect between radial modes and their recombination to yield noise reduction is a new mechanism for HQ tubes in the presence of multiple duct modes.

In the previous example where the HQ system was optimized to provide a maximum sound reduction, it was noticed that the scattered components allowed to reduce the amplitude of mode (1,1) in an optimal way. The scattering of energy into different radial modes and reconstruction of components in each mode; actually depends on the characteristics of the HQ tubes such as centerline length, cross sectional area, distance between tube ends, and so forth. As an illustration, Figure 4-6 shows the modal breakdown analysis for the incident mode (1,0) as a function of the system parameters. Figure 4-6a first shows the result for a range of values of the distance between tube ends, i.e. $D=0.06$ to $0.11\ m$. Figure 4-6b then shows the effect of centerline tube length on the scattering mechanism for a range of length L from 0.105 to $0.145\ m$.

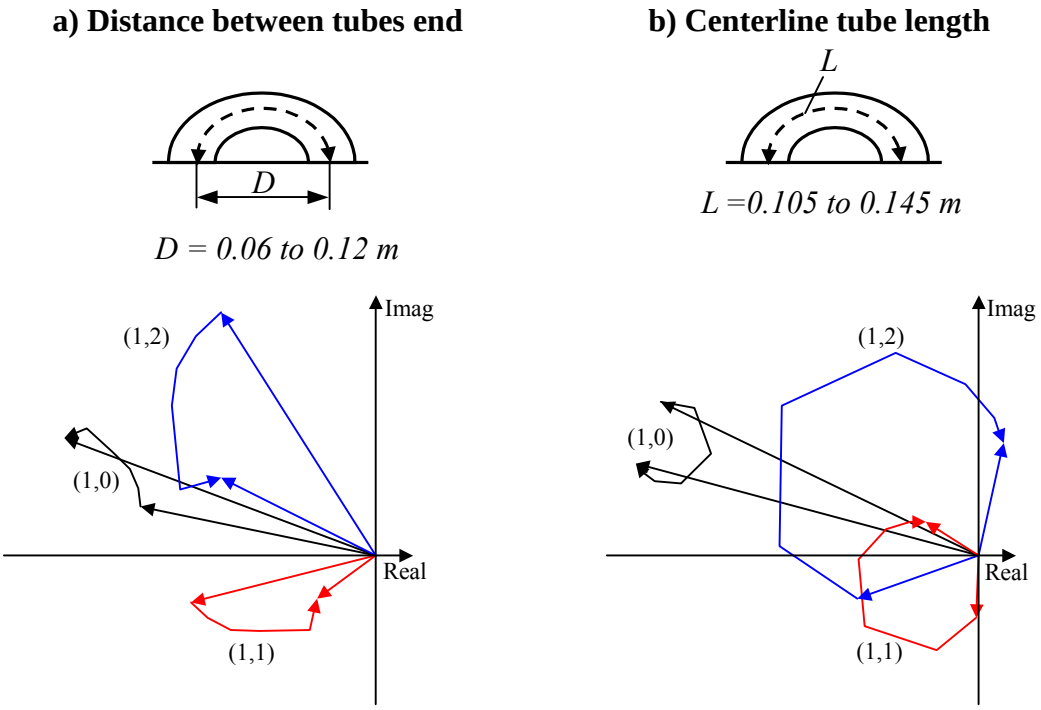

Figure 4-6: Transmitted mode amplitudes for incident mode (1,0) as a function of a) distance between tube ends and b) centerline tube length.

In Figure 4-6, the range of transmitted modal amplitudes corresponding to the parameter values are indicated by the curve connecting the two vectors associated to the lower to upper values of the range. Figure 4-6a shows that the magnitude and phase of the modes created by the scattering of energy is also greatly affected by the distance between tube ends. In the case of the tube length, the effect on the scattering shown in Figure 4-6b is even more dramatic. Therefore, in the process of designing the HQ tube system, it is important to choose the parameters such that the scattering and recombination of energy in each mode occurs in an optimal way.

4.3 Circumferential Scattering

In the previous section, it was shown that the noise attenuation mechanisms for an array of tubes involve reflection of the modes back towards the fan, as well as modal scattering and recombination among radial modes of same circumferential order m. It was assumed that all the modes present in the duct had the same circumferential order m_D as the disturbance. However, for a given input disturbance mode with circumferential order m_D, some of the modes present in the duct with the HQ tubes system can have circumferential order different than the disturbance m_D. This effect takes place because of the spatial alliasing of the discrete number of tubes in the array. The circumferential order of the modes present in a HQ system are predicted by

$$m_{HQ} = m_D \pm kN_T \tag{4.4}$$

where N_T is the number of tubes in the array and k is any integer, i.e. $k=0, \pm1, \pm2, \pm3,\ldots$ Equation (4.4) shows that given an incident disturbance mode of order m_D, acoustic energy will result in modes with circumferential order m_{HQ} (if they are cut-on). Thus, some energy from the m_D disturbance mode will be scattered into m_{HQ} circumferential modes, which it is referred as circumferential scattering.

A simple example can be used to illustrate this circumferential scattering. Assume the disturbance mode is of circumferential order m_D=4 and there are 8 HQ tubes. The tubes will be driven by the disturbance mode and the particle velocity between tubes will have the same magnitude but the phase between adjacent tubes will be 180°. This is shown in the schematic of Figure 4-7. Selecting k=2 from equation gives $m_{HQ} = 4 - 2\times 8 = -12$. Therefore, a mode of circumferential order 12 and spinning in the opposite direction as the disturbance mode, will be excited by the HQ system.

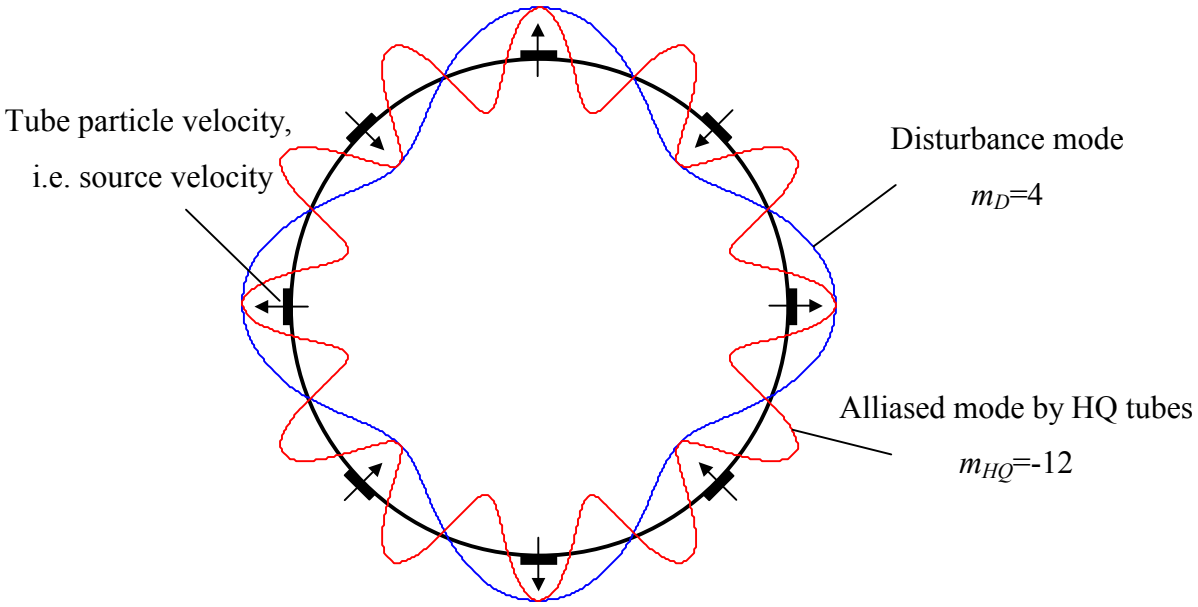

Figure 4-7: Spatial alliasing due to an array of 8 tubes with a disturbance mode of circumferential order m_D=4.

Thus, the previous effect leads to two possible design strategies for the HQ tubes system. First, the number of tubes can be designed to be sufficient enough so that there is no acoustic content scattered into cut-on m-order modes at the frequency of analysis. On the other hand, the number of tubes can be selected such that additional m-orders are excited by the HQ tube system (i.e., m_{HQ} for $k \neq 0$ that are cut-on). Results from these two different design approaches will be investigated here.

In this example, the disturbance again contains modes (1,0), (1,1) and (1,2) at a frequency of 2320 Hz and the mode amplitudes are those measured on the JT15D engine. The sound reduction results provided by two different HQ systems are investigated. The first system contains 20 tubes and the second has only 10 tubes. The efficiency of both systems is measured in term of the total sound power reduction and is shown in Table 4-1. This table also shows the reduction in each propagating transmitted mode.

Mode	20 Tubes	10 Tubes
(1,0)	8.0	1.6
(1,1)	16.4	2.6
(1,2)	7.5	4.2
(-9,0)	*Not present*	-113.6
Total	8.6	1.1

Table 4-1: Modal and total Sound Power reduction in dB for arrays of 20 and 10 HQ tubes applied to the inlet of the JT15D engine.

The transmitted modal content for the inlet with 20 tubes is shown in the second column of Table 4-1. It shows a sound power reduction of 8.0, 16.4 and 7.5 dB of the three radials, (1,0), (1,1) and (1,2), respectively, for an overall reduction of 8.6 dB. The lowest *m*-order mode excited by the 20 tubes system is $m_{HQ}=-19$ (see equation (4.4) and Table 3-1), which is cut-off at 2320 Hz. Thus, the only modes present with the HQ tubes system are those modes that were present in the disturbance (no scattering between *m*-order modes). The noise control mechanisms happening in this case are only the reflection of incident energy and recombination of scattered energy among the three radial modes. As seen in this table, the HQ system is very efficient in this case.

On the other hand, the transmitted modal content for the inlet with 10 tubes is shown in the third column of Table 4-1. In this case, there is energy scattered into mode (-9,0) from the incident modes (1,0), (1,1) and (1,2) ($m_{HQ}=-9$ for $k=-1$ in equation (4.4) and Table 3-1). The results show a power reduction of 1.6, 2.6 and 4.2 dB for the (1,0), (1,1) and (1,2) modes, respectively. Note that there is now 113.6 dB of acoustic content in the (-9,0) mode, which was scattered into. The overall noise reduction is now only 1.1 dB. That is, the overall reduction is greatly diminished with only 10 tubes (allowing scattering effects between *m*-order modes) as compared to 20 tubes (without scattering).

To examine in depth the scattering mechanisms taking place here, the modal breakdown will be shown for both systems. Figure 4-8a and b show the modal

breakdown of the incident mode (1,1) in the case of an array of 20 and 10 HQ tubes, respectively.

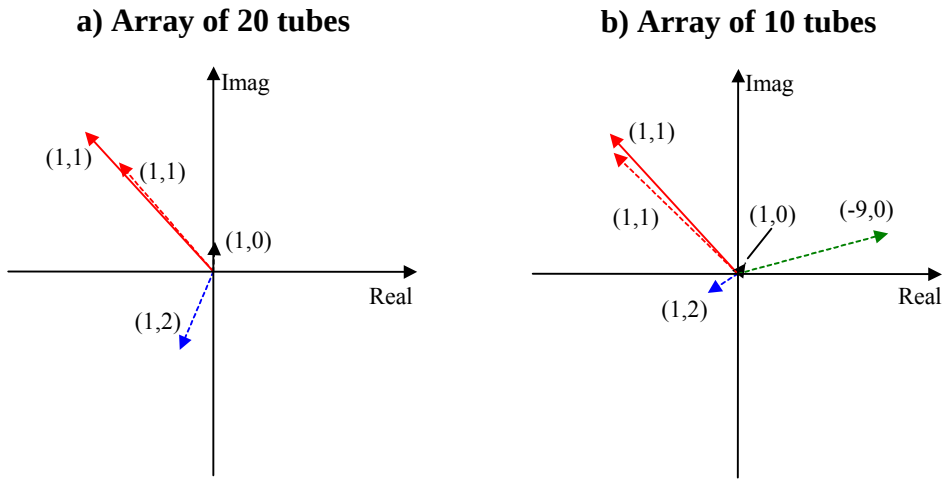

Figure 4-8: Scattering of mode (1,1) with an array of 20 or 10 HQ tubes applied to the inlet of the JT15D engine.

In Figure 4-8, the straight red line represent the amplitude of incident mode (1,1), whereas the dashed lines show the transmitted amplitudes in the scattered modes (1,0), (1,1), (1,2) and (-9,0). By comparing both plots in Figure 4-8a and b, it is clear that a significant portion of the incident mode (1,1) energy scatters into the (-9,0) mode and that the amount of energy scattering from the (1,1) to the other radial modes is very small in the case of 10 tubes. It can also be noticed that the transmitted amplitude in mode (1,1) is smaller in the case of 20 tubes.

As the scattering mechanism depends on the number of tubes in the system, the recombination of energy in each mode will obviously be different for both systems. The modal recombination of scattered energy for the suppression of mode (1,1) in the case of 20 and 10 HQ tubes is shown in Figure 4-9.

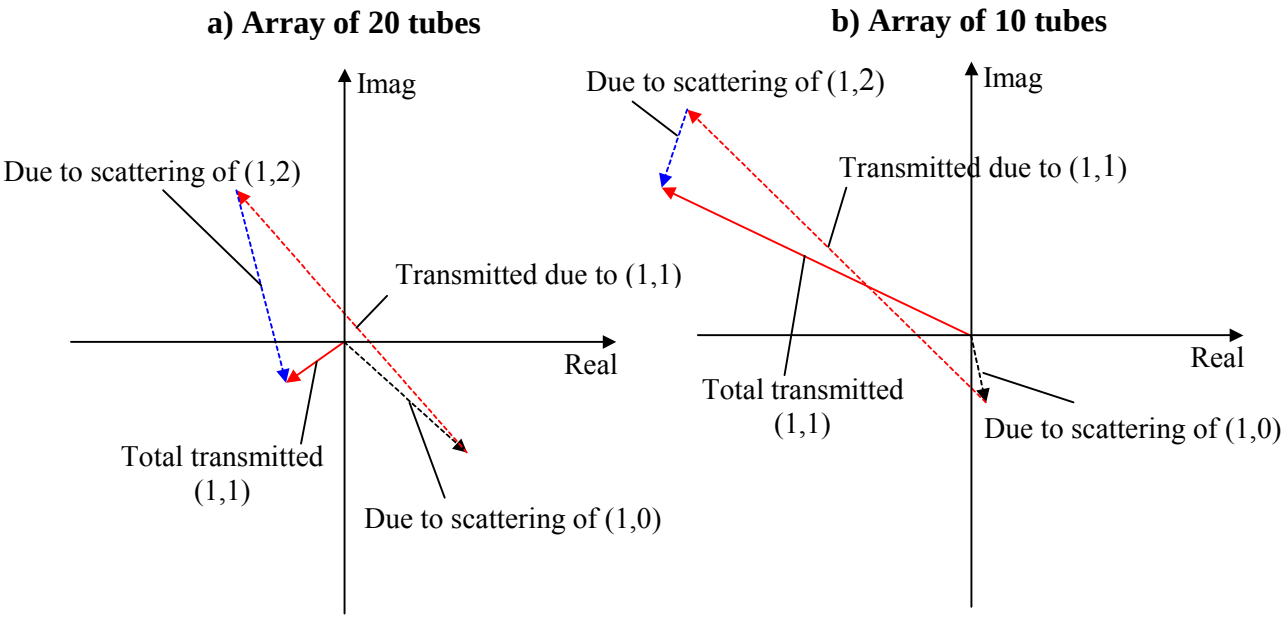

Figure 4-9: Suppression of mode (1,1) with 20 and 10 HQ tubes applied to the inlet of the JT15D engine.

It is clear in Figure 4-9 that the recombination mechanism is less effective with 10 tubes than in the case of 20 tubes. When scattering into other *m*-order modes is allowed, the attenuation mechanism provided by the recombination of scattered energy is severely reduced.

This analysis showed that scattering the acoustic content only among radial modes by using a high number of tubes results in significant cancellation of the radial modes. On the other hand, allowing the energy to scatter to another *m*-order mode by choosing a low number of tubes reduces the effect of the HQ tubes phase cancellation mechanism. Thus, the scattering and recombination of acoustic energy among radial modes of a single circumferential order is shown to be a primary mechanism of attenuation.

In the previous analysis, the disturbance only contained modes of the same circumferential order *m=1*. In this case, the energy scattered into the other circumferential order mode causes an increase in the sound radiation. An interesting issue would be to investigate the effect of this scattering mechanism in the case of incident modes of different circumferential order. This is the case of the AlliedSignal engine,

where incident modes of circumferential orders –8, 2 and 12 simultaneously propagate at the BPF of 2250 Hz. In this case, an array of 10 tubes would allow scattering of energy from one circumferential mode into the other two and if the recombination of energy in each mode happens optimally, this HQ system could eventually be very effective. Therefore, one can wonder if allowing the scattering into circumferential modes could, in this case, result in better performance than with a system with a high number of HQ tubes. In order to answer this question, a system with 27 tubes will be compared to a system with only 10 tubes. In the case of 27 tubes, there is no scattering of energy between circumferential modes but only into cut-on radial modes. The dimensions of the tubes (centerline length and distance between tube ends) in both cases were optimized using genetic algorithms to provide maximum reduction at 2250 Hz. In the case of 27 tubes, the centerline tube length was found to be 12.3 cm and the distance between tube ends 6.6 cm. In the case of 10 tubes, the centerline tube length is 11.4 cm and the distance between tube ends is 6.2 cm. The tube cross-sectional areas were chosen in both systems to keep the cross-sectional area ratio equal to 0.1. The result of this study is shown in Figure 4-10.

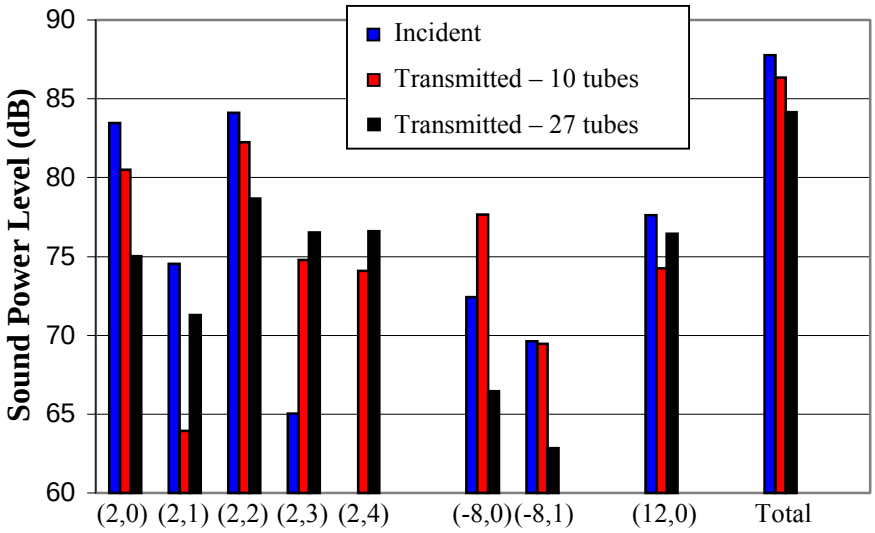

Figure 4-10: Modal and total sound power reduction for arrays of 27 and 10 HQ tubes applied to the AlliedSignal engine at 2250 Hz.

As seen in Figure 4-10, the total sound power reduction is 1.4 dB with 10 tubes and 3.7 dB with 27 tubes. Therefore, the system with a higher number of tubes (no scattering into circumferential modes) allows to achieve a better total sound power reduction. Although the system with 10 tubes was optimized to provide maximum reduction at 2250 Hz, it still has lower performance than the system with 27 tubes. Therefore, allowing the scattering between circumferential modes did not allow to increase the sound power reduction.

After looking at the individual transmitted modal amplitudes, the following conclusions could be drawn. When the number of tubes is high enough to avoid scattering into other *m* order modes, the reflection of the incident energy is more important as well as the scattering effect between radial modes. On the other hand, when scattering into circumferential modes is allowed (by having a low number of tubes), the reflection effect is less important and more energy tends to be scattered into circumferential modes than in radial modes. Another interesting conclusion is that the scattering into circumferential modes effect tends to be more important from low order into higher-order modes than vice-versa. This mechanism was observed previously in the case of scattering between radial modes. These conclusions were made by investigating the amplitudes of the transmitted modes with only one incident mode propagating at a time. These amplitudes are not shown here to avoid getting into too much complexity. However, these conclusions are illustrated in Figure 4-10 and will be explained next.

As seen in Figure 4-10, modes (2,0) and (2,2) show great reduction with 27 tubes. This is due to the important reflection of the incident energy in these two modes and also to a good recombination of the scattered energy from all the other modes. However, the energy transmitted in modes (2,3) and (2,4) is higher in the case of 27 tubes. This is due to the fact that more energy is scattered into these modes with 27 tubes and the scattered energy does not recombine optimally. Modes (8,0) and (8,1) show very little reduction or even increase in the transmitted sound power level with 10 tubes. This is mainly due to the important scattering of energy from modes of circumferential order *m=2*. Finally, mode (12,0) shows a better reduction in the case of 10 tubes. In this case, an important part of the incident content in this mode is scattered into all the other lower-order modes,

largely reducing the amount of energy left in this mode; whereas with 20 tubes, the only reduction happening is due to reflection.

The previous study illustrated the main noise control mechanisms involved in the HQ system. A new mechanism takes place in the case of higher-order modes, i.e. not only is the incident energy reflected as in the plane wave case, but recombination of scattered energy and phase cancellation also contributes to the noise reduction. The number of tubes was shown to be a determinant criterion governing the scattering process. In general, the HQ system tends to show better performance with a higher number of tubes. In this case, the propagation of energy into other circumferential order modes can be avoided and the only scattering effect occurs between radial modes. However, it is important to remark that these conclusions are applicable only in the case of a hard-wall inlet. If the HQ tubes are combined with a liner, it could be very effective to scatter energy into *m*-order modes that the liner can effectively attenuate. In particular, the scattering effect seems to be more important from lower to higher order modes, which is a very interesting issue in the case of a liner. The attenuation provided by a liner is indeed much higher as the order of the mode increases.

4.4 Parametric Study

In this section, a parametric study will be performed to analyze the influence of the various parameters of the HQ system on the sound reduction. The parameters investigated here are the axial position of the array of tubes, centerline tube length, distance between tube ends, number of tubes, and tube cross-sectional area. Besides these parameters defining the geometry of the HQ system, the effect of uniform flow velocity will also be investigated.

In this study, the dimensions and configuration of the JT15D engine will be used. The effect of the HQ system will be investigated for the control of the BPF tone, with BPF frequencies ranging from 2200 to 2400 Hz. The basic configuration of the HQ system used in this parametric study corresponds to the optimal system, i.e., one array of 20 tubes located at 0.45 m upstream from the fan. The HQ tubes have a centerline length of 0.118 m and the distance between the tube ends is 0.092 m. The tube diameter is 0.038 m yielding to a cross-sectional area of 0.00113 m^2. The computations will be done by including 25 circumferential and 20 radial modes in the Green's function.

The effect of the various parameters will first be investigated over the BPF range and in the case of three incident propagating modes. The amplitudes of these three modes of order (1,0), (1,1) and (1,2) correspond to those measured in the JT15D engine. Then, the effect of the centerline tube length will be investigated for a more general case. For this purpose, the sound power reduction will be shown while having each cut-on mode individually propagating in the disturbance. This will allow to know if the performance of the HQ system is related to the disturbance modal content.

4.4.1 Axial location of array

The effect of axial location of the array is first studied and is shown in Figure 4-11. The sound power reduction in dB is plotted as a function of the blade passage frequencies (BPF) and the axial position of the array. In this figure, the variation of colors

corresponds to the level of sound power reduction. The array location ranges from 10 to 60 cm upstream from the fan.

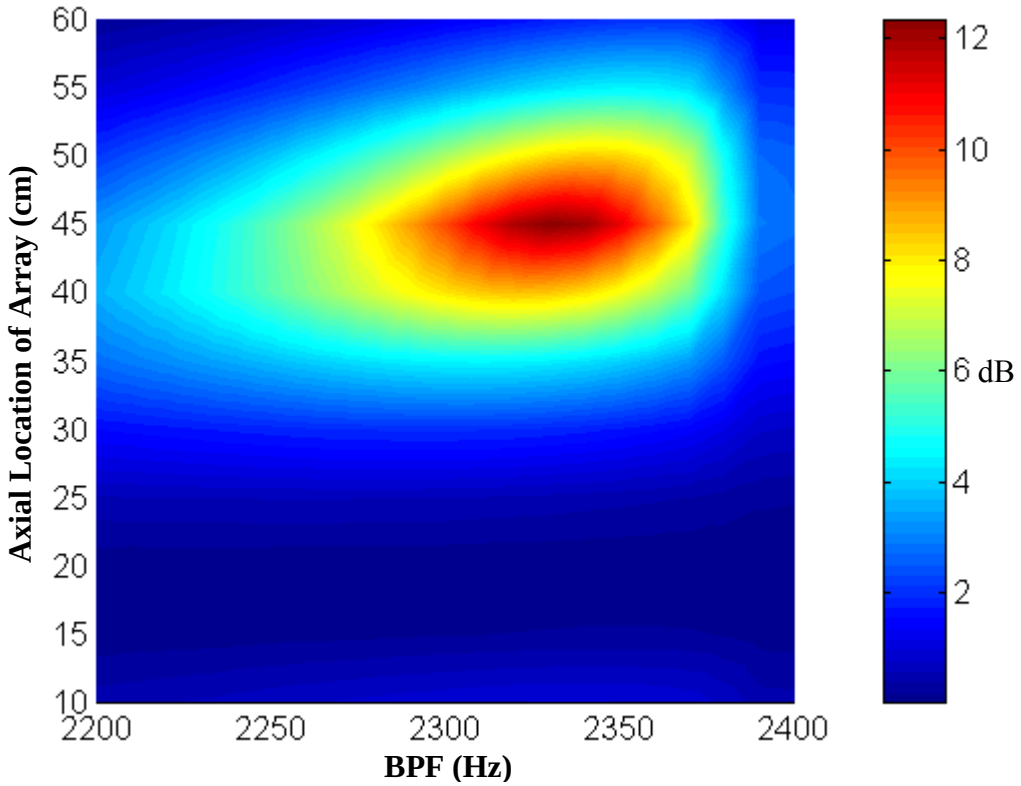

Figure 4-11: Effect of axial location of array on sound power reduction.

Figure 4-11 shows an extreme sensitivity of the noise reduction to the axial position of the tubes on the inlet wall. The optimum location is 45 cm upstream from the fan. At that position, the sound power reduction is higher than 10 dB at frequencies from 2300 up to 2350 Hz. As the array is moved away from this position from as little as 10 cm, the sound power reduction rapidly decreases and becomes less than 5 dB. It eventually drops out under 1 dB as the array is moved further away from the optimum location.

Since the three modes present in the disturbance are of different radial order, i.e. 0, 1 and 2, they do not propagate and spin the same way. Therefore, the recombination and cancellation of energy in each mode illustrated in the previous section will depend on the axial location of the array. Some locations exist for the array where the acoustic energy

from the three incident modes optimally recombines and results in maximum sound reduction. This location is 45 cm upstream from the fan in this case.

Although the model shows sensitivity of the system to the axial position of the array, this behavior was not observed in the experimental tests. The experimentally measured noise reduction is indeed not very sensitive to the axial location of the array. This divergence between the experimental results and the predictions is probably due to simplifications made in the development of the model. The reflection of the acoustic energy at the open end of the inlet and at the fan is indeed a mechanism that certainly takes place in a real engine. These effects are not taken into account in the modeling technique developed here and are probably the main factor in the difference between experimental and analytical results.

4.4.2 Centerline Tube length

The variation of the sound power reduction as a function of BPF and the centerline tube length is investigated here. Figure 4-12 shows the effect of this parameter for tubes having a length from 105 to 130 mm.

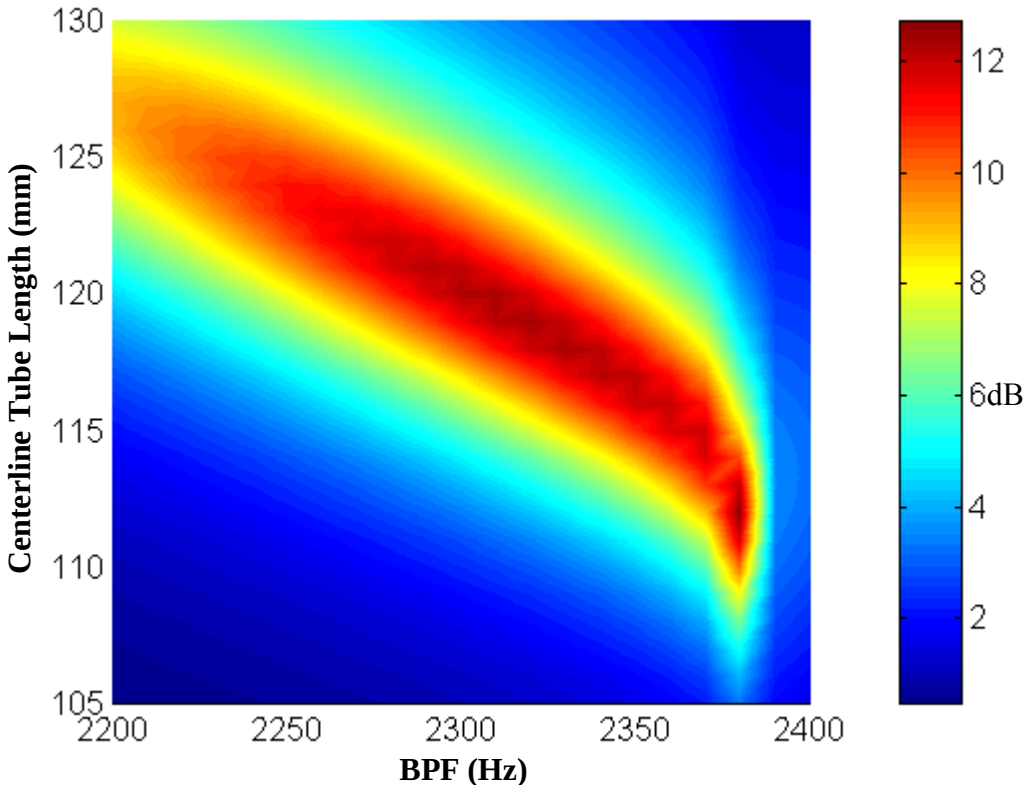

Figure 4-12: Effect of tube length on sound power reduction.

Figure 4-12 shows an important correlation between the frequency of maximum sound reduction and the centerline tube length. Increasing the tube length from 114 to 127 mm causes the resonant frequency of the system to decrease linearly from 2380 to 2200 Hz. Above 2380 Hz, the sound power reduction suddenly drops from 12 dB to less than 5 dB. This is due to the fact that mode (1,3) starts to be propagating above this particular frequency. Therefore, some acoustic energy from the incident modes (1,0), (1,1), and (1,2) is scattered into mode (1,3) and radiated in the far field.

It is important to notice that the HQ system is very sensitive to a change of the centerline tube length. Changing the tube length by only 10 mm (less than 10%) may shift the frequency of reduction by more than 100 Hz. Therefore, in the process of designing the HQ tube system to provide reduction at a specific frequency, the tube length will be a determinant parameter.

4.4.3 Distance between tube ends

Figure 4-13 shows the sound power reduction as a function of BPF and distance between tube ends. This length corresponds to the distance along the inlet axis between the centers of the two openings of a tube. The distance between tube ends ranges from 40 to 115 mm, which is the largest possible range for a tube with centerline length 118 mm and diameter 38 mm.

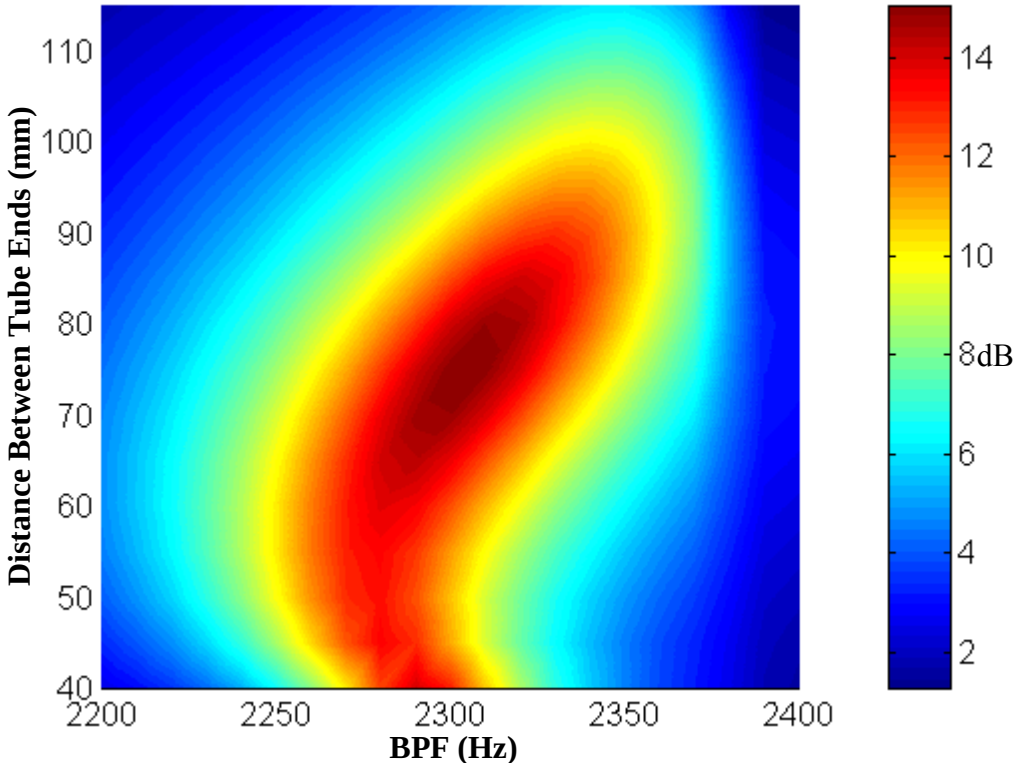

Figure 4-13: Effect of distance between tube ends on sound power reduction.

As seen in Figure 4-13, the HQ system provides optimal sound reduction for a distance between tube ends ranging from 60 to 85 mm. The power reduction for these distances is higher than 13 dB and concentrated on BPF from 2280 to 2330 Hz. At these optimum values, there is more scattering of energy between modes and the recombination of scattered energy is optimum. However, this parameter does not seem to affect significantly the optimum frequency of reduction of the system.

4.4.4 Tube length by keeping the tube shape constant

Previous work on HQ tube was mainly concentrated on control of plane wave in ducts of small diameters. The frequency of optimum reduction of such systems was shown to be directly proportional to the ratio of centerline tube length over distance between tube ends [10]. In order to know if this assumption could be applied to the present systems where several higher-order modes are propagating, the centerline length of the tubes was changed while the ratio of tube length over distance between ends was held constant. This is what is meant here by "keeping the tube shape constant". The sound power reduction in this case is shown in Figure 4-14 where the tube length ranges from 105 to 130 mm. The ratio of tube length over distance between tube ends is kept constant at 1.28. Therefore, the corresponding distance between tube ends spans from 82 to 105 mm.

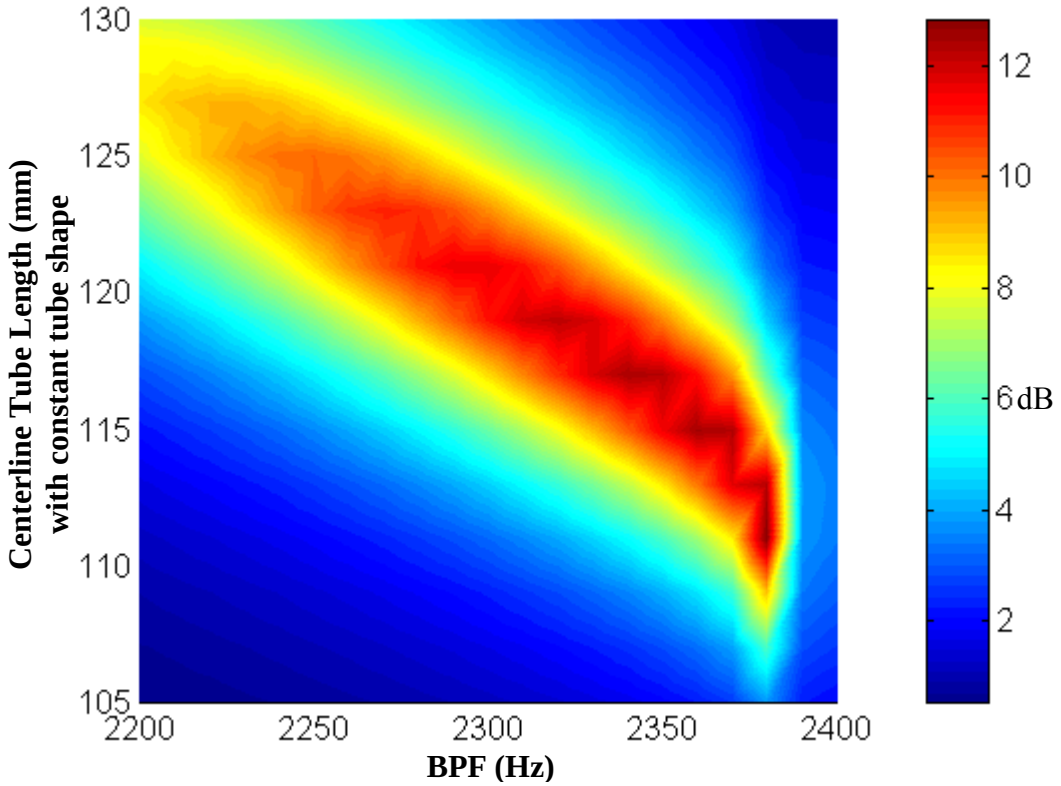

Figure 4-14: Effect of tube length on sound power reduction when shape of tube stays the same.

It should be expected no variation in the frequency of optimum reduction when the tube length is changed. However, it is clear in Figure 4-14, that this frequency is changing linearly with the tube length, even if the ratio of tube length over distance between tube ends is held constant. This clearly demonstrates that the parameter that dictates the frequency of reduction of the HQ system is the tube length and not the ratio of tube length over distance between tubes as for the plane wave case.

4.4.5 Tube Cross-sectional Area

Figure 4-15 shows the effect of tube cross-sectional area on the sound reduction. The values of tube cross-sectional areas range from 6 to 30 cm^2. The corresponding tube cross-sectional area ratios (ratio of total tube cross-sectional area over cross-sectional area of the engine inlet) range from 0.05 to 0.27.

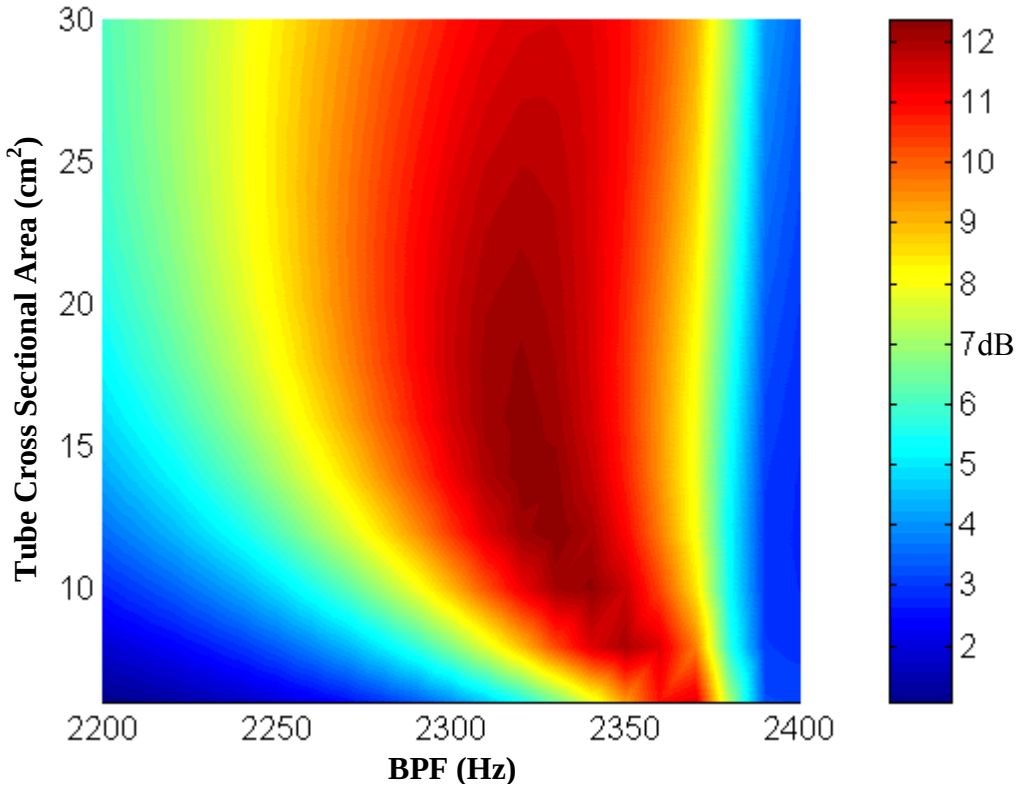

Figure 4-15: Effect of tube cross-sectional area on sound power reduction.

Figure 4-15 shows that the sound power reduction remains higher than 12 dB from 2310 to 2340 Hz for values of tube cross-sectional area spanning from 12 to 30 cm^2. For cross-sectional area less than 12 cm^2, the HQ system seems to be less efficient. This is due to the fact that, as the area of the tubes decreases, the acoustic energy radiated by these tubes also decreases and the system becomes less and less efficient at reducing the incident energy. This shows that the tube cross-sectional area is not a determinant criterion for the efficiency of the HQ system because it does not affect much the frequency or the level of noise reduction.

4.4.6 Number of tubes

The variation of the sound power reduction as a function of BPF and the number of tubes in the array is investigated here. The number of tubes in the array will vary from 4 to 36. For this study, the number of modes included in the Green's function was increased to 40 circumferential and 40 radial modes. As the number of tubes in the array increases, the distance between the piston sources corresponding to the tube ends decreases; therefore, the near-field effects due to cut-off modes become more and more important. To reach convergence, the number of modes in the Green's function needs to be sufficiently high. This is the reason why the number of modes included in the calculation of the Green's function was increased. Figure 4-16 shows the results of this parametric study.

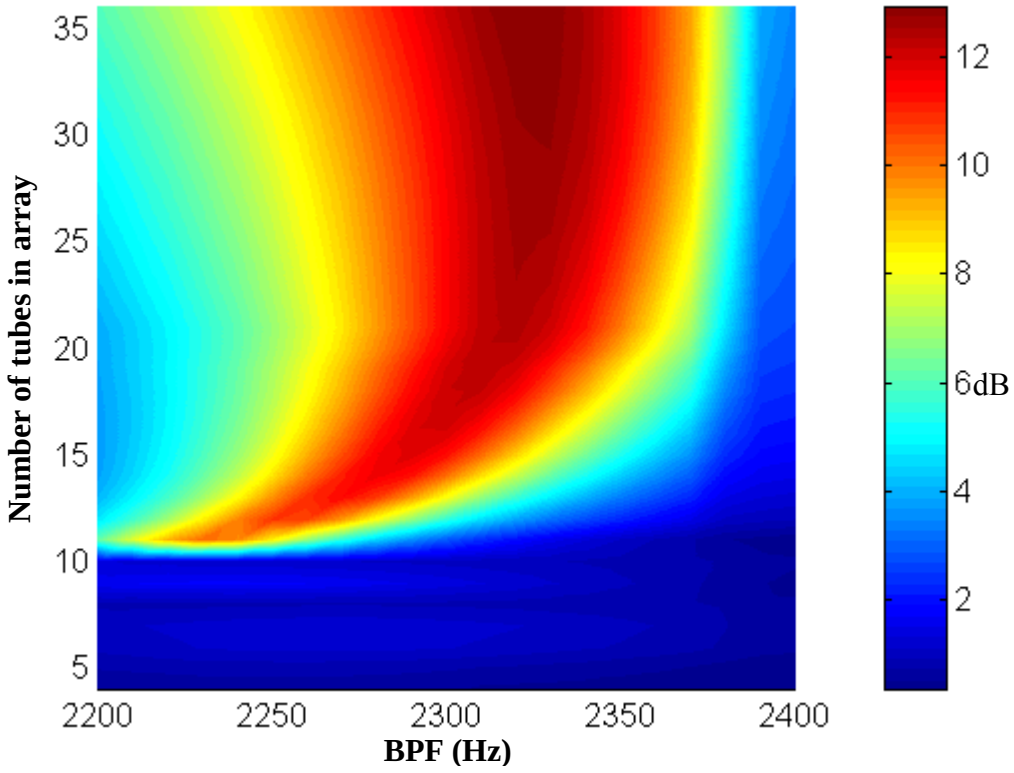

Figure 4-16: Effect of number of tubes on sound power reduction.

As shown in Figure 4-16, the most significant reduction occurs when the number of tubes exceeds 10. In particular, arrays of more than 20 tubes achieve sound power reduction of more than 12 dB over a frequency span from 2300 to 2350 Hz. However, an array of less than 10 tubes, only achieves reduction of 2 dB maximum.

This strong impact of the number of tubes on the sound reduction is once again due to scattering effects. From the scattering equation earlier presented, $m_{HQ}=m_D\pm kN_T$, the minimum number of tubes for no cut-on circumferential modes to be excited is $N_T=11$. Therefore, if there are less than 11 tubes in the array, energy from the three incident modes (1,0), (1,1) and (1,2) will be scattered into a propagating circumferential mode. This mode will then radiate acoustic energy and cause the sound power level to increase.

Figure 4-16 also shows that increasing the number of tubes from 20 to 36 does not necessarily improve the efficiency of the HQ system. It just allows to slightly broadening the frequency span of reduction, making the system more robust.

4.4.7 Duct uniform flow effect

Figure 4-17 shows the sound power reduction as a function of BPF when the uniform flow velocity and direction changes. The flow Mach number spans from –0.4 to 0.4. A negative flow Mach number corresponds to the case where the sound field is propagating in the opposite direction as the flow.

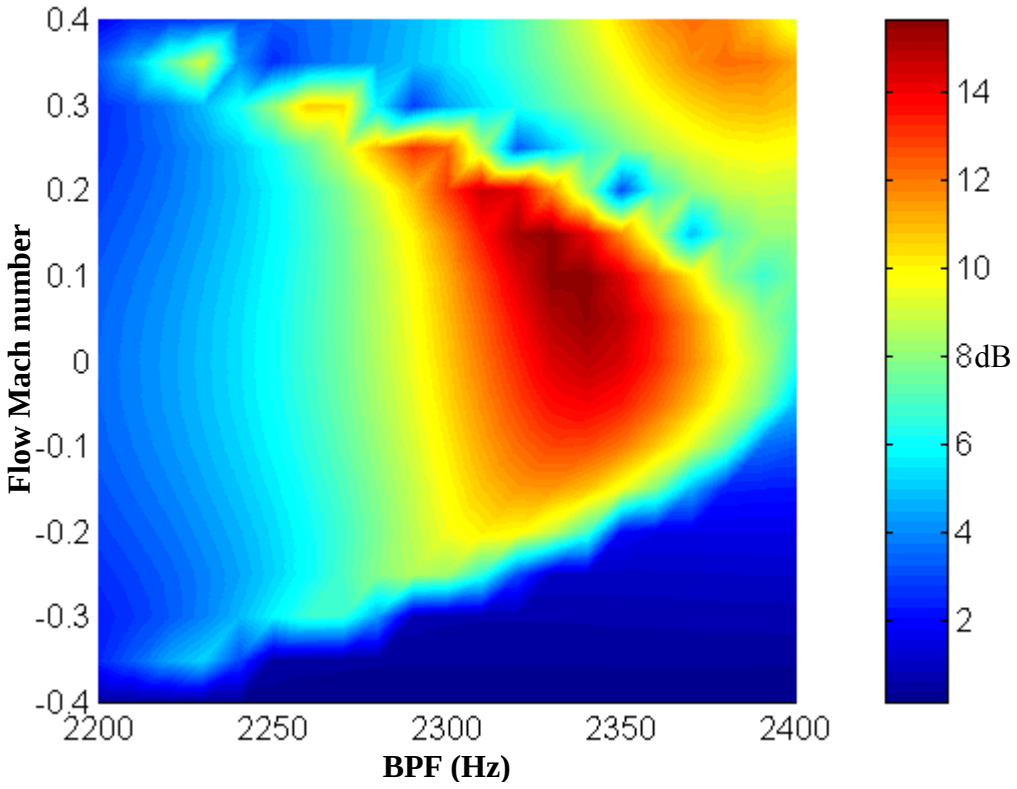

Figure 4-17: Effect of uniform flow velocity on sound power reduction.

Figure 4-17 shows that the HQ system is more efficient when the flow Mach number is small. The sound power reduction is indeed higher than 10 dB for flow Mach numbers smaller than 0.2 for both direction of flow. When the flow velocity becomes larger, the reduction rapidly drops off. It can also be noticed that the sound reduction is higher when the flow is propagating in the same direction as the sound field, i.e. for positive Mach numbers. However, this plot does not necessary show that the HQ system is inefficient at high Mach flow numbers. The HQ system was investigated at higher

Mach numbers. Thus, the HQ system was optimized to provide good reduction at flow Mach number of 0.4, which corresponds to values present in real engines. With tubes of centerline length 12.3 cm and distance between ends of 11 cm, the HQ system provides indeed 11.6 dB power reduction at 2320 Hz. Therefore, the flow condition in which the HQ system will be used, has to known in order to be design the system.

4.4.8 Mode order

In the previous study, the centerline tube length was shown to be the dominant parameter to dictate the frequency of maximum reduction of the HQ system. An increase in the tube length caused the frequency of reduction to decrease linearly. This was for the case of 3 incident modes propagating in the inlet. However, an interesting issue would be to know if this linear variation depends on the order of the incident modes. In order to investigate this effect, each mode cut-on at 2200 Hz was put individually in the disturbance and the length of the tubes was changed to see the effect on the sound power reduction.

Figure 4-18 shows the effect of changing the centerline tube length from 105 to 135 mm for different incident modes. Each of the plots corresponds to a case where there is only one incident mode propagating in the inlet. Figure 4-18a through j show the sound power reductions for the incident modes (0,2), (1,1), (2,1), (3,1), (4,0), (5,0), (6,0), (7,0), (8,0) and (9,0), respectively. In fact, there are 20 modes cut-on at 2200 Hz; however, the plots corresponding to modes of same circumferential order look very alike. The effect of the tube length is very similar, only the level of power reduction is slightly different and increases with the radial order of the modes. Therefore, for the seek of clarity, plots are shown here only for modes of different circumferential order.

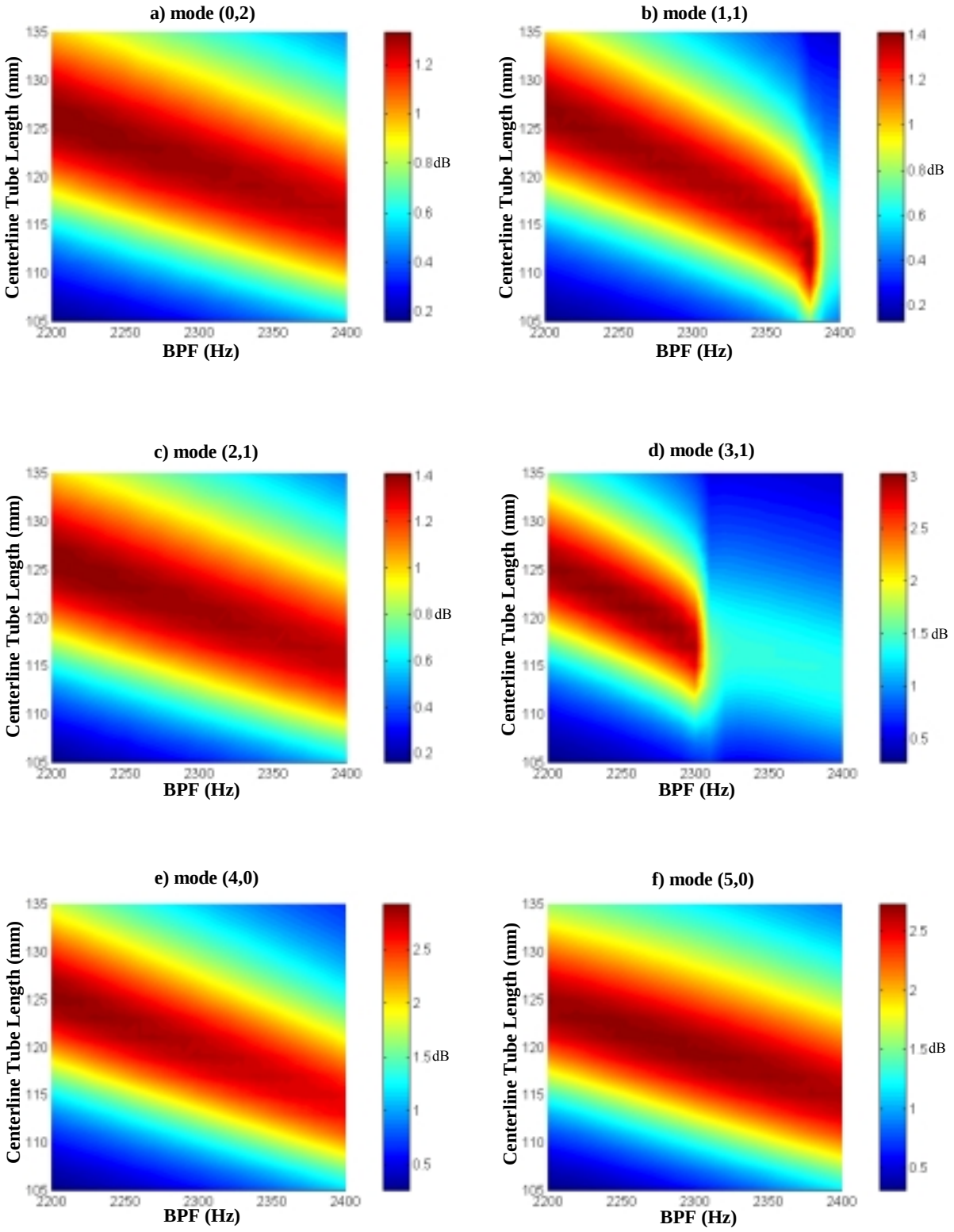

Figure 4-18a-f: Effect of tube length on sound power reduction for different incident modes.

Figure 4-18a through f very clearly show the linear variation of the optimum frequency of reduction with the tube length observed previously in the case of the three incident modes. Increasing the centerline tube length from 114 to 125 causes the frequency of optimum reduction to decrease proportionally from 2400 to 2200 Hz. The order of the incident mode does not seem to alter this behavior.

However, Figure 4-18b and d, corresponding to modes of circumferential order 1 and 3, respectively, show a sudden decrease in the sound reduction at frequencies higher than 2381 and 2307 Hz, respectively. These two frequencies correspond to the cut-off frequency of modes (1,3) and (3,2), respectively. This effect is due to the scattering of energy between radial modes. In the case of the modes of circumferential order 3, i.e. Figure 4-18d, the HQ system effectively works for frequencies lower than 2307 Hz, where modes (3,0) ad (3,1) are well cut-on. However, as soon as a new radial mode starts to propagate, mode (3,2) cut-on at 2307 Hz here, energy from the incident mode (3,0) or (3,1) is scattered into this new propagating mode (3,2) and propagates through the inlet, causing a sudden decrease in the sound power reduction.

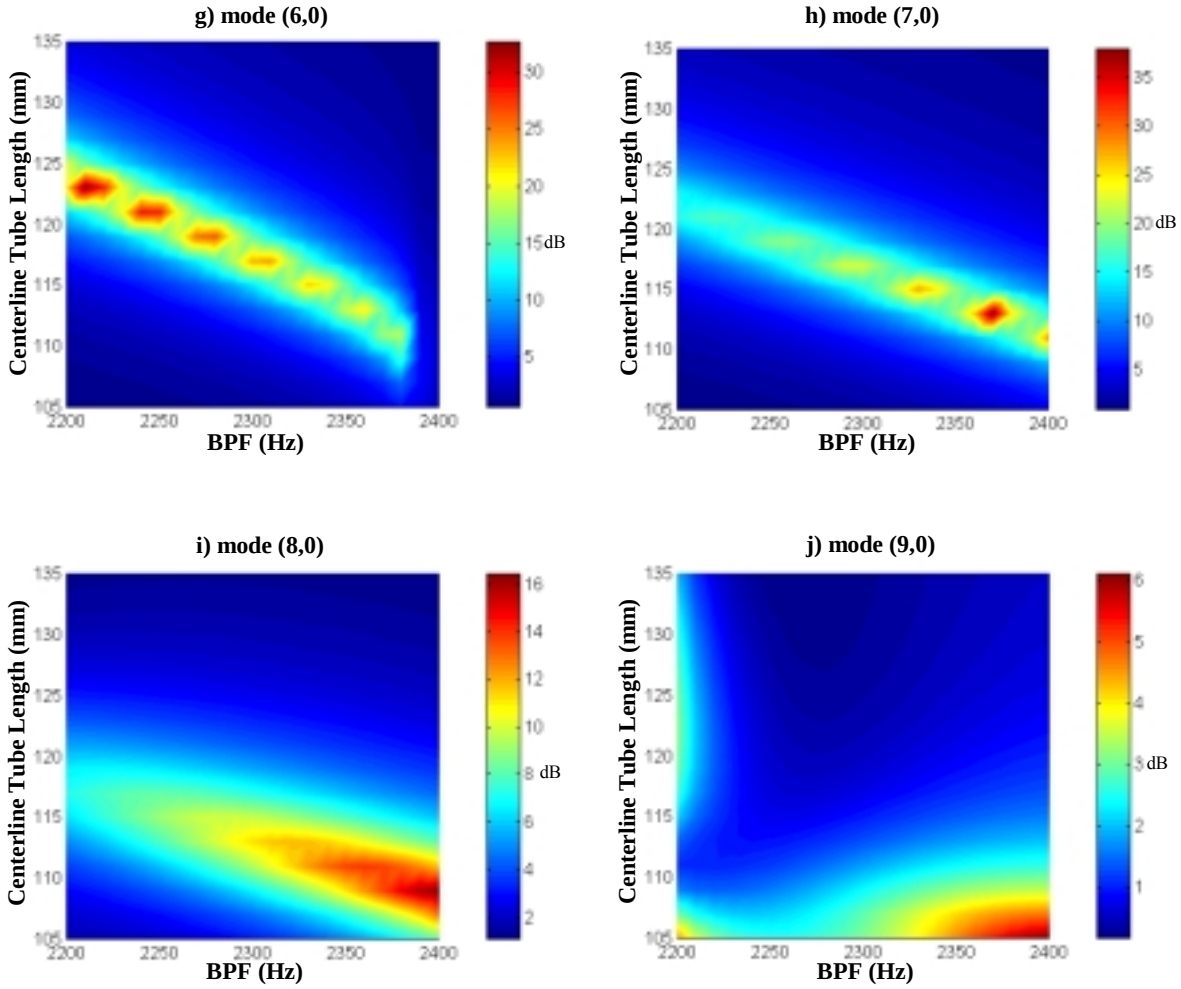

Figure 4-18g-j: Effect of tube length on sound power reduction for different incident modes.

Figure 4-18g through j show the effect of the centerline tube length for incident modes (6,0), (7,0), (8,0) and (9,0). Figure 4-18g and h first show the sound power reduction for modes with circumferential order 6 and 7, respectively. For these particular circumferential order modes, there is only one radial mode cut-on over the frequency range from 2200 to 2400 Hz. This is the reason why these two figures show very good sound power reduction, exceeding 20 dB. The only reduction mechanism happening in this case is reflection of the incident acoustic energy. There is no scattering of energy into other order modes as in the previous figures. The linear variation of the frequency of reduction with the centerline tube length still appears here.

Figure 4-18i and j show the effect of changing the tube length with modes (8,0) and (9,0) in the disturbance, respectively. Although there is only one radial mode cut-on in these cases, the HQ system does not provide a good reduction of the sound field. Whereas for the mode (8,0), the trend seen with the lower order modes is still visible at higher frequencies, there is no clear relation between the frequency of reduction and the tube length in the case of the incident mode (9,0).

4.5 New geometries for the HQ system

In the previous parametric study, the influence of each parameter on the performance of the HQ system was investigated. The tubes considered were parallel to the inlet axis and placed in a circumferential array, each tube being at the same axial location upstream from the fan and distributed evenly around the circumference. However, as discussed earlier, the acoustic field inside the inlet is made up of rotating modes, each of them contributing to the total sound radiation. These modes are spinning as they propagate upstream from the fan; in other words, they are propagating inside the inlet in helix patterns. Therefore, one can wonder if placing the HQ tubes along helixes instead of having a circumferential array of tubes could lead to any improvement in the performance of the HQ system. The effectiveness of the system could eventually be better when the angle of the helical array of tubes matches the angle of propagation of the incident modes. This issue will be investigated in the next four sections.

First, the characteristics of the modes propagating along a helix will be explained. The equation relating the value of helix angle to the mode order and the frequency of analysis will thus be presented. Then, three different systems will be investigated based on this helix propagation idea. First, the HQ tubes will be placed in a helix pattern while the tubes are lined up with the engine axis. The effect of this system will be studied at a higher frequency, and then at a frequency where a mode is just cut-on. Since the angle of propagation of a mode along a helix is directly related to the frequency of analysis, this will allow to investigate cases where the angles of propagation of the modes are different. Then, the HQ tubes will be placed in a circumferential array while the tubes are at an angle with respect to the engine axis. Finally, both systems will be combined and the tubes will be placed in a helix pattern while each tube is rotated at the same angle as the helix.

4.5.1 Propagation of modes along a helix

The propagation characteristics of a mode in the engine inlet are governed by the total wavenumber k_T. The total wavenumber can be expressed as the vector summation of the axial and the circumferential wavenumbers. Figure 4-19 shows the helix along which a mode of circumferential order m will propagate.

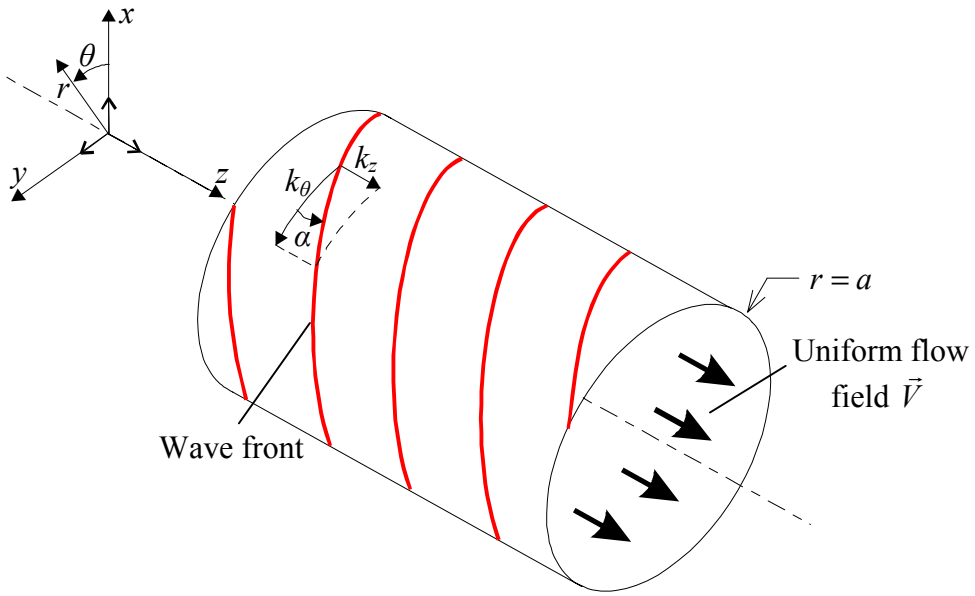

Figure 4-19: Propagation of mode in the inlet along a helix.

For a positive traveling mode, the axial wavenumber takes the form (see (2.21))

$$k_z = \frac{-Mk_o + \sqrt{k_o^2 - \left(1-M^2\right)k_{mn}^2}}{1-M^2} \tag{4.5}$$

where M is the flow Mach number, k_o is the free field wavenumber ($k_o=\omega/c$), k_{mn} is the eigenvalue written as $k_{mn}=\chi_{mn}/a$, where χ_{mn} are the inflection points of the Bessel's function of the first kind of order m.

On the other hand, the circumferential wavenumber k_θ depends on the circumferential order m of the mode. Figure 4-20 shows the variation of the acoustic pressure on the inlet wall along the circumference at an arbitrary axial location. This pressure variation corresponds to a mode of circumferential order $m=4$.

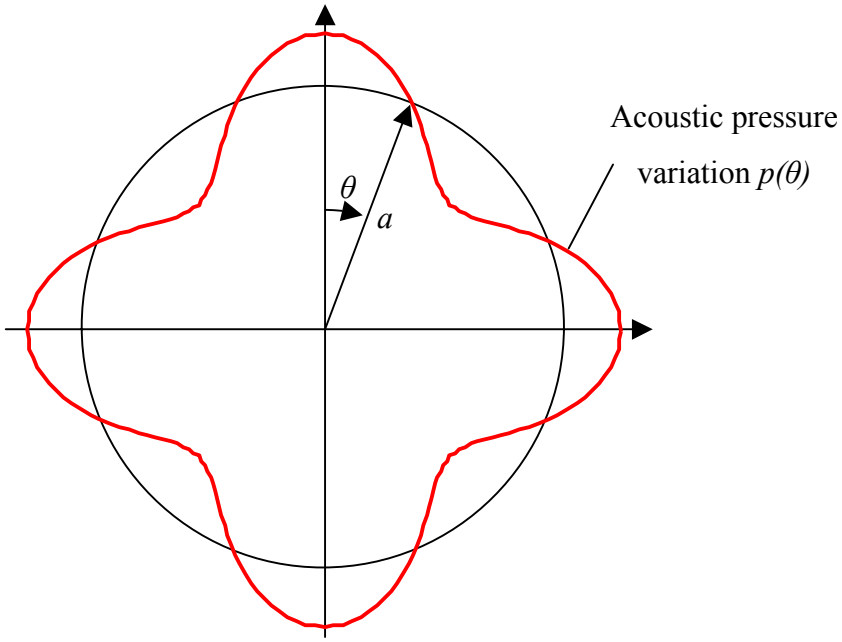

Figure 4-20: Variation of the acoustic pressure on the inlet wall along the circumference.

As seen in Figure 4-20, the number of pressure lobes along the circumference corresponds to the circumferential order of the mode. Here there are 4 lobes so there are 4 wavelengths along the circumference. In a more general approach, for a mode of circumferential order m, there will be m wavelengths λ_θ along the circumference. Therefore, the circumferential wavenumber is given as

$$k_\theta = \frac{2\pi}{\lambda_\theta} = \frac{2\pi}{\left(\frac{2\pi a}{m}\right)} = \frac{m}{a} \tag{4.6}$$

As defined in Figure 4-19, the angle of the helix α is given as

$$\alpha_{mn} = \tan^{-1}\left[\frac{k_z}{k_\theta}\right] = \tan^{-1}\left[\frac{\left(\frac{-Mk_o + \sqrt{k_o^2 - \left(1-M^2\right)k_{mn}^2}}{1-M^2}\right)}{\left(\frac{m}{a}\right)}\right] \tag{4.7}$$

As shown in equation (4.7), since k_z depends on the order of the mode considered, the angle of propagation will be different for each mode. For this study, the HQ system will be applied to the JT15D engine inlet at the frequency of 2320 Hz. At this frequency,

there are 21 cut-on modes. The angle of propagation α_{mn} for each mode is shown in Table 3-4 as a function of its circumferential order *m* and radial order *n*.

		Radial order *n*			
		0	**1**	**2**	**3**
Circumferential order *m*	**0**	90.0	90.0	90.0	90.0
	1	85.4	85.0	83.6	-
	2	80.7	79.2	73.8	-
	3	75.8	72.3	44.2	-
	4	70.6	63.3	-	-
	5	65.0	48.9	-	-
	6	58.8	-	-	-
	7	51.6	-	-	-
	8	42.8	-	-	-
	9	30.3	-	-	-

Table 4-2: Angle of propagation α in degree for each cut-on mode at 2320 Hz.

As modes of circumferential order *m=0* are not spinning, they are not propagating along a helix, therefore the angle of propagation is 90°, as shown in Table 3-4. It can also be noticed in Table 3-4 that the angle of propagation of modes is very high and decreases as the order of the mode increases. This is due to the fact that the angle of the helix is directly related to the frequency. When a mode is just cut-on, the angle is 0°, and as the frequency increases, the angle will tend to approach 90°.

4.5.2 Array in a helix pattern with tubes parallel to the engine axis

In this section, the tubes will be placed along the inlet duct such that the array of tubes has a helix shape. As previously explained, the angle of the helix is measured from an axis perpendicular to the engine axis, such that an angle of 0° corresponds to a circumferential array. The angle of the helix defined by the array of tubes will be changed and the effect on the sound power reduction will be observed.

The first case investigated here will consist of placing the tubes to form 4 helixes, each of them being made of 5 tubes. The reference system is a circumferential array of 20 tubes of length 11.8 cm. Figure 4-21 shows an unwrapped view of the inlet mounted with a circumferential array of tubes and with the HQ tubes placed in helix patterns.

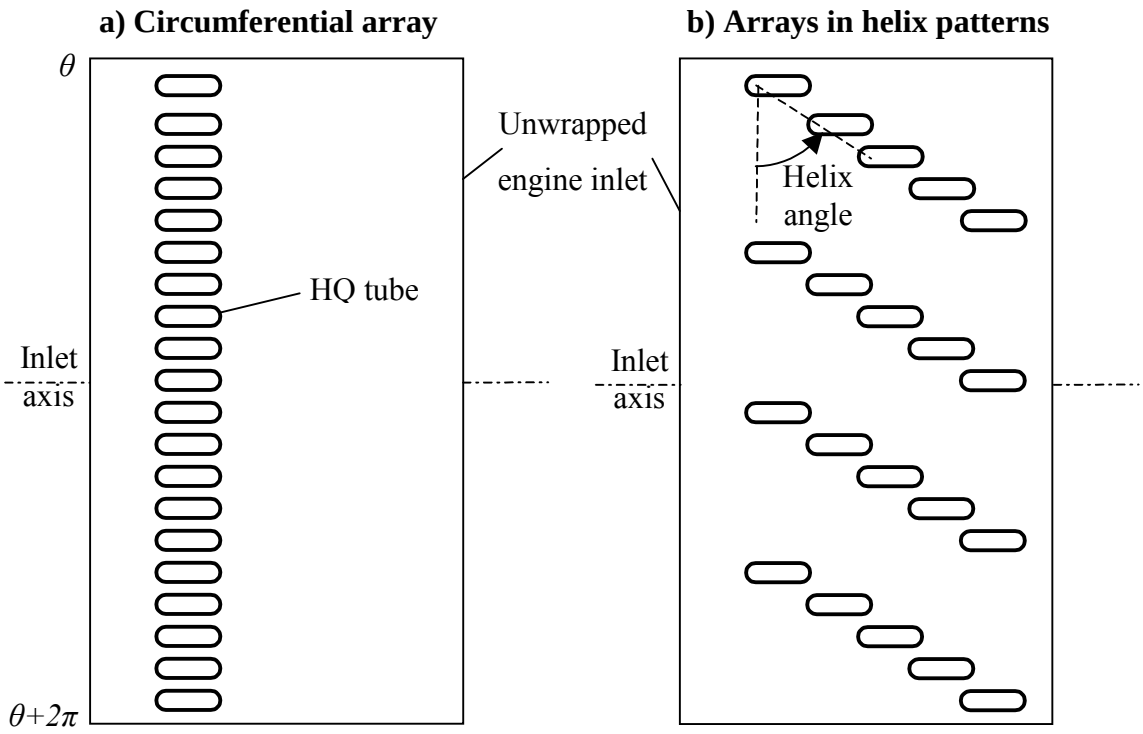

Figure 4-21: Expanded view of the inlet with HQ tubes placed a) in a circumferential array or b) in 4 helixes of 5 tubes.

There are several possible options to place the tubes in helixes based on the reference system. Two configurations will be studied here. First the distance between the tubes in the circumferential direction will be kept constant as the angle of the helix changes. Then, the distance between the tube ends is kept constant as the angle of the helix changes. These two cases are illustrated in Figure 4-22a and b and will be referred to as configuration 1 and configuration 2 in the next paragraphs.

a) Configuration 1: Constant distance between tubes in circumferential direction

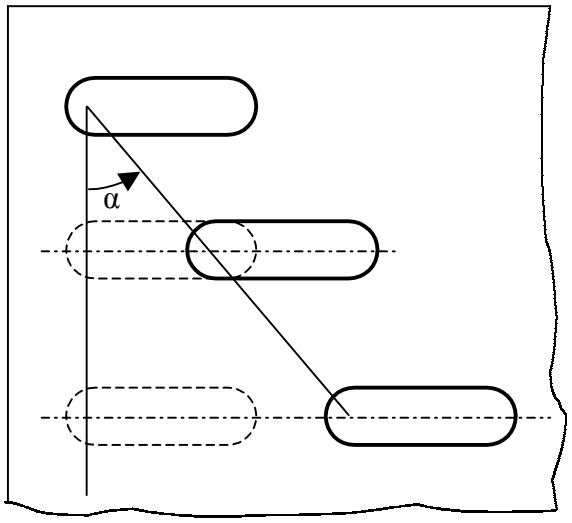

b) Configuration 2: Constant distance between tube ends in same helix

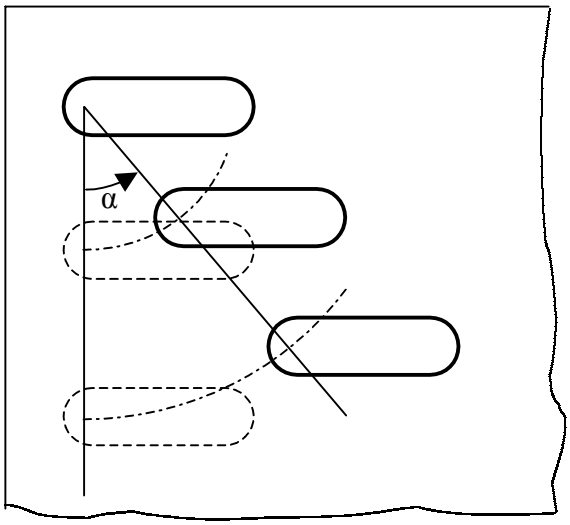

Figure 4-22: Configurations used to place tubes in helix patterns.

For the simulations performed here, the disturbance contains 3 modes, (1,0), (1,1) and (1,2) whose amplitudes are those measured on the JT15D engine at 2320 Hz. However, besides the case of the disturbance containing these 3 modes simultaneously, the effect of the helix angle will be investigated for the three modes individually propagating in the inlet. Results for the configuration 1, i.e. constant distance between tubes in circumferential direction, are illustrated in Figure 4-23. This figure shows the sound power reduction as a function of the helixes angle. The helix angles ranges from – 85° to 85°. This range was selected to theoretically investigate the effect of the helix arrays on the performance of the system and see if there is a trend. However, the required inlet length for such large angles would not be practical (4 meters for helixes at 85°) making such systems physically unrealizable.

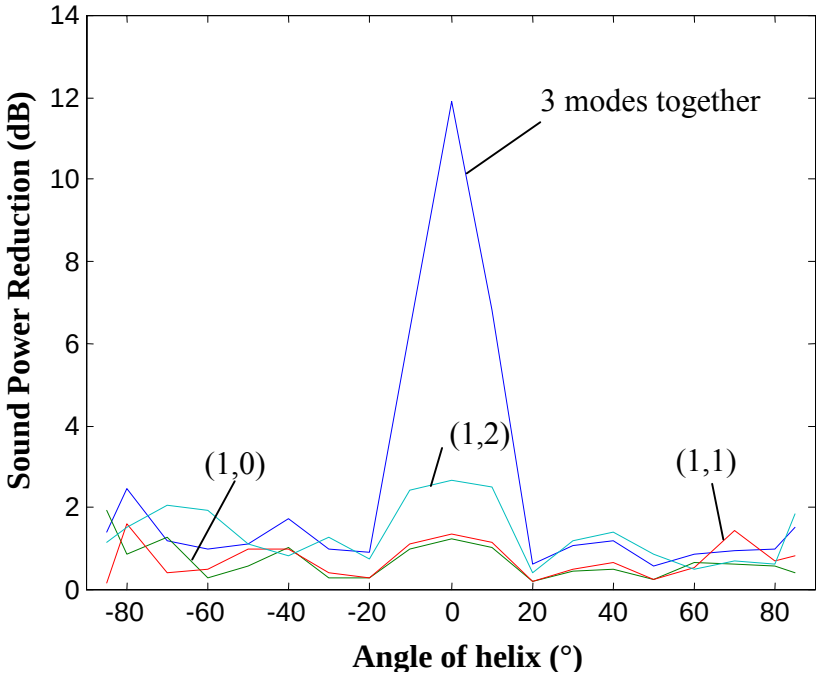

Figure 4-23: Effect of the helix angle on the sound power reduction for 4 helixes of 5 tubes in configuration 1.

Figure 4-23 shows that the maximum sound reduction occurs with a circumferential array of tubes, i.e. when the helix angle is 0°. With the three incident modes, the sound power reduction suddenly drops from 12 dB to less than 2.5 dB when the tubes are placed in helixes. In the case of the incident modes individually propagating in the inlet, there is no improvement of the reduction observed either when the tubes are placed in helixes.

As shown in the previous section, incident modes (1,0), (1,1) and (1,2) propagate through the inlet along helixes of angles 85.4°, 85.0° and 83.6°, respectively, at 2320 Hz. These angles are extremely high and are almost out of the range for the helix angles investigated here. However, placing the tubes at angles of 80° or 85° does not seem to provide any improvement in the sound reduction here.

Results for configuration 2, i.e. constant distance between tube ends in the same helix, are shown in Figure 4-24. In this case, the helix angles ranges from –60° to 60°, which corresponds to the maximum possible range for the system.

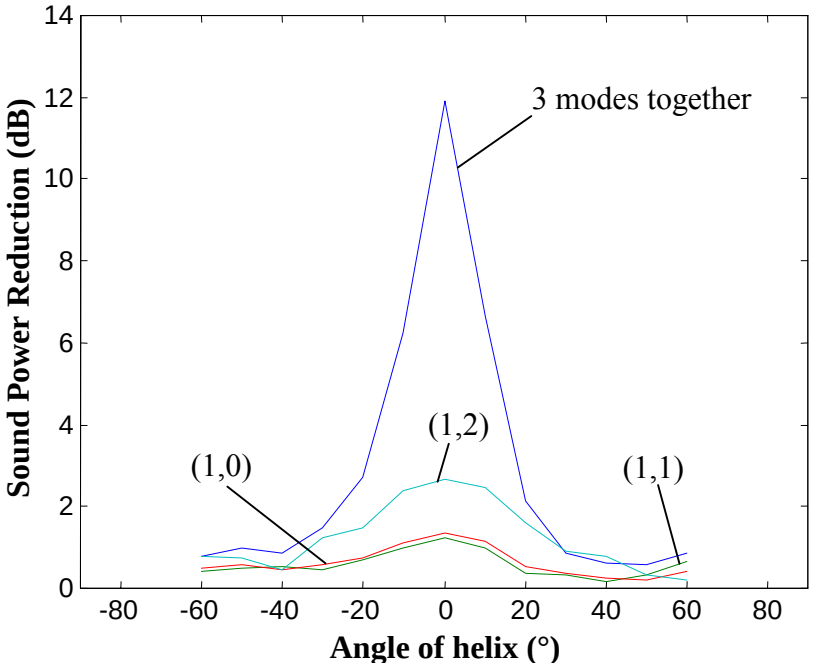

Figure 4-24: Effect of the helix angle on the sound power reduction for 4 helixes of 5 tubes in configuration 2.

Once again, putting the tubes in 4 helix arrays does not achieve any improvement in the sound reduction. The best sound power reduction is obtained with a circumferential array of tubes whether the modes (1,0), (1,1) or (1,2) are propagating individually or simultaneously through the engine inlet.

By looking at the configuration of the system, it can easily be understood why the helix concept does not work here. Placing the tubes in 4 helixes of 5 tubes is the same as having 5 successive circumferential arrays of 4 tubes placed at a different angle relative to the top of the inlet duct. Therefore, the scattering effect will cause the incident energy from modes (1,0), (1,1) and (1,2) to be scattered into other circumferential modes that are cut-on. That is, from the scattering equation ($m_{HQ}=m_D\pm kN_T$), energy will be radiated through modes of circumferential orders –7, -3, +5 and +9. Therefore, in order for the HQ system placed in helix patterns to be efficient, the number of helixes must be high enough, such that no energy is scattered into other circumferential propagating modes.

This case is presented in the next study where the case of 11 helixes of 2 tubes is investigated.

The HQ tubes are now placed such that they form 11 helixes along the engine inlet, each helix being made of 2 tubes. The reference system is then a circumferential array of 22 tubes. Once again, configurations 1 and 2 will be investigated here. Figure 4-25 first shows the effect of helix angle on the sound power reduction for helixes in configuration 1.

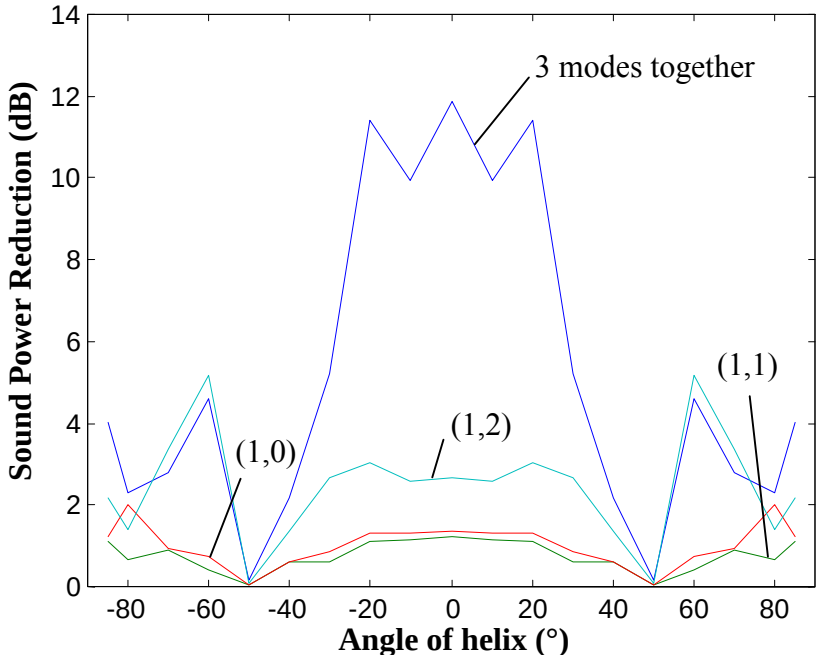

Figure 4-25: Effect of the helix angle on the sound power reduction for 11 helixes of 2 tubes in configuration 1.

It is clear in Figure 4-25 that a better sound reduction is achieved when the angle of the helixes is small. When the 3 modes are in the disturbance, reduction of more than 10 dB is indeed observed with helixes at an angle less than 20°. Figure 4-25 also shows a critical angle, 50°, where the reduction dramatically drops. For higher angles, the reduction increases but remains under 5 dB. Placing the tubes such that the helix angle is 60° seems to reduce the noise propagating through mode (1,2). The sound reduction for this mode is 5.2 dB at this angle, whereas it was only 2.7 dB with a circumferential array.

However, it does not seem to be a relation between the angle of propagation of modes and the angle of the helix. The sound power reduction at angles higher than 80° is indeed much smaller than in the case of a circumferential array.

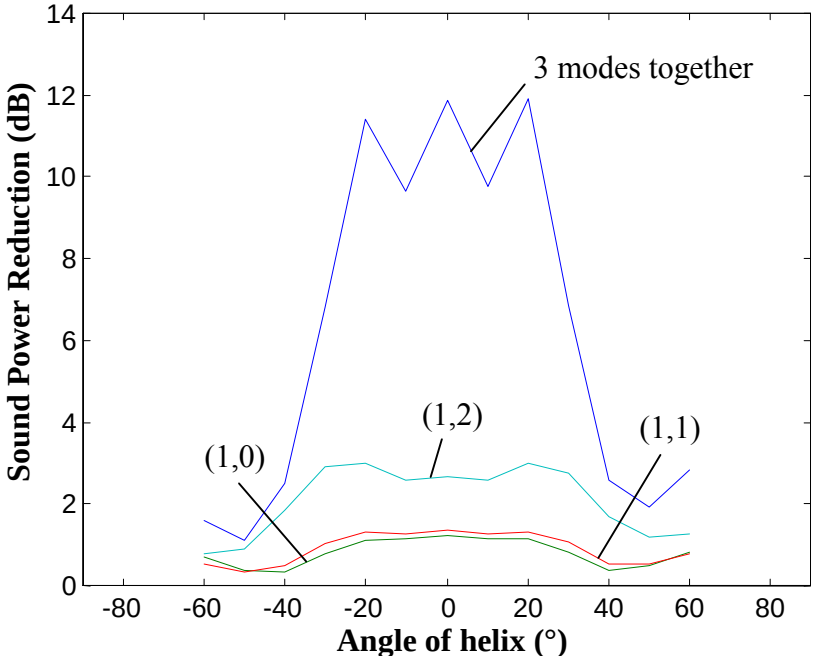

Figure 4-26: Effect of the helix angle on the sound power reduction for 11 helixes of 2 tubes in configuration 2.

The case of 11 helixes of 2 tubes placed as in configuration 2 is shown in Figure 4-26 for helix angles ranging from –60° to 60°. As shown in Figure 4-26, the HQ system provides good reduction for helix angles smaller than 20°. However, the sound power reduction decreases as the helix angle increases.

The previous results do not really show any correlation between the angle of the tube helixes and the angle of propagation of the incident modes. The best reduction is still achieved with a circumferential array of tubes and there is no real improvement of the HQ system efficiency by placing the tubes in helix patterns.

However, in the previous study, the three incident modes (1,0), (1,1) and (1,2) had an angle of propagation higher than 80° at 2320 Hz. In order to know if the helix arrays concept would be more efficient at lower propagation angles, the frequency of analysis will now be chosen just after a mode is cut-on. The case of mode (1,1) will be illustrated here. This mode is cut-on at 1084 Hz. Table 4-3 shows the angle of propagation of this mode for frequencies just above 1084 Hz.

Frequency (Hz)	**Angle of propagation (°)**
1085	40.4
1089	49.1
1093	53.2
1097	55.9
1101	58.1
1105	59.7

Table 4-3: Angle of propagation of mode (1,1) at frequencies just after cut-off.

As seen in Table 4-3, at frequencies just above cut-on, mode (1,1) is propagating in helix at smaller angles. As the frequency increases, the angle of propagation also increases. The tubes were then placed to form 10 helixes of 2 tubes and the effect of the helix angle on the sound reduction was investigated at frequencies just after cut-off. For this study, the HQ tube system was optimized in order to provide maximum reduction with a circumferential array of 20 tubes at 1085 Hz. Thus, the tubes have a centerline length of 14.2 cm and the distance between tube ends is 12.0 cm. Figure 4-27 first shows the sound power reduction as a function of helix angle and frequency in the case of configuration 1.

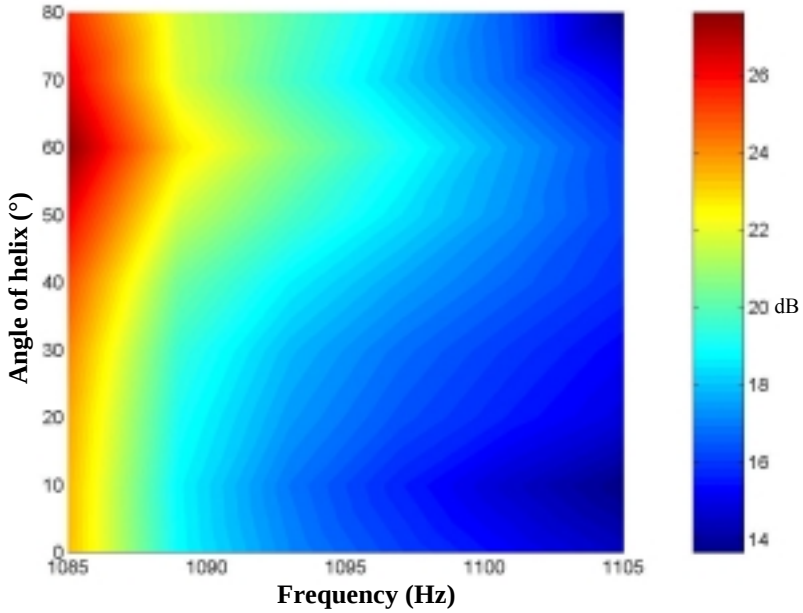

Figure 4-27: Effect of the helix angle for incident mode (1,1) at frequencies just above cut-on – configuration 1.

As seen in Figure 4-27, placing the HQ tubes in a helix with angle 60° allows to increase the sound power reduction up to 27 dB at 1085 Hz. However, the reduction provided by the HQ system in circumferential array was already more than 23 dB at that frequency. Moreover, the improvement achieved by the helical array very rapidly drops out as the frequency increases. At 1105 Hz, which is only 20 Hz above cut-off frequency, the improvement achieved by the HQ system placed in a helix array is indeed quite insignificant.

Figure 4-28 shows the same study applied to configuration 2. The range for the helix angles is now –60 to 60°.

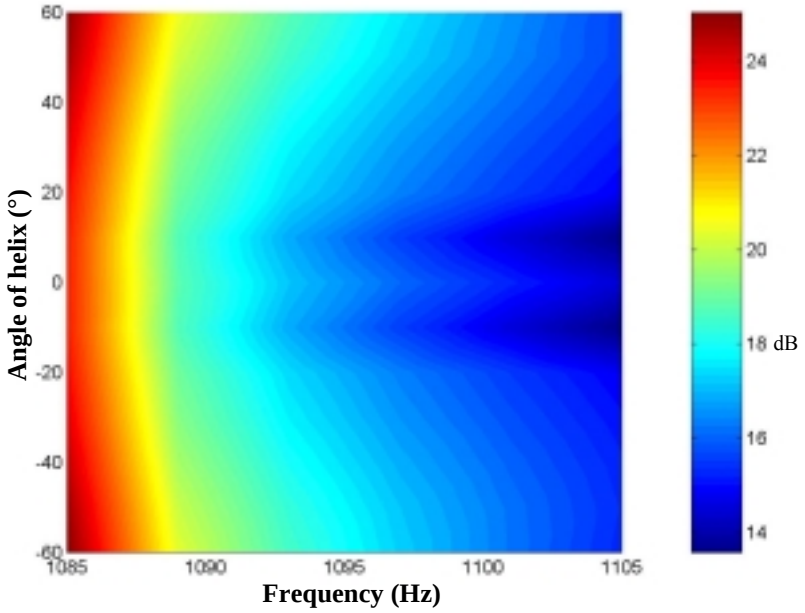

Figure 4-28: Effect of the helix angle for incident mode (1,1) at frequencies just above cut-on – configuration 2.

Again, placing the HQ tubes in helix patterns provides a slight increase in the sound power reduction. At 60°, the sound reduction is 25 dB whereas a circumferential array provided 23.5 dB reduction in the sound power at 1085 Hz. The results seem to be identical for positive or negative angles of the helix. However, once again, the sound power reduction very rapidly decreases as the frequency increases. The improvement in the efficiency of the system in helix pattern is only visible at frequency very close to the cut-off frequency. Therefore, there is no direct relation between the angle of maximum reduction and the angle at which the incident mode is propagating in the inlet.

This study investigated a new configuration for the HQ system based on placing the HQ tubes in helixes. As the modes are propagating in the inlet along helixes, it was proposed that the new helix configurations could improve the noise reduction. However, the various cases showed here did not show satisfactory improvement. Although the system with arrays in helix patterns allowed to increase the sound reduction of a mode just cut-on, the amelioration in the results was only noticeable on a very short frequency

range. Moreover, the amelioration occurs in a frequency range where the system with circumferential array was already very efficient.

4.5.3 Circumferential array with tubes at an angle with respect to the engine axis

Based on the previous idea that modes are propagating in the inlet along helix, another configuration will be investigated here. The HQ tubes are now placed in a circumferential array and are rotated such that they form an angle with respect to the inlet axis. Unlike the previous where the tubes were placed in helix patterns, this system is very practical and could be easily built. This system is illustrated in Figure 4-29.

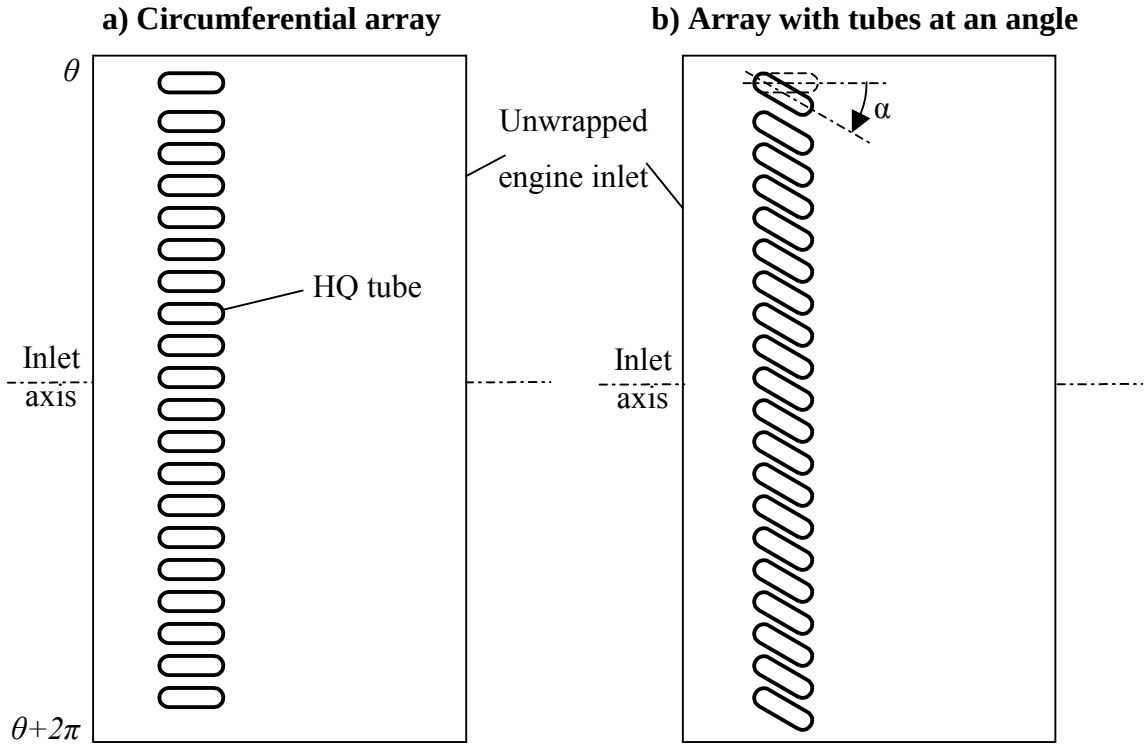

Figure 4-29: Expanded view of the inlet with HQ tubes placed a) in a circumferential array or b) in an array with tubes at an angle with respect to inlet axis.

The angle α is measured from the inlet axis and the positive direction for this angle is chosen to be the same as the direction of rotation of the fan. As in the previous study, the results will be presented for three incident modes of order (1,0), (1,1) and (1,2). The

dimensions of the inlet are those of the JT15D engine. The reference HQ tube system consists of a circumferential array of 20 tubes with centerline length 11.8 cm.

The sound power reduction provided by the system as a function of the BPF is shown in Figure 4-30. In this case, the three incident modes (1,0), (1,1) and (1,2) are propagating simultaneously in the inlet. The tube angles range from –65° to 65°, which is the maximum possible range.

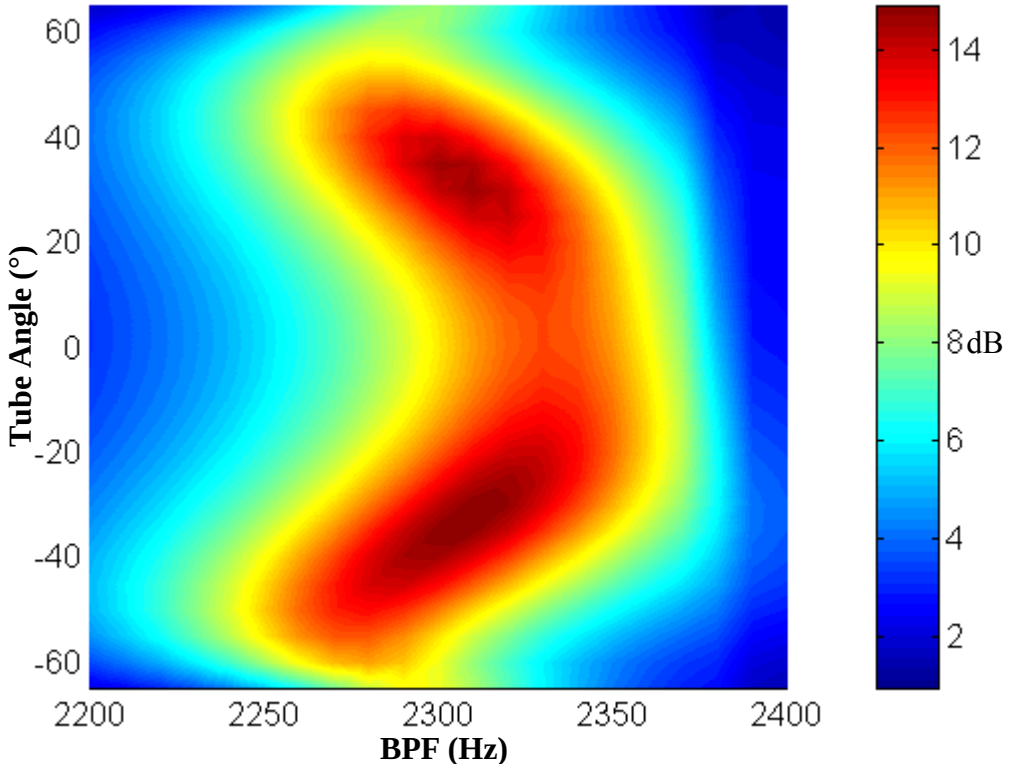

Figure 4-30: Effect of tube angle on sound power reduction for 3 incident modes propagating in inlet of the JT15D engine.

Figure 4-30 clearly shows that placing the tubes at an angle from 20° to 45° provides a significant increase in sound power reduction as compared to having the tubes parallel to the engine axis (α =0°). Both positive and negative tube angles result in better performance in this range. As the angle of the tubes increases from 0° to -40°, the maximum sound power reduction over the frequency range increases from 12.3 to 14.5 dB. It is obvious that the plot will flip if the modes are spinning in the opposite direction.

Although the system with tubes at an angle allows to improve the sound reduction, the optimum angle does not correspond to the angle of propagation of the three incident modes (1,0), (1,1) and (1,2) which are less than 10° (with respect to the inlet axis) on the frequency range investigated here (the calculation of these angles was presented in the previous section).

As the angle of the tubes changes up to ±40°, the reduction provided by the tubes increases; however at the same time, the frequency of optimum reduction is shifted down from 2330 to 2300 Hz. To account for this frequency change, the geometry of the tubes needs to be adjusted as the tube angle changes to provide optimum sound reduction at a given frequency. The centerline tube length was previously shown to be the dominant criterion to set the frequency of resonance of the system, therefore this parameter will be adjusted here as an example to provide reduction at 2330 Hz. Figure 4-31 shows the sound power reduction as a function of BPF for an optimum reduction at 2330 Hz with straight tubes and tubes at an optimum angle.

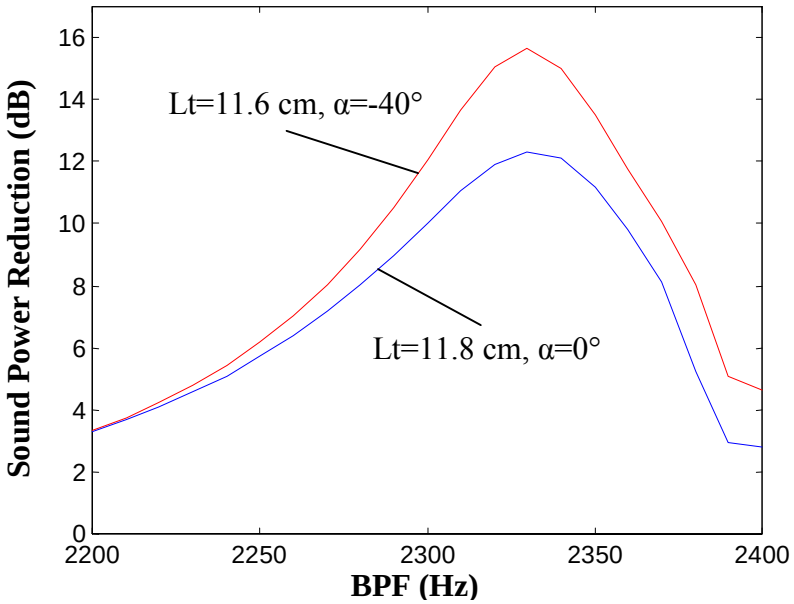

Figure 4-31: Sound power reduction for an array of straight tubes and an array of tubes placed at an angle relative to the inlet axis – 3 modes propagating in the inlet of the JT15D engine.

In Figure 4-31, the blue curve corresponds to an array of tubes parallel to the inlet axis ($\alpha = 0°$) and of centerline length 11.8 cm. The reduction at 2330 Hz is then 12.3 dB. On the other hand, the red curve corresponds to an array with tubes at an angle of –40°. The centerline tube length was optimized to provide maximum reduction at 2330 Hz and is thus 11.6 cm. Now, the reduction at 2330 Hz is 15.6 dB, so 2.3 dB higher than in the previous case.

The previous results showed that placing the tubes at an angle allowed to improve the performance of the system. The transmitted mode amplitudes were looked at and compared in the case of an array of straight tubes and for an array with tubes at the optimum angle of –40°. The values of the modal amplitudes will not be shown here to avoid getting into too much complexity and keep the exposition clear. However, it can be concluded from these results that two noise control mechanisms are involved here. First, the system with tubes at an angle seems to increase the reflection of the incident energy from each individual incident mode as compared to the case with straight tubes. On the other hand, the scattered energy from each incident mode into the two other radial modes tends to be more important when the tubes are placed at an angle. As there is more energy scattered between the three propagating modes, the recombination mechanism and suppression of energy in each mode is more efficient and thus the transmitted acoustic energy tends to be lower.

As seen in the previous results, the system tends to be more efficient when tubes are rotated at a certain angle, regardless if this angle is positive or negative. Therefore, this system could eventually be used in a case where the disturbance includes modes, which are spinning in the positive as well as in the negative direction. Therefore, the same study will be performed based on the AlliedSignal engine. At the BPF of this engine there are incident modes rotating in the positive direction ($m=2$ and $m=12$) as well as in the negative direction ($m=-8$). The effect of the tube angle is shown in Figure 4-32. The reference HQ system is a circumferential array of 27 tubes optimized to provide reduction at 2150 Hz. The centerline tube length is then 12.7 cm. As the number of tubes along the circumference is high and the distance between tube ends will be small

for high tube angles, the near-field effect will have a stronger effect. Therefore, the number of modes included in the Green's function for these simulations is 40 circumferentials and 40 radials.

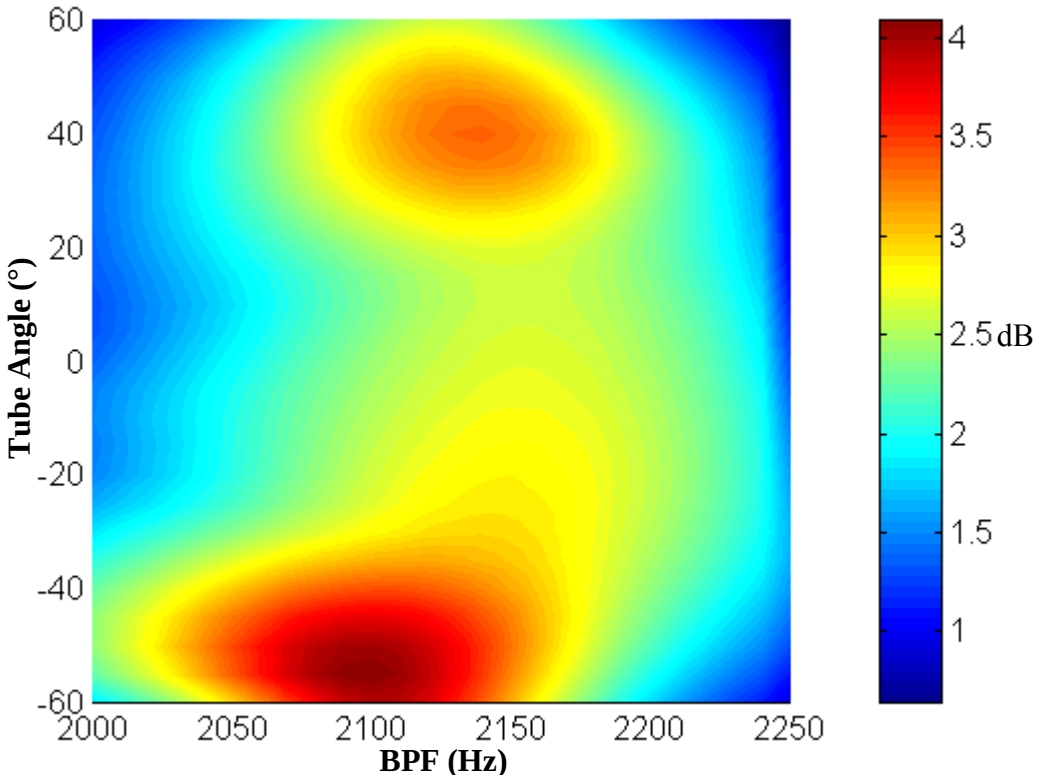

Figure 4-32: Effect of tube angle on sound power reduction for positive and negative rotating modes propagating in the inlet of the AlliedSignal engine.

As seen in Figure 4-32, a significant improvement in the performance of the system is provided with tubes at an angle of –55°. The maximum reduction at this angle is 4.1 dB whereas maximum reduction achieved with the circumferential array is 2.7 dB. However, as observed previously, the frequency of maximum reduction is shifted down as the angle of the tubes increases. The centerline of the tubes was next optimized to provide maximum reduction at 2150 Hz with tubes at an angle of –55°. The results in this case are shown in Figure 4-33.

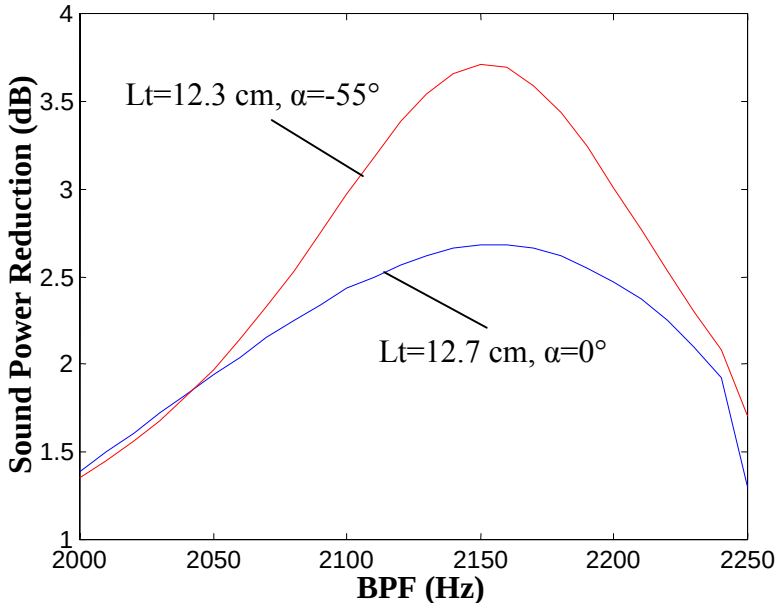

Figure 4-33: Effect of tube angle on sound power reduction for positive and negative rotating modes propagating in the inlet of the AlliedSignal engine.

In Figure 4-33, the blue curve corresponds to an array of tubes parallel to the inlet axis ($\alpha = 0°$) and of centerline length 12.7 cm. The reduction at 2150 Hz is then 2.7 dB. On the other hand, the red curve corresponds to an array with tubes at an angle of –55°. The centerline tube length was optimized to provide maximum reduction at 2150 Hz and is 12.3 cm. Now, the reduction at 2150 Hz is 3.7 dB, so 1.0 dB higher than in the previous case.

4.5.4 Array in a helix pattern with tubes rotated at the same angle

The two previous sections investigated configurations of the HQ tubes based on the helical propagation of modes. The first system consisted in placing the HQ tubes in helix patters and the second in rotating the tubes placed in a circumferential array. Both systems will now be combined now in a system where the arrays of tubes are placed at an angle with tubes rotated at the same angle as the helix. The tubes will be placed along the inlet as illustrated in Figure 4-34.

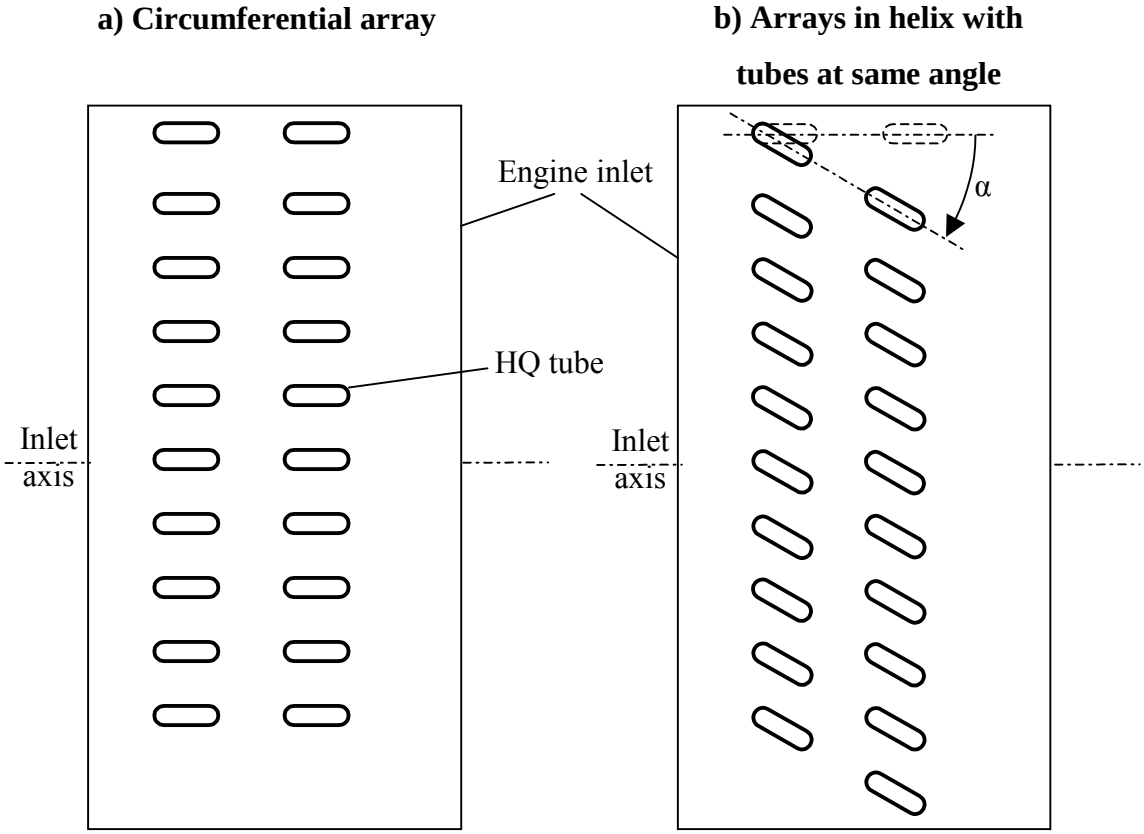

Figure 4-34: Expanded view of the inlet with HQ tubes placed a) in a circumferential array or b) in helixes patterns with tubes at an angle.

In this study, the system was optimized to provide maximum reduction at 2320 Hz in the reference configuration when the incident modes (1,0), (1,1) and (1,2) are propagating in the inlet. The reference system consists of 2 arrays of 11 tubes located at 0.25 and 0.45 m from the fan respectively. The tubes have a centerline length of 11.8 cm

and the distance between ends is 9.2 cm. The sound power reduction is shown in Figure 4-35 where the helix angle α as defined in Figure 4-34, ranges from –60° to 60°.

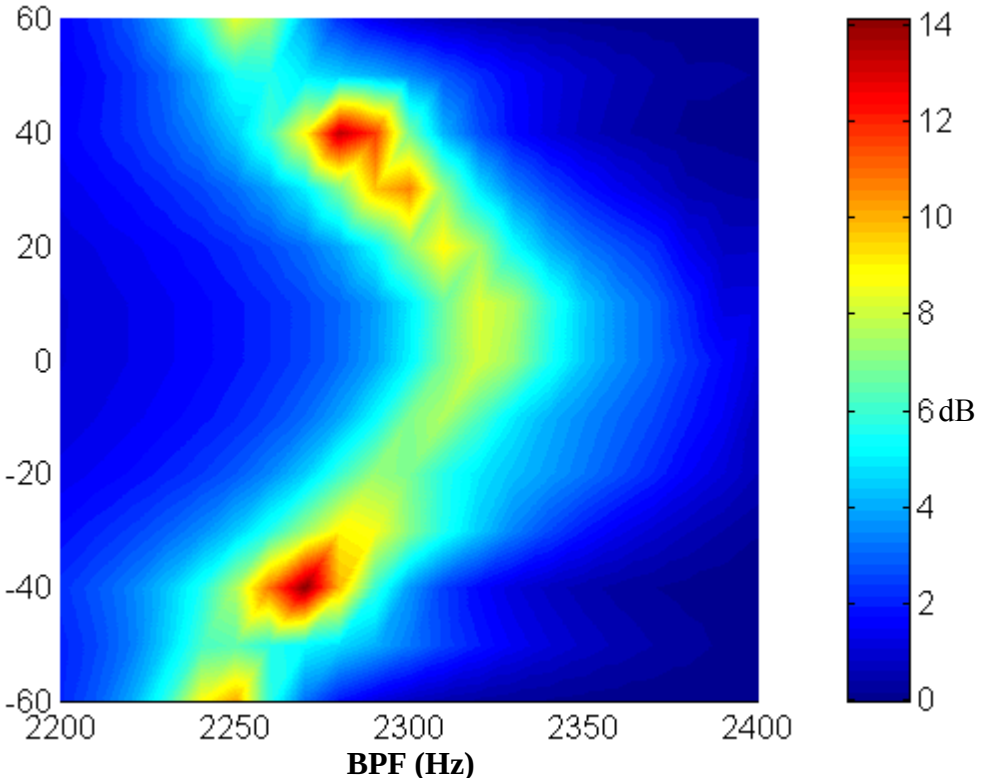

Figure 4-35: Effect of helix angle on the sound power reduction for 11 helixes of 2 tubes at the same angle as the helix.

As seen in Figure 4-35, improvement in the sound reduction is achieved with a helix at ±40°. As the helix angle increases from 0° to 60°, the frequency of maximum reduction is shifted down from 2320 to 2250 Hz. This mechanism was already observed when only the tubes were rotated at an angle with respect to the inlet axis. Placing the tubes in a helix with the tubes rotated at the same angle seems to improve the performance of the HQ system. However, the maximum reduction provided by this system is 14 dB, which is not significantly higher than the reduction provided by a circumferential array with 20 tubes. Moreover this system is rather complex and would be very complicated to build. Once again, no relation is shown between the optimum angle of reduction and the angle of propagation of the three incident modes (4.6° for mode (1,0), 5.0° for mode (1,1) and 6.4° for mode (1,2) at 2320 Hz).

Chapter 5. Conclusions and Recommendations

5.1 Conclusions

An innovative implementation of the Herschel-Quincke tubes concept for the reduction of noise from turbofan engines was investigated in this thesis. The main objective of this research was to analytically investigate the noise control mechanisms involved in the HQ system. In order to reach this objective, a modeling technique was developed and a computer code was written to predict the effect of the HQ tubes on the noise radiated by the inlet of turbofan engines. This modeling technique allows to apply the HQ tubes to a cylindrical duct in the presence of higher-order modes in uniform flow, as opposed to the simple case of plane waves considered in the past. The analytical technique involved modeling the HQ tubes-duct interfaces as finite piston sources that couple the acoustic field inside the inlet duct with the acoustic field within the HQ tubes. The prediction code was also used in parallel with genetic algorithms to optimize the geometry of the HQ system when needed.

The results provided by the model were compared to experimental data taken on two real engine inlets on which the HQ system was applied. Both tonal and broadband results showed good agreement between the predictions and the experimental results and therefore allowed to validate the modeling technique. In particular, the model allows to predict very accurately the frequency of attenuation of system. However, a significantly

high number of modes need to be included in the calculations in order to get accurate results.

Then, the model was used to investigate the noise attenuation mechanisms involved in the HQ system. An impedance analysis first allowed to show that the HQ system provides good reduction at discrete frequencies corresponding to the resonance of the coupled HQ tube-duct system. The dynamics of the inlet duct actually modifies the resonance behavior of the tube itself and causes the tube resonant frequencies to shift down. Then, the noise control mechanisms were investigated by studying the modal amplitudes of the incident, reflected and transmitted modes. This allowed to show that in the presence of the HQ system, incident modes not only are reflected back to the fan but also are scattered into other radial and circumferential order modes. Thus, the reduction of the acoustic energy in a particular mode is due to the recombination of scattered energy due to the other incident modes. It was shown that a preferable design strategy consists of using a higher number of HQ tubes in order to avoid scattering of energy into propagating circumferential modes. A parametric study was then performed to investigate the effect of the geometry of the HQ system on its performance. The centerline tube length was shown to be the determinant criteria dictating the frequency of noise reduction.

Based on the idea that higher-order modes are propagating in the inlet duct along helixes, new geometries for the HQ system were investigated. Tubes were first placed in helix patterns with tubes parallel to the inlet axis. Then, the HQ system was based on a circumferential array with tubes placed at an angle relative to the inlet duct axis. Finally, both systems were combined and tubes were placed in a helix and rotated at the same angle as the helix. The configurations where tubes are placed in helixes did not show any clear improvement in the effectiveness of the HQ system. However, the performance of the system was improved by placing the HQ tubes at an angle relative to the inlet axis. However, no relation between the angle of propagation of the modes and the angle at which the tubes were placed was observed.

5.2 Recommendations for future research

A number of suggestions for future work are as follows:

- An interesting extension of this work would consist of combining the HQ tubes system with the more traditional passive liner system. Strategic design of the combined system, such as using the HQ tubes to reduce the low frequency tone or broadband noise, and implementing the liner to reduce higher frequency noise could result in a very effective noise reduction.

- This work was focused on the HQ system applied to the inlet of the turbofan engine. However, this concept could be easily applied to the aft of the engine. However, in this case, the modeling approach would have to be modified since the aft radiation consists of a conical duct.

- The model presented in this report allows to compute the transmitted as well as the reflected sound power. However, it does not take into account the reflection of the energy on the fan. Therefore, it would be interesting to include the impedance of the fan in the modeling technique to investigate if the reflection mechanisms modify the performance of the HQ system.

- It was shown that the frequencies of optimal performance of the HQ tube system were greatly affected by the centerline tube length. Adapting the tube length with a control system as the running speed and operating conditions of the engine change could eventually allow to track the BPF frequency and result in good noise reduction for different engine operating conditions.

Bibliography

[1] Tyler J. M. and Sofrin, T. G., "Axial Flow Compressor Noise Studies," SAE Transaction no. 70, 309-332, (1962).

[2] Kantola, R.A., and Gliebe, P.R., "Effects of Vane/Blade Ratio and Spacing on Fan Noise," AIAA Paper no. 81-2033, Oct. (1981).

[3] Dittmar, J. H. and Woodward, R. P., "An Evaluation of some Alternative Approaches for Reducing Fan Tone Noise," NASA Technical Memorandum 105356, February (1992).

[4] Mangiarotty, R. A., "The Reduction of Aircraft Engine Fan-Compressor Noise Using Acoustic Linings," Journal of Sound and Vibration, **18** (4), 565-576, (1971).

[5] Thomas, R.H., R. A. Burdisso, C. R. Fuller and W. F. O'Brien, "Active Control of Fan Noise From a Turbofan Engine," AIAA paper no. 93-0597, January (1993).

[6] Smith, J. P. and Burdisso, R. A., "Active Control of Inlet Noise From a Turbofan Engine Using Inlet Wavenumber Sensors," CEAS/AIAA-99-1808, Seattle, WA, May (1999).

[7] Burdisso, R. A., Fuller, C. R. and Smith, J. P., "Experiments on the Active Control of a Turbofan Inlet Noise using Compact, Lightweight Inlet Control and Error Transducers," CEAS/AIAA-95-028, pp. 177-185, (1995).

[8] Herschel, J. F. W. ,"On the absorption of light by coloured media, viewed in connexion with the undulatory theory," *Philosophical Magazine and Journal of Science*, **3**, 401-412, (1833).

[9] Quincke, G., "Ueber interferenzapparate fur schallwellen," *Annalen der Physik und Chemie*, **128**, 177-192, (1866)

[10] Stewart, G. W., "The theory of the Herschel-Quincke tube," *Physical Review*, **31**, 696-698, (1928)

[11] Selamet, A., Dickey, N. S., and Novak, J. M., "The Hershcel-Quincke tube: a theoretical, computational, and experimental investigation," *J. Acoust. Soc. Am.*, **96** (5), 3177-3185, (1994)

[12] Zhichi, Z., Song, L. , Rui, T., Rui, G., Genhua, D., and Peizi, L., "Application of Quincke tubes to flow ducts as a sound attenuation device," Noise Control Eng. J., **46**(6), 245-255, Nov-Dec (1998)

[13] Brady, L. A., Burdisso, R. A., and Smith, J. P., "Investigation of the Herschel-Quincke Tube Concept for the Suppression of Higher-order Modes in a Duct," Proceedings of Internoise 99, pp. 545-550, Fort Lauderdale Florida, December (1999).

[14] Burdisso, R.A. and Smith, J.P., "Control of Inlet Noise from Turbofan Engines Using Herschel-Quincke Waveguides," 6th AIAA/CEAS 2000-1994, (2000).

[15] Morse, P. M. and Ingard, K. U., "Theoretical Acoustics," Princeton University Press, page 701, (1986).

[16] Ingard, U. and Ising, H., "Acoustic Nonlinearity of an Orifice," Journal of Acoustical Society of America, **42** (1), pp6-17, (1967).

[17] Goldberg, D., "Genetic Algorithms in Search, Optimization and Machine Learning," Addison-Wesley, (1989).

Appendix A. Computer code

A.1 Computer code

Based on the modeling technique presented in Chapter 2, a matlab code was first developed to model the effects of the HQ tubes in a circular duct. The computer code allows to compute the transmitted modal amplitudes in term of sound pressure and sound power for any configuration of the HQ system. Although this code was providing satisfactory results, it is clear that the computation involved in this model is rather intensive and the computational time needed to run the simulations rapidly became an issue. In certain cases, the time needed to run a simulation was no less than several days. The computing time also increases with the accuracy of the results due to the large number of modes included in the Green's function and the complexity of the HQ system, i.e. mainly, the number of HQ tubes. Therefore, instead of trying to optimize the actual matlab code, it was decided to choose another programming language, which could provide extremely faster results. Thus, a Fortran code was built on the same basis as the previous code and gave some very satisfactory performance in term of accuracy of the results and running time. This Fortran routine will be presented in this section.

A.2 Structure of code

The flow chart in Figure A-1 shows the main steps of the code. The details for the successive computation steps were given in Chapter 2, therefore, it will not be covered again here. However, the information provided in the input and output files will be described in the following sections.

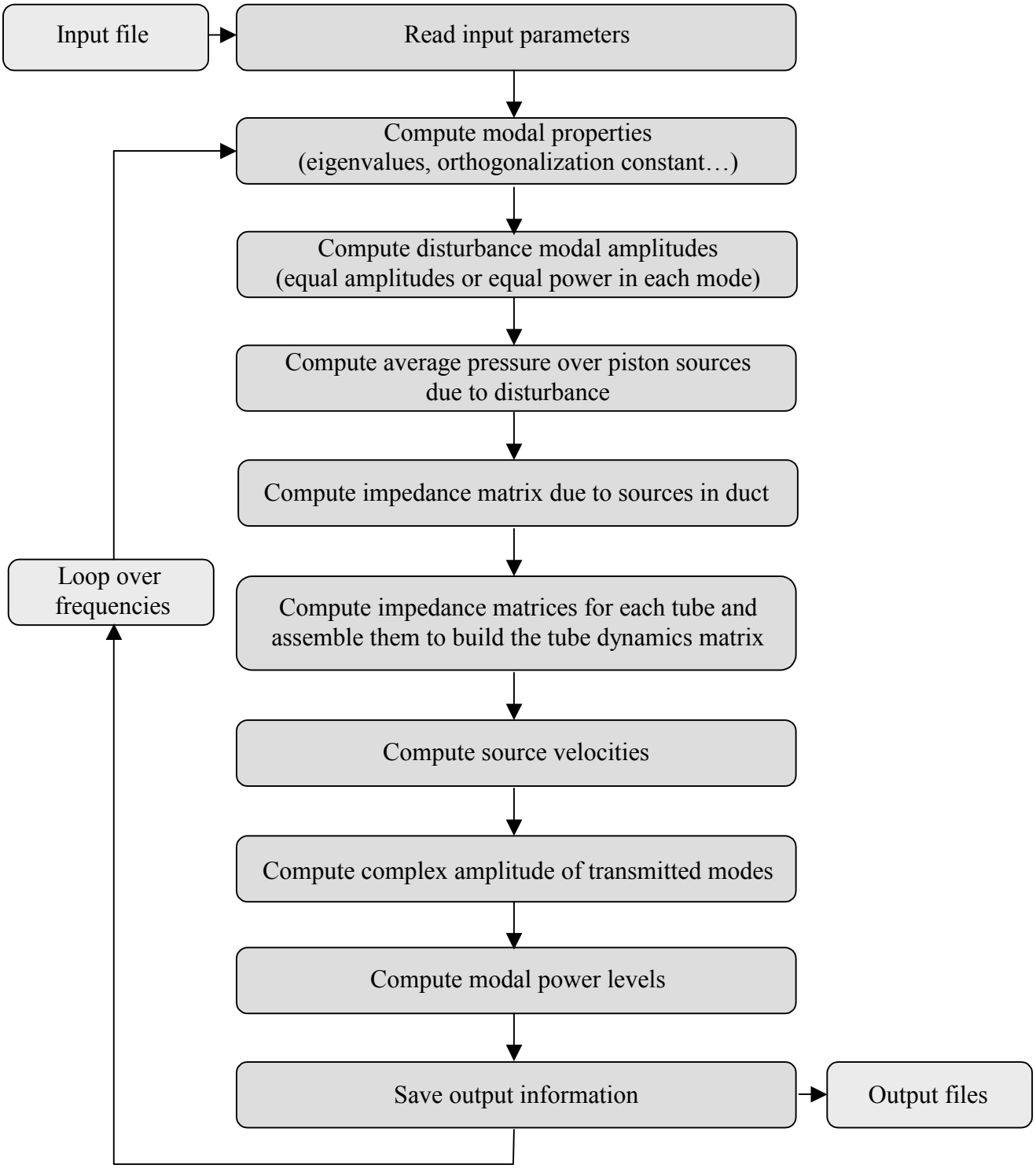

Figure A-1: Main steps in the computer code that models the Herschel-Quincke tubes in the duct.

A.3 Input file

The code was developed to allow a large flexibility in the possible simulations. In order to fully describe the system, the following information needs to be given in the input file.

General:

- Fluid density, sound velocity, flow Mach number,
- Duct radius,
- Lower frequency of analysis, frequency resolution and total number of frequencies,
- Number of radial and circumferential modes included in the Green's function,
- Axial position of the observer point where the transmitted mode amplitudes are computed.

Disturbance:

Three options are possible for the incident modal content. If the incident modal amplitudes are known, which is often the case for a BPF or tone analysis, these amplitudes can be directly given as input (in this case, one needs to give the m and n order of each mode and its complex amplitude). However, for a broadband analysis, the mode amplitudes can be chosen such that, for each frequency, all cut-on modes have equal amplitude, or each cut-on mode generates the same amount of sound power.

HQ system:

The HQ system is first defined by the number of arrays of tubes. The characteristics of each array are then given, assuming that the tubes in an array have the same properties. For each array, one needs to specify the number of tubes, centerline tube length, distance between tube ends, tube cross-sectional area, axial position of array, angle in the circumferential direction of first tube in array relative to the top of the duct, angle of tubes in the axial direction relative to duct axis.

The perforated screens characteristics are then needed: screen thickness, percentage of open area and orifice radius. Then, it is possible to choose to account for just the resistive term (responsible for dissipation of energy), the reactive term, or both terms in the screen impedance.

Output file:

It can be chosen to print all information (tubes and duct impedance matrices, source velocities…) or just the sound power information in the main output file. The modal power information can be saved in a second output file for particular modes. For this option, the order of the modes for which the power amplitudes will be saved need to be given in the input file.

A.4 Output files

The information given by the code is saved into two different output files. The main output file can take two different forms depending on the option chosen in the input file. In its shortest version, it contains the total incident, transmitted as well as the sound power reduction levels at each frequency. In its more complete form, it contains not only the total power levels at each frequency but also displays it for each individual mode. At each discrete frequency, it also shows the sound pressure modal amplitudes, the tube and duct impedance matrices and the source velocities.

The second output file allows to save modal power information at each frequency for particular modes, specified in the input file. In this case, it shows the incident and transmitted sound power amplitudes for the chosen modes at each frequency.

Vita

Raphaël Hallez was born on July 23, 1977 in Les Lilas, France. After graduating from Lycée S^{t} Rémy, Soissons in 1995, he joined the Université de Technologie de Compiègne (UTC). He received a Diplôme d'Études Universitaires de Technologie in July 1997 after two years of general engineering studies. He then specialized in the Acoustics and Vibrations branch of the Mechanical Engineering Department. He earned his engineer degree from the Mechanical Engineering Department in October 2000. During his last year of studies at UTC, he moved to the United States and began graduate studies in the Mechanical Engineering Department of Virginia Polytechnic Institute and State University in August 1999. With Professor Ricardo Burdisso as his advisor, he completed his master degree in January 2001.